The University of Nottingham

UNITED KINGDOM · CHINA · MALAYSIA

Capturing CO_2 from an Integrated Steel Mill

A techno-economic analysis through process modelling

Zahras Mohamed Duwahir (BEng Hons)

A thesis submitted to the University of Nottingham for the degree of Doctor of Engineering

Supervisors: Dr Paul Langston, Dr John Robinson

July 2016

Acknowledgement

I am extremely fortunate to get an opportunity to do research under University of Nottingham with partnership of TATA Steel. The EngD course has given me an extensive knowledge and wisdom through many enduring experiences. It has allowed me to travel, take part in political and technical conferences, and meet people with similar interest. The journey has allowed me to continuously develop and learn from mistakes, while preparing me to face the next chapters of my life.

I thank RCUK, University of Nottingham International Office and TATA Steel for their financial support for this research. I thank with my whole heart my supervisors Dr Paul Langston, Dr John Robinson and Prof Trevor Drage, without there guidance and intellectual input I would not have been able to achieve this thesis. Their wide knowledge in chemical engineering and process modelling has been a light in the dark parts of this journey. I once again thank you for your unmeasurable support and continuous guidance throughout this course. I hope that I can use the skills and knowledge gained from you all, beyond this research degree.

Dr Chris Treadgold, my industrial supervisor, who has continuously believed in me and guided me with his diverse knowledge will never be forgotten. I thank you for your continuous support, even when you had a busy work schedule. I would also like to thank Dr Bruce Adderley, my second industrial supervisor for his mentoring and guidance at TATA Steel. I would like to mention a heartfelt thank you for the employees at TATA steel, who embraced my research and provided enormous support.

My parents, who always believe in me even if they do not understand what my work enfolds, cannot be forgotten at this point. A thank you would not be enough for the love and care you have given me. With my parents I would like to remember my aunt, Mazoona, who has always been a well-wisher. Finally I remember my wife, thank you dear. You have been my companion through this journey. I do not think I can ever repay the support you have given, but will always remember it.

I dedicate this thesis to my father.....

Abstract

The increase in global carbon dioxide emission has raised concerns about climate change. This has caused nations to consider different carbon dioxide mitigation pathways to reduce emissions. The iron and steel industry contributes to approximately 30% of total global CO_2 direct emission in the industrial sector. It is an energy intense industry. Many steel mills are operating close to thermodynamic limits in efficiency. Therefore decarbonising the steel industry through process improvements is limited. Breakthrough technologies such as carbon capture and storage (CCS) is an alternative and attractive solution.

In this research I have explored the application of a retrofit carbon capture technology to an existing steel mill. The steel mill chosen, combusts gases arising from the steel making processes. Different locations within the steel mill were analysed, the in-house power station and the turbo blower house were chosen for retrofit post-combustion carbon capture.

Two different separation technologies were process modelled to capture the carbon dioxide from the flue gas of the in-house power station and the turbo blower house. The technologies were chemical absorption and adsorption. The two technologies were techno-economically studied.

Chemical absorption, with solvent MEA, showed capability of recovering 86% of CO_2 with a purity of more than 99 mol%. Adsorption using sorbent zeolite 13X was able to achieve 82% recovery with purity of 96 mol%. Sorbent activated carbon showed a capability of recovering 67% of carbon dioxide with a purity of 95 mol%.

The cost of CO_2 avoidance for the process using chemical absorption (MEA) was equal to \$44.92/tonne CO_2. For the process using adsorption (zeolite 13X) the CO_2 avoided cost was equal to \$44.90/tonne of CO_2. Activated carbon was the most expensive capture process, out of the three processes studied. It costs \$45.81/tonne of CO_2 avoidance.

List of Figures

List of Tables

List of Equations

List of Mathematical Nomenclature

a_s	External surface area of pellet (m^2)
b	Langmuir isotherm constant (bar^{-1})
C	Concentration (mol/m^3)
C_e	Purchased equipment cost, factorial method
CO_3^-	Carbonate ion
D_c	Inter-crystalline diffusivity (m^2/s)
D_e	Effective diffusivity (m^2/s)
D_k	Knudsen diffusivity (cm^2/s)
D_L	Axial dispersion coefficient (m^2/s)
D_m	Molecular diffusivity (m^2/s)
d_p	Pore diameter (Å, m)
fc	installation factor for civil engineering work, factorial method
fel	installation factor for electrical work, factorial method
fer	installation factor for equipment erection, factorial method
fi	installation factor for instrumentation and control, factorial method
fl	installation factor for lagging, insulation or paint, factorial method
fm	material factor if a material different to carbon steel is used, factorial method
f_{molar}	Flow rate of gas (mol/h)
fp	installation factor for piping, factorial method
fs	installation factor for structures and building, factorial method
H	Enthalpy
H^+	Hydrogen ion
HCO_3^-	Hydrogen carbonate ion
i	Interest rate
IP_1	Isotherm parameter in ADSIM (kmol/kg)
IP_2	Isotherm parameter in ADSIM (kmol/kg)
IP_3	Isotherm parameter in ADSIM (bar^{-1})
IP_4	Isotherm parameter in ADSIM (K)
k	Mass transfer coefficient (s^{-1})
k_a	Adsorption constant
k_d	Desorption constant
k_f	Boundary film mass transfer resistance (ms^{-1})
M	Total number of pieces of equipment
	Molecular weight (g/mol)
n	Plant life time
OH^-	Hydroxyl ion
P	Pressure (bar, Nm^{-2})
q	Amount of sorbate adsorbed onto the sorbent (mol/kg)
q^*	Equilibrium amount of sorbate adsorbed (mol/kg)
q_m	Monolayer adsorbed capacity (mol/kg)
r	Micro particle crystal radius (m)
R	particle radius (m)
Re	Reynolds number
R_g	Universal gas constant ($Jmol^{-1}K^{-1}$)
R_p	Pellet radius (m)
r_p	pore radius (cm)
S	Size parameter
	Entropy (J/K)
Sc	Schimdt number
Sh	Sherwood number
t	time (s, h)
T	Temperature (K)
W	Work (J)
u_o	Interstitial velocity (m/s)
v	Diffusion volume
w	Adsorption loading (mol/kg)
Δ	change
θ	fractional coverage
σ_{AB}	collision diameter (nm)
ϵ_p	Inter-pellet void fraction
τ	tortuosity factor
ρ	density (kg/m^3)
η	efficiency

Acronyms and Abbreviations

AC	Activated carbon
ASU	Air separation unit
BF	Blast furnace
BFG	Blast furnace gas
BOF	Basic oxygen furnace
BOF gas	Basic oxygen furnace gas
CAPEX	Capital expenditure
CCS	Carbon Capture and Sequestration
CEPCI	Chemical engineering plant's cost index
CO	Carbon monoxide
CO_2	Carbon dioxide
COG	Coke oven gas
CPS	Central Power Station
CS	Carbon steel
DEA	Di-ethanolamine
DR	Direct reduction
DRI	Direct reduced iron
EAF	Electric arc furnace
ETS	Emission trading system
FCI	Fixed capital investment
FGD	Flue gas desulphurisation
FOC	Fixed operating cost
GHG	Greenhouse gas
H_2	Hydrogen
H_2O	Water
IEA	International Energy Agency
IGCC	Integrated gasification combined cycle
IPCC	Intergovernmental Panel on Climate Change
ISBL	Inside battery limit
kWh	kilo-watt hour
LDF	Linear drive force
M	Million, Mega
MEA	Monoethanolamine
N_2	Nitrogen
NO_x	Nitrogen oxides
O_2	Oxygen
OHF	Open hearth furnace
OPEX	Operational expenditure
OSBL	Outside battery limit
P	Pressure
ppm	Particle per million
PSA	Pressure swing adsorption
PTSA	Pressure and temperature swing adsorption
QDF	Quadratic drive force
R^2	Coefficient of determination
SO_2	Sulphur dioxide
T	temperature
t	tonne
TACC	Total annual capture cost
TBH	Turbo Blower House
TEA	Tri-ethanolamine
TGRBF	Top gas recycling blast furnace
TOC	Total operating cost
TSA	Temperature swing adsorption
ULCOS	Ultra Low CO_2 Steel Making
US	United States
v	valve

Contents

1 Decarbonising the Steel Industry – CCS and its Role

The working group assessment report on climate change published by Intergovernmental Panel on Climate Change (Alexander et al., 2013) has confirmed that human actions are the principal cause for climate change. The report mentions that the target of limiting the global temperature rise below $2^{o}C$, to pre-industrial period, is becoming unachievable with the current pace of greenhouse gas[1] (GHG) emissions. There have been drastic changes to weather conditions and climate events due to the increase in atmospheric temperature even below $2^{o}C$. Some parts of the globe are affected by series of heat waves while others continue to see high rainfall. Significant losses in ice mass in the hemispheres are visible, causing a rise in global sea level (Alexander et al., 2013).

Increasing concerns about climate change is causing us to rethink and strive to reduce GHG emissions. The synthesis report published by IPCC in 2007 (Bernstein et al., 2007) mentions that 77% of the total atmospheric anthropogenic GHGs is carbon dioxide (CO_2), and is considered as the most important GHG. The annual CO_2 emission has increased by 80% in the last three to four decades (IEA, 2010). Figure 1-1 is a replica of the chart showing the share of anthropogenic GHGs emission in 2004. It is clear that the largest

[1] Greenhouse gases (GHGs) are atmospheric gases present both as natural and anthropogenic (produced by humans). They have the capability of absorbing and emitting radiation onto the earth's troposphere. An increase in GHGs would cause an increase in temperature of the troposphere resulting in an enhanced greenhouse effect.

contribution to the emission is due to mankind's high dependency on fossil fuel[2].

Fossil fuel has been the main source providing primary energy globally. It has constantly contributed to more than four fifth of the energy share since 1970 (IEA, 2014). According to the IEA (International Energy Agency) fossil fuels contributed 82% of the global total primary energy in 2011 (IEA, 2012b). The world's demand on primary energy has also doubled in the last four decades (IEA, 2010). This has seen a rise in anthropogenic CO_2 emissions; it is reported that in 2011 the world experienced a total emission of 31.3 Gt CO_2. With predictions that energy usage would double by 2050, low carbon technologies needs to be implemented on a large scale to offset carbon emissions.

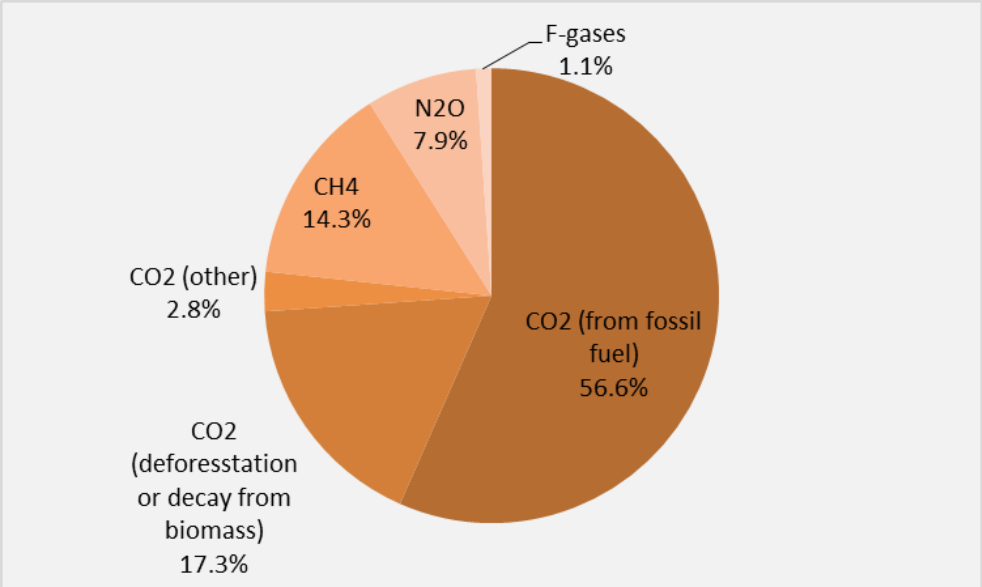

Figure 1-1: Anthropogenic GHG emissions in 2004 (Bernstein et al., 2007)

[2] Fossil fuels are hydrocarbons in form of coal, oil or gas. They are resulted from the anaerobic decomposition of organic compounds millions of years ago. The combustion of fossil fuel would result in emitting CO_2 as a by-product.

It is agreed, by many experts, that the current trend of emissions without any hindrance would result in an average global temperature rise by $6^{o}C$ (IEA, 2012a). A worrying prediction after experiencing drastic climate changes around the globe with global temperature rise below $2^{o}C$ (Field and Van Aalst, 2014). Global temperature rise to $6^{o}C$ would mean devastating changes causing inhabitants in some part of the world to experience disastrous impact. Global energy demand, controlled by energy intense consumer goods and services humans consume as part of their lifestyle, is expected to double by 2050 (IEA, 2012a). The Energy Technology Perspective published by the IEA explains; with the current government pledges and improvements in energy efficiency the path is leading to a global temperature rise of $4^{o}C$ in the long term. It is arguable that $4^{o}C$ would not be considered as enough to prevent catastrophic climate events, but IEA mentions it as an optimistic ambitious scenario. It requires strict climate change policies implemented and substantial changes to human lifestyle to achieve. The window of opportunity to limit global temperature to $2^{o}C$ is narrowing; the report mentions global CO_2 emission in 2050 needs to be cut by half to the levels of 2009. This would require a diverse energy mix, changes to human behaviour and less energy intense economy (IEA, 2012a).

The pathway to $2^{o}C$ or $4^{o}C$ limitation of rise in global temperature would require three routes to reduce total CO_2 emissions; reduction of the carbon intensity, improve energy efficiency and mitigation by sequestrating captured CO_2 (Yang et al., 2008). To reduce carbon intensity, non-fossil fuel energy such as hydrogen and renewables should fill the global energy mix. Energy efficiency is a process improvement route that reduces the process energy used,

therefore indirectly reducing the CO_2 emission. Sequestration of captured CO_2 known as Carbon Capture and Storage[3] (CCS) can be applied to the current fossil fuel saturated energy mix to reduce CO_2 emission. This would reduce the overall CO_2 emissions from fossil fuel combustion. It can also be applied for sources using biomass as fuel, and therefore would enable to achieve negative emissions to the atmosphere if the biomass is obtained sustainably with no carbon emissions (Metz et al., 2005). CCS is considered as an important process that could be applied globally, and would enable movement towards a low carbon future. It is considered to be technically feasible and applicable to large emitting sources such as industries and power generators. Its global application depends on its technological maturity, public acceptance, cost to implement and environmental impact (Metz et al., 2005).

1.1 Carbon Capture and Storage

The initial stage of CCS involves capturing CO_2 from the processed fossil fuel or capturing it from the flue gas after combustion. It is then transported by pipelines or ships to designated storage locations, where it is finally stored for the long term. Storage of CO_2 can be achieved by injecting the captured CO_2 into deep underground geological formations, or into deep sea. It can also be stored as inorganic carbonates by industrial fixation. Captured CO_2 can also be used in manufacturing processes, in which it is stored in the industrial product (Metz et al., 2005). There are three main different approaches that can be applied for the capturing CO_2; post combustion, pre combustion and oxy

[3] Carbon capture and storage is a process that captures carbon dioxide and stores it, preventing emissions to the atmosphere. The carbon dioxide is preferably captured from large emitting sources.

combustion. The choice of which method to use varies in accordance to its application.

1.1.1 Post-combustion CO_2 capture

Post combustion capture involves separating the CO_2 from flue gas, by applying a capture technology to capture the CO_2 from the combusted flue gas. Flue gas contains the products of fossil fuel combustion. Post combustion process can be applied as a retrofit technology to an existing coal or gas fired power plant. It can also be applied as a retrofit to the sources that combust industrial gases (Metz et al., 2005). Figure 1-2 shows the schematic of the process flow for capturing using post combustion. There are many different technologies available that can be used in the CO_2 separation stage. The most matured and widely used technology is chemical absorption using amines. There is a good understanding of this technology, because it has been widely used in natural gas processing for many years (Yang et al., 2008). Other technologies such as adsorption and membranes are less mature, but are applicable and considered to be less energy consuming in comparison to chemical absorption.

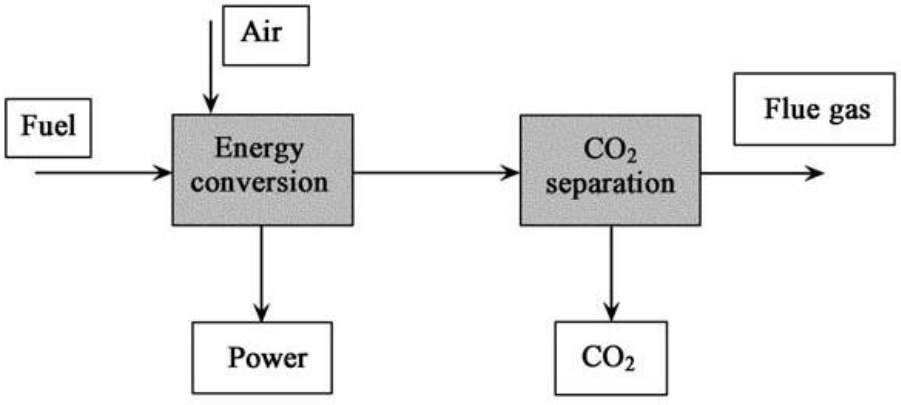

Figure 1-2: Process flow for post combustion CO_2 capture process (Yang et al., 2008)

1.1.2 Pre-combustion CO_2 capture

As the name states, this process uses technology before combustion to decarbonise the fuel. It involves fossil fuel reaction with steam or air to obtain a fuel gas known as synthesis gas (syngas). The syngas mainly consists of carbon monoxide (CO) and hydrogen (H_2). The syngas is then further processed through a water gas shift reactor, which converts the CO in the syngas to CO_2 and H_2. The final product stream then undergoes a separation process in which CO_2 is separated for storage and H_2 is used as fuel (Metz et al., 2005, Wilcox, 2012). The process flowsheet representing pre-combustion CO_2 capture is shown in Figure 1-3.

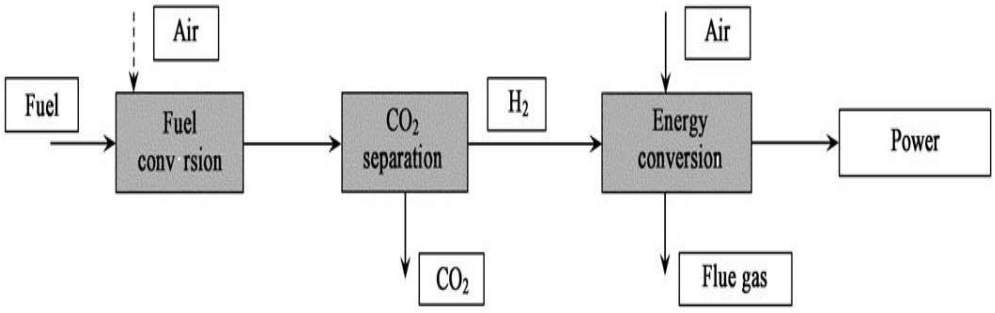

Figure 1-3: Process flow for pre-combustionCO_2 capture process (Yang et al., 2008)

The separation of CO_2 can be achieved by different technologies, but unlike post-combustion capture the processed syngas has a higher CO_2 partial pressure. This enables using technologies such as physical absorption, adsorption using sorbents and membranes, which are much more effective at high CO_2 partial pressures (Yang et al., 2008, Kanniche et al., 2010). According to Yang et al. (2008) pre-combustion process is potentially less expensive than post-combustion process. It will be efficient when applied to an integrated gasification combined cycle (IGCC).

1.1.3 Oxy-combustion CO_2 capture

This process involves combustion of the fossil fuel using pure oxygen (O_2). This gives a flue gas with a high CO_2 partial pressure, which is significantly higher than flue gas from combustion using air. Yang et al. (2008) mentions that the oxy combustion flue gas consists approximately 90% dry volume of CO_2. This is variable and depends on the purity of O_2 used for combustion. The CO_2 from the flue gas can then be further purified using cryogenic separation or membranes. The process flow diagram representing an oxy combustion capture is shown in Figure 1-4.

The advantages of this technology are; elimination of nitrogen oxides (NO_x) and lesser energy penalty for CO_2 separation (Rackley, 2010). Reduced boiler size from using a lower volume of combustion oxygen instead of air is also an advantage. The disadvantages include a higher concentration of sulphur dioxide (SO_2) in the flue gas, which causes excessive corrosion. This will increase the cost of equipment material. An additional investment cost with energy penalty will be from the air separation unit (ASU) (Yang et al., 2008). In conclusion Yang et al. (2008) mentions the oxy-combustion CO_2 capture process is less matured and the capital cost is similar to post-combustion CO_2 capture process. The flexibility of retrofitting post-combustion CO_2 capture process to an existing coal fired power plant makes it the primary choice.

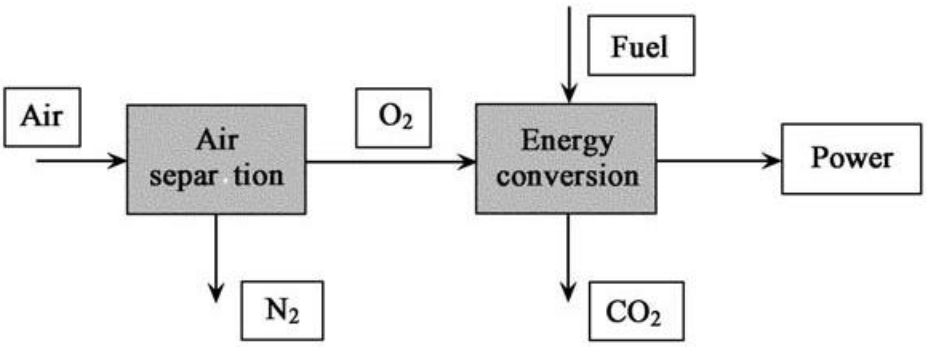

Figure 1-4: Process flow for oxy-combustion CO_2 capture process (Yang et al., 2008)

1.2 Industrial CO_2 Emissions

In similar to the power sector a large percentage of CO_2 is emitted from heavy industries (steel, paper etc.). In industry there are two forms of CO_2 emissions (Brown et al., 2012)

- Direct emission: CO_2 emitted from consuming raw materials with a carbon factor e.g. coke for making steel. Emissions are emitted to the atmosphere directly within the manufacturing process.

- Indirect emissions: Emissions from consuming utilities that emitted CO_2 during its production e.g. electricity consumed. Emissions are emitted by the supplier of the utility.

In the year 2005, 37% of total global CO_2 emissions were from industries. A total of 9.9 Gtonnes of CO_2 were emitted by industries that year, of which direct emissions were approximately 67% (IEA, 2008). The breakdown of the percentage direct CO_2 emission for year 2005 is shown in Figure 1-5.

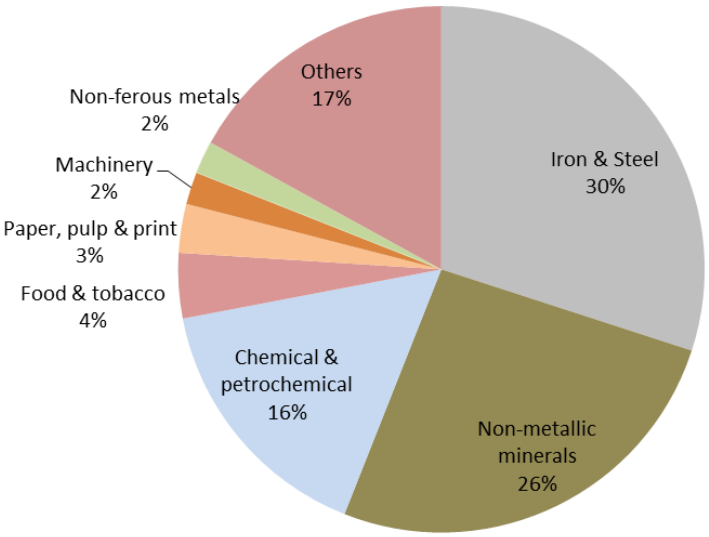

Figure 1-5: Direct industrial CO_2 emissions by sector for 2005 (IEA, 2008)

Iron and steel industry contributed to 30% of industrial direct emissions in 2005, and is highlighted as one of the largest industrial emitters. Process improvement with alternative fuel could reduce emission, but CCS needs to be applied alongside it to achieve 50% emission reduction by the year 2050 (Kuramochi et al., 2012).

1.2.1 Steelmaking and its CO_2 emissions

The conventional blast furnace plus basic oxygen furnace (BOF) is the most common route in producing steel globally. The World Steel Association assumes approximately 66% of total steel produced globally in the year 2007 was by the conventional route. The electric arc furnace (EAF) route uses electricity to melt direct reduced iron (DRI) or recycled metal in the EAF. Steel production through EAF in the year 2007 was approximately 31% (WSA, 2008). The two different methods of steel production are illustrated in Figure 1-6.

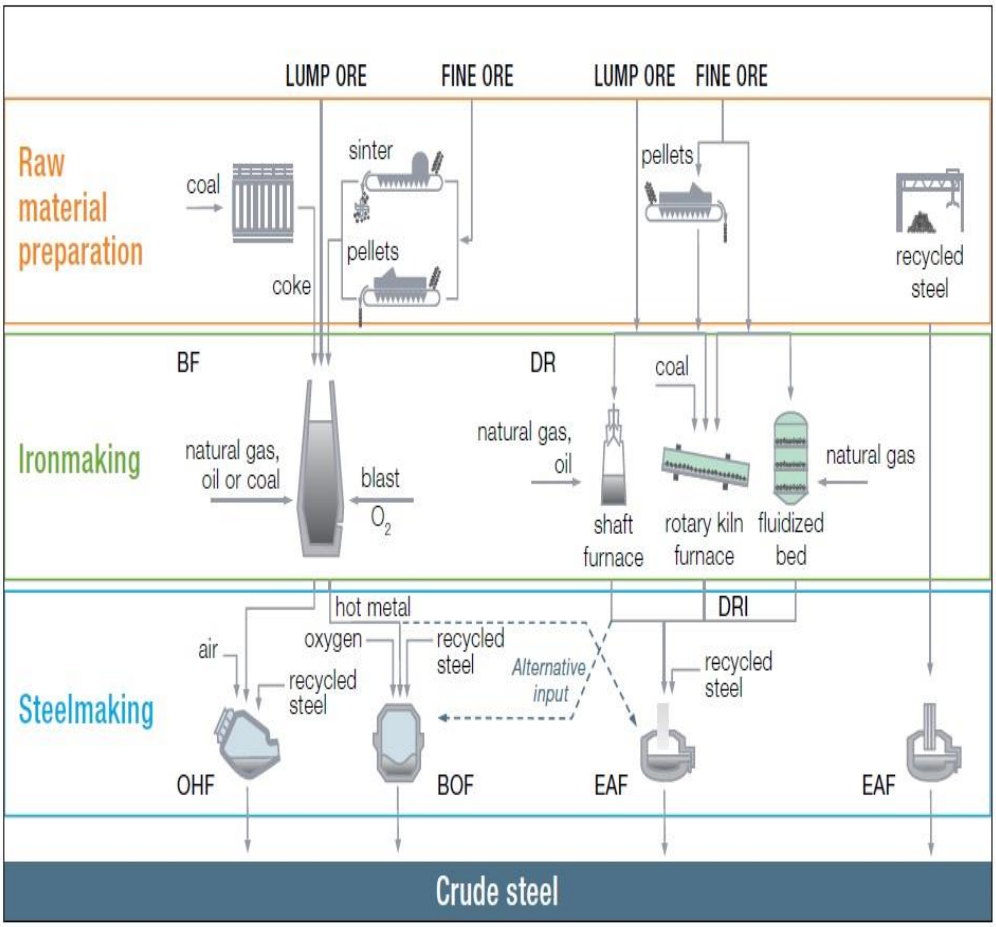

Figure 1-6: Conventional and EAF routes of steel making (WSA, 2014b)

The conventional steel making route using a blast furnace and BOF emits approximately 2.2 tonne of CO_2 per tonne of steel. The EAF route emits approximately 0.6-0.9 tonne of CO_2 per tonne of steel. The conventional steelmaking route remains to be popular, despite a higher CO_2 emission. The lack of high quality scrap steel for the EAF route is a reason for the conventional route to be popular. The conventional route is also known to produce a high quality crude steel with less undesired residual material (Wiley et al., 2011).

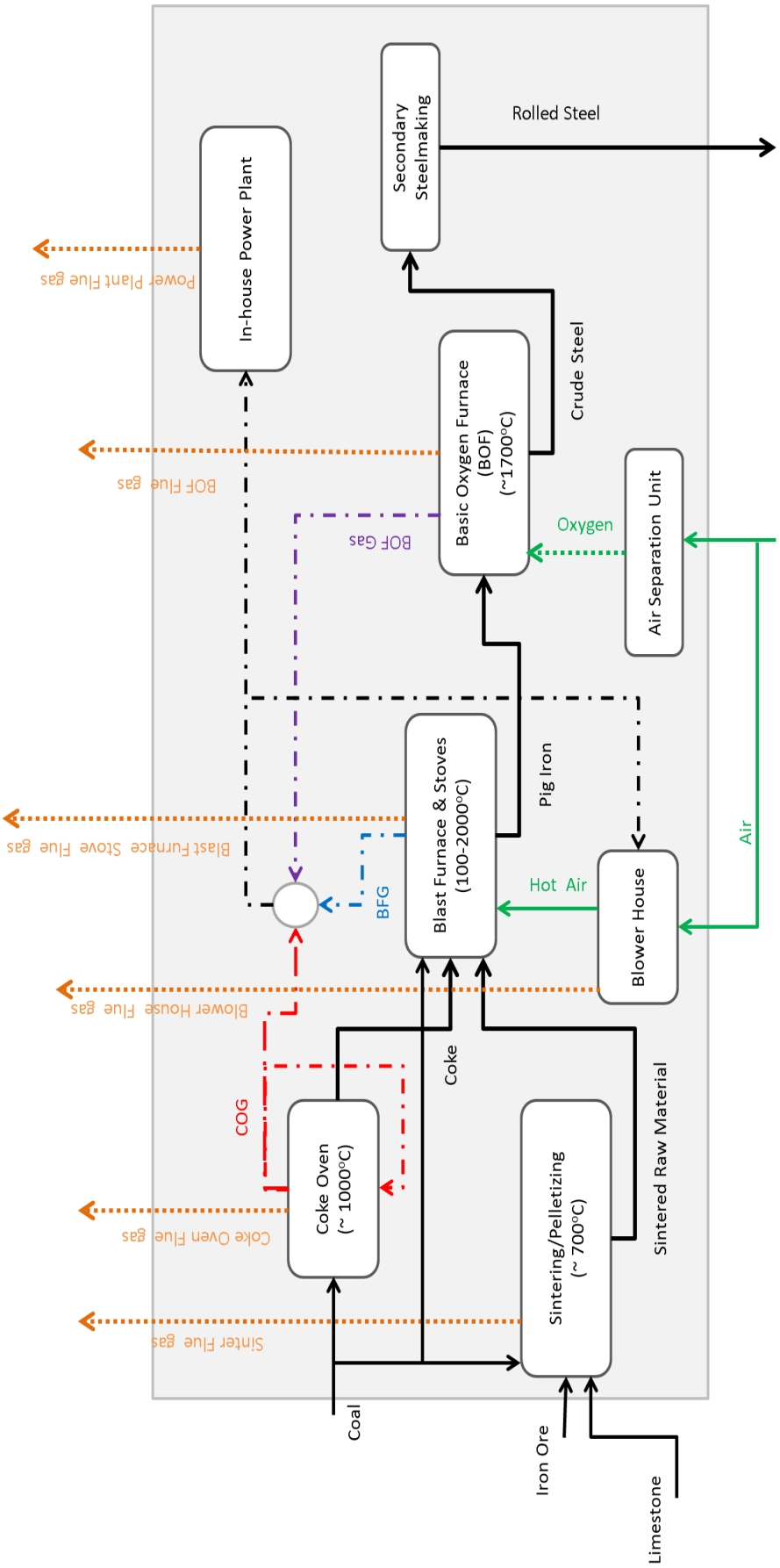

Figure 1-7 : A simplified process flowsheet of the conventional steelmaking route adapted from (Kuramochi et al., 2012)

Integrated steel mills producing steel through the conventional route have many different point sources of CO_2 emissions as shown in Figure 1-7. The main processes in steelmaking consist of the coke oven, sinter production, iron production and steel making. The coke oven carbonates the coal at a high temperature (approx. 1000^{o}C) in the absence of oxygen. The oxygen deficient process enables production of carbon concentrated coke. Coke is an important raw material added into the blast furnace. Coke should be able to support the descent of the blast furnace burden with little degradation as possible. It also provides thermal energy and contributes to iron ore reduction. The coke also allows permeability of blast furnace gases and molten metal. The off-gas from the coke ovens is called the coke oven gas (COG). COG is used to heat the coke ovens and as fuel in other parts of the steel mill (Valia, 1994).

The sinter production involves converting raw materials; iron ore, limestone, coke breeze and recycled materials to form an agglomerated product. Coke breeze enables ignition. The product sinter is charged into the blast furnace with coke and limestone. The sinter production emits a flue gas with a low calorific value, and therefore has no further use in the steel mill (Remus et al., 2013).

Iron production takes place in the blast furnace. Iron bearing materials (iron ore lumps and sinter), additives (limestone) and reducing agents (coke) are continuously fed through to top of the blast furnace. This prevents the blast furnace gas (BFG) from escaping. Hot air and additional reducing agents are blasted up the tuyeres of the blast furnace. This provides counter-current iron ore reduction. The hot air blast reacts with the reducing agents to produce

carbon monoxide, which reduces the iron ore to a hot metal (pig iron). The pig iron is collected in the hearth of the blast furnace and transported to the basic oxygen furnace, where steel making starts. The slag from the blast furnace is also collected and has further use in cement production a road making. The BFG is transported as fuel to be used in various other parts of the steel mill (Remus et al., 2013).

Steel making begins in the basic oxygen furnace (BOF) after pre-treatment of the pig iron to reduce sulphur content. In the BOF scrap metal and pig iron are reacted with oxygen to remove undesirable impurities. High purity oxygen is injected to the BOF. The oxidation process eliminates excess carbon, which is fumed as part of the off-gas from the BOF. Other impurities such as silicon, magnesium and potassium are also oxidised and removed as BOF slag. The reactions in the BOF are exothermic; therefore it provides the necessary heat to melt the scrap and enables tapping of the hot metal at desired temperature. The off-gas from the BOF is used as fuel in the other parts of the steel mill (Remus et al., 2013). Crude steel from the BOF is transported to the rolling mills, where steel is rolled and cooled to desired shapes.

Integrated steel mills have an in-house power plant. The power plant utilises the off-gases from iron/steel making processes. The off-gases are known as works arising gases (WAGs) and mainly consist of BFG, COG and BOF gas. The power plant can utilise these WAGs to produce electricity power, steam and/or district heat. In appropriate and feasible conditions the power plants also utilises purchased fuel (e.g. natural gas and oil). The flue gas

from the power plants is released to atmosphere through stacks (Remus et al., 2013).

The compositions and the conditions of the WAGs and flue gases from the integrated steel mill are dependent on raw materials and process technology. Table 1.1 illustrates the properties and the compositions of the flue gases from point sources of steel making shown in Figure 1-7.

Table 1-1 Compositions and conditions of the flue gas from point sources of steel making (Wiley et al., 2011)

	Sinter flue gas	*Coke oven flue gas*	*Blast furnace stove flue gas*	*BOF flue gas*	*Power plant & Hot air blower flue gas*
Temperature (°C)	*100*	*100*	*300*	*300*	*300*
Pressure (kPa)	*101.3*	*101.3*	*101.3*	*101.3*	*101.3*
Compositions (%vol)					
N_2	70	67	68	13	68
H_2O	21	5	10	2	8
CO_2	8	27	21	15	23
O_2	-	1	1	-	1
CO	1	-	-	70	-
H_2	-	-	-	-	-

The steel making process has matured over many years, and many advanced conventional steel mills around the world operate with close to thermodynamic limits in efficiency. Process improvements to reduce energy within the conventional route are limited. To reduce CO_2 emissions significantly, drastic changes to the conventional process needs to be implemented. This has to be achieved through innovative technologies or breakthrough technologies (Orth et al., 2007, Wiley et al., 2011). The World Steel Association has identified and proposed a few changes and they are as follows (Wiley et al., 2011, WSA, 2014a)

- Using hydrogen (H_2) as an alternative to fossil fuel for reducing iron ore. The H_2 needs to be sourced from carbon-lean process, and will be used in direct reduction (DR) reactors. DR process is an alternative to the blast furnace route as shown in Figure 1-6. H_2 can be used in its pure form or as syngas. The H_2 production process can be paralleled with CCS.

- Biomass which is sustainable and sourced through lean CO_2 emission routes can be used as a reducing agent. Biomass converted to charcoal can be used in the blast furnace, or syngas processed from the biomass can be used in reactors of DR process.

- Electrolysis, which uses electricity to reduce iron ores instead of fossil fuel.

- Application of CCS. CCS can be applied to a conventional route steel mill or to an altered innovative mill with different set up for iron making. The multiple points of CO_2 emission in a conventional route makes it difficult to apply carbon capture. Modifications to iron making would enable it to concentrate the CO_2 emissions to a single point and apply CCS.

CCS is considered as a key CO_2 abatement process that would decarbonise steel industries while it continues to use fossil fuel. It needs to be applied in parallel to steel making and would require alterations to the conventional route to make CCS economically feasible (Kuramochi et al., 2012).

1.2.2 Steelmaking and CCS

According to Tsupari et al. (2013) the three capture approaches (post-capture, pre-capture and oxy combustion) can be implemented to an integrated steel mill. The point of application is important and needs to be assessed, in order to reduce a larger quantity of CO_2 emissions. According to the IEA (2008) the blast furnace emits approximately 1-1.5 tonne of CO_2 per tonne of iron produced. Applying CCS to the blast furnace can theoretically decarbonise steel making by approximately 60-70%, since about 70% of the carbon introduced into steel making passes through the blast furnace. Carbon is introduced into steelmaking as fossil fuel (coal) as shown in Figure 1-7. Iron ore reduction takes places in the blast furnace, where the fossil fuel is consumed as a reducing agent. The blast furnace therefore is the largest CO_2 emitter in the steel mill (Kuramochi et al., 2012).

There are two ways to apply carbon capture to the blast furnace, with or without further processing of the top blast furnace gas. The top blast furnace gas has a CO_2 partial pressure of approximately 17-25%. The gas has other gaseous molecules such as nitrogen (N_2) H_2 and CO. Applying carbon capture directly to the top gas will not capture CO. The CO will be converted to CO_2 after combustion and emitted to the atmosphere. The other option of application is to apply after the CO in the top gas is converted or combusted to CO_2. The latter method would enable a higher recovery of CO_2 (Kuramochi et al., 2012).

Other options of carbon capture involve a modification to the air blown blast furnace. Ultra Low CO_2 Steel Making (ULCOS) is a consortium made up

of leading steel companies from around the world collaborating with academia and other industries specialising in CCS. ULCOS is currently investigating different modifications to the conventional blast furnace that would enable carbon capture to be more efficient. The top gas recycling blast furnace (TGRBF) is a retrofit technology to the existing blast furnace. TGRBF uses oxygen instead of air to obtain CO and CO_2 rich top gas. CO is recycled back into the blast furnace to act as a reducing agent after separation. The recycling of the top gas reduces the overall coke combustion in the blast furnaces, therefore reducing the overall CO_2 emissions by approximately 76%. Two different separation technologies have been investigated; vacuum pressure swing adsorption (VPSA) and chemical absorption using monoethanolamine (MEA). VPSA was more cost effective due to the high partial pressure of CO_2 in the top gas from TGRBF (IEA, 2008, Kuramochi et al., 2012).

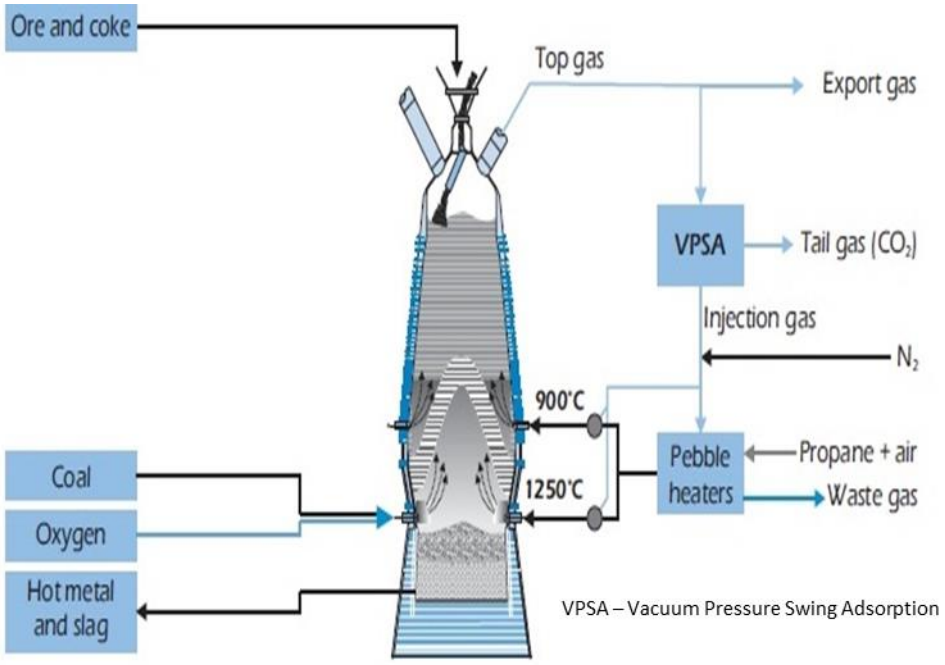

Figure 1-8: Top gas recycling blast furnace schematic (IEA, 2008)

Another novel alternative to the conventional blast furnace is the smelting reduction process. It is considered that the hot metal produced through the smelting process is cheaper than that produced through the blast furnace route. The most matured smelting reduction process used at commercial scale is COREX, a two stage iron ore reduction process that uses non coking coal and a wide range of iron ores. The COREX process is commercially operating worldwide. The smelt reduction process is more feasible for carbon capture because the flue gas has a higher CO_2 concentration, approximately 25-35 vol%. Further development of the smelting reduction process would directly use iron ores in the reduction shaft (FINEX). Other developments involve operation without N_2 input into the smelting process (HIsarna), which is developed by ULCOS. HIsarna is novel technology designed to decarbonise steel making by approximately 95% and is in its development phase. HIsarna process involves direct input of non-coking coal and iron ores, and the carbon is fully oxidised in the smelter. This high concentration of CO_2 in the flue gas enables capturing it easily by cryogenic separation. The currently available smelting reduction process has a low output rate of hot metals when compared to the conventional blast furnace (Gojiæ and KoÞuh, 2006, Kuramochi et al., 2012).

In an integrated steel mill the top gas from the blast furnace is exported to other parts of the steel mill to be combusted, therefore the blast furnace is not the largest emission point to the atmosphere. Similar to the blast furnace gas other process arising gases, such as coke oven gas and BOF gas are also combusted. The combustion of these low grade fuels is used to heat other units or is used to generate electricity. Generating its own electricity makes the steel

mill energy efficient and self-sufficient to a certain extent. A capture technology applied to the power plant could capture approximately 36-40% of total CO_2 emissions (Wiley et al., 2011).

1.3 Project Objectives

The aim of this project was to produce a detailed techno-economic analysis of capturing CO_2 from the steel mill studied. This was achieved through the following objectives.

- Conduct a literature survey to find the most suitable separation technology for CO_2 capture in conditions representing a steel mill
- Analyse and understand different point source CO_2 emissions in a steel mill
- Conduct a CO_2 mapping on the studied steel mill, to apply a retrofit carbon capture technology
- Process model one or two technologies to understand the technical feasibility of applying carbon capture to the studied mill
- Conduct an economic analysis to understand the overall feasibility of applying carbon capture for the steel mill

1.4 Novelty in this Study

This study has investigated capturing CO_2 from an integrated steel mill. An in-depth process flow was analysed for the steel mill studied. This gave a picture on the different flue gas composition arising from steel making. Wiley et al. (2011) have conducted a similar work, but every steel mill is different.

The processes and the flue gas arising differs depending on the raw materials and process technology.

Arasto et al. (2013) have studied capturing CO_2 using MEA scrubbing from an existing steel mill in Bothnia. Arasto et al. (2013) have considered capturing from the flue gas arising from the in-house power station and hot stoves. Chapter 5 of this study is very similar to the work of Arasto et al. (2013), because it considers capturing CO_2 from combined flue gas from central power station (CPS) and turbo blower house (TBH). As mentioned above the flue gas composition differs from one steel mill to the other. Arasto et al. (2013) study had a flue gas CO_2 concentration of approximately 28 mol%. This study analysed capture from flue gas with CO_2 concertation of 24 mol%. Another difference from the work by Arasto et al. (2013) is the procedure of process modelling. This study uses equilibrium based CO_2 separation for amine scrubbing, while Arasto et al. (2013) has used rate based CO_2 separation.

The economic analysis for the work of Arasto et al. (2013) was done by Tsupari et al. (2013). They do not show individual equipment costing, and have equated the cost as loss in electricity generation from the steel mill. This study has used the traditional costing term "CO_2 avoidance cost"; this enables to compare with adsorption and other published literature on amine scrubbing.

The "leap" in novelty is in Chapter 6, where adsorption is modelled using ADSIM. The software was previously known as Aspen Adsorption, and is still in its developing phase. Unlike HYSYS it has not got a property library for the sorbents. It also lacks information on adsorption isotherms and adsorption kinetics. A large scale CO_2 capture using adsorption has not been process

modelled before. Simpler methods of mass balance relationships have been used to model large scale CO_2 capture from coal fired power plant (Ho et al., 2008b). Conditions representing capture from steel mill flue gas is even rarer.

This study analyses adsorption using zeolite 13X and activated carbon, in conditions of the steel mill. A comparative analysis of these two sorbent at large scale and high CO_2 concentrated flue gas is novel. In addition to that adsorption models were also compared with a mature technology (MEA scrubbing).

A techno-economic comparison of adsorption and MEA scrubbing is novel in terms of the scale of this study. This study considers capturing CO_2 from flue gas flow rate of approximately 700,000 kg/h. Most of the adsorption studies have only considered lab scale flow rates (Wang et al., 2013).

2 Literature Survey – Search for the Most Suitable CO_2 Separation Technology

The literature survey conducted as part of this research investigated different CO_2 separation technologies that can be applied for steel making conditions. The flue gas rising from steel mills have different properties to that rising from power stations using coal or natural gas as fuel. The CO_2 concentration in the flue gas rising from steel mill is approximately 25-35 vol%. Coal power stations emit flue gas with CO_2 concentration of approximately 13-15 vol%, and natural gas has the lowest concentration 3-5 vol%. The flue gas for all three scenarios, mainly consist N_2 and CO_2 (Singh et al., 2003, Wiley et al., 2011). There is currently a vast literature on applying separation technologies for conditions using coal or natural gas. Literature describing separation technologies for the conditions of steel mills is limited, but the technologies are similar to that applied to other fossil fuel CO_2 capture. It can therefore be cross linked and applied for steel making conditions. A wide range of capture is adaptable to capture from steelmaking (Figure 2-1).

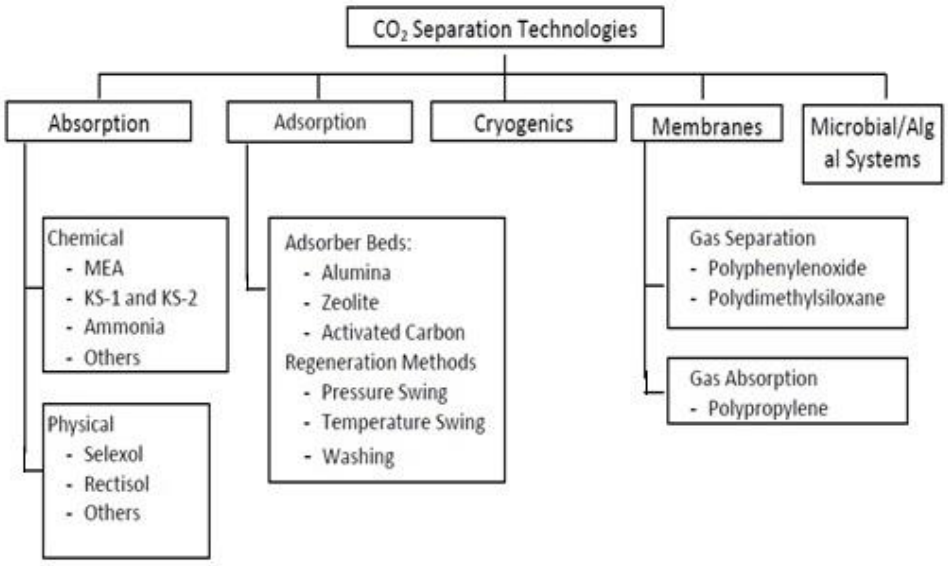

Figure 2-1: CO_2 capture technologies that can be applied for conditions representing a steel mill. Obtained from (Wang et al., 2011)

The capture technologies represented in Figure 2-1, were not initially designed for carbon capture from flue gas or syngas. They were applied to smaller scale different processes that required separation of gaseous molecules. The technologies can be adapted and applied to large scaled process involving CO_2 capture. The choice of the technology is dependent on the characteristic of the flue gas or syngas (Rao and Rubin, 2002).

The literature survey has reviewed chemical absorption, adsorption, membranes and physical absorption. These technologies are applicable to conditions representing capture of CO_2 from flue gas arising from steel making. They have been analysed against the following design and performance parameters.

- Maturity
- Capital Investment

- Reliability
- CO_2 selectivity
- Operational cost
- Environmental friendliness

2.1 Chemical Absorption

Chemical absorption is a matured technology with years of use in natural gas processing. The process is ideal for post combustion processes which have low CO_2 partial pressure (Metz et al., 2005). CO_2 in the flue gas chemically reacts with the aqueous alkaline solvent to form reversible weak bonds. This chemical reaction is used to capture and separate CO_2 through a continuous absorption and regeneration process. The process flow sheet for chemical absorption is shown in Figure 2-2. Flue gas is initially cooled to 40-50^oC to enhance absorption and is blown into the absorber column (Rao and Rubin, 2002, Wang et al., 2011). The absorber column provides a surface area for the contact of flue gas with the counter flowing lean solvent. The solvent and the CO_2 react through a series of exothermic chemical reactions to produce a rich solvent with CO_2 absorbed. The cleaned flue gas is vented to the atmosphere after water wash to reduce solvent leakage. The rich solvent is then heated through a cross heat exchanger and pumped to the top of the stripper (or regenerator). The solvent is regenerated in the stripper at a pressure slightly above atmospheric pressure (1.5 – 2atm) and using raised temperatures (100-140^oC). The regenerated lean solvent is recycled back to the absorber column

after cooling through the cross heat exchanger (Metz et al., 2005, Wang et al., 2011).

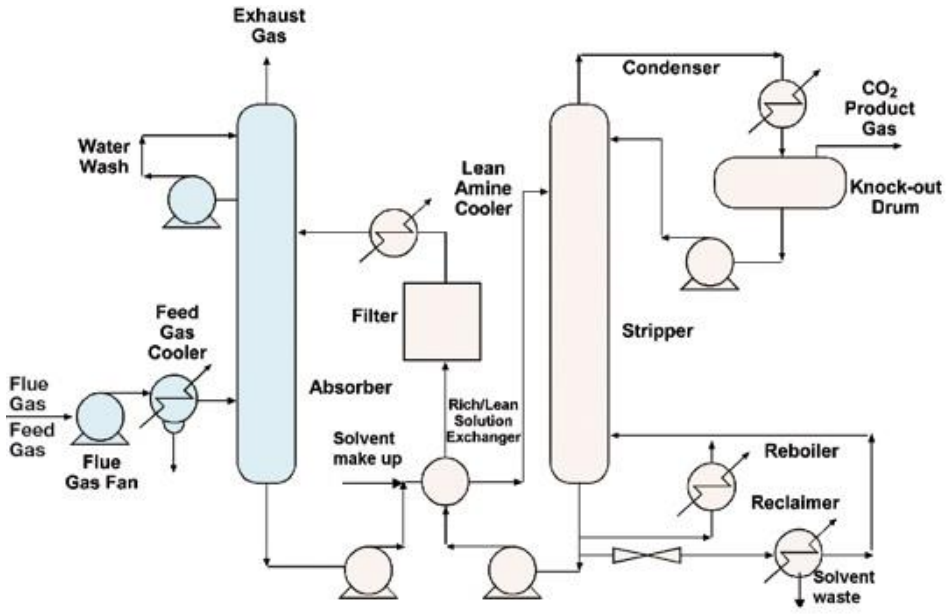

Figure 2-2: Process flow of chemical absorption (Metz et al., 2005)

Wang et al. (2011) has mentioned that the flue gas needs to pre-treated before capture, to remove sulphur dioxide (SO_2) and oxides of nitrogen (NO_x). The presence of these in the flue gas can form heat stable salts with some solvents such as monoethanolamine (MEA). NO_x can be reduced by low NOx designed burners or selective catalytic reduction. SO_2 reduction design requirement is 10ppm according to Wang et al. (2011). Other authors (Singh et al., 2003, Abu-Zahra et al., 2007b, Karimi et al., 2011) have also mentioned this level of SO_2 reduction for efficient capture minimising solvent loss.

The presence of O_2 in the flue gas can increase the rate of corrosion of the equipment according to Wang et al. (2011). It is also mentioned that O_2 present in flue gas can degrade some solvents such as MEA. O_2 levels should be restricted to less than 1ppm, if no corrosion inhibitors are used.

2.1.1 MEA for chemical absorption

Amine solvents can be categorised into primary, secondary and tertiary groups according to the number of hydrogen atoms replaced by alkanol chains. The reaction rates and corrosive characteristics of the solvents differ from one group to the other. The reaction rate is highest for primary amines while tertiary amines are least corrosive. MEA is a primary group amine and has been widely used at commercial scale. It is able to capture CO_2 at low partial pressures. It will be suitable for application to capture from post combustion pulverised coal power plants (Rao and Rubin, 2002). It is mentioned by Metz et al. (2005) that more than 99% CO_2 purity is achievable with 85% or more CO_2 recovery, by applying MEA absorption as a post combustion capture technology.

MEA is proven to achieve high recovery with purity. These are attractive characteristics of the solvent, but the solvent is highly corrosive in the presence of O_2. Flue gas from pulverised coal power stations has approximately 5 mol% O_2 and this would increase the rate of MEA corrosion. MEA which is a primary amine is more corrosive than di-ethanolamine (DEA), a secondary amine. DEA is more corrosive than tri-ethanolamine (TEA), a tertiary amine. Inhibitors should be deployed to prevent corrosion of the solvent. Flue gas should have a minimum of 1.5 vol% O_2 to maintain the activity of the inhibitors (Chapel et al., 1999). Other alternative options to reduce O_2 concentration can involve use of catalytic reactors or controlling of the laminar flame in the burners (Metz et al., 2005, Wang et al., 2011).

Thermal degradation of MEA is common in the stripper and is concentrated within the reboiler of the stripper. The work done by Davis and Rochelle (2009) used 135^{o}C reboiler temperature in their studies and produced a result showing thermal degradation of 2.5 - 6% per week. The paper explained that increase in loading of CO_2 and amine concentration increases the solvent degrading rate. The paper further concluded that thermal degradation of MEA could be reduced if working temperature is less than 110^{o}C.

The formation of thermally stable salts when MEA reacts with NO_x and SO_2 is undesirable and leads to solvent degradation. It is mentioned by Rao and Rubin (2002), that the concentration of SO_2 needs to be limited to approximately 10ppm to reduce solvent loss. SO_2 reduction in flue gas is achieved by flue gas desulphurisation (FGD). The flue gas typically contains 700-2500ppm of SO_2 for pulverised coal-fired plants before FGD. Chapel et al. (1999) mentions, the currently used FGDs for pulverised coal-fired plant will not be able to reduce SO_2 concentration to less than 10ppm. This is because of the high sulphur content found in coal used today. Increasing the CO_2 loading in the liquid phase would reduce SO_2 degradation as explained by Wang et al. (2011). It is mentioned that having more CO_2 available for reaction with MEA would reduce SO_2 and O_2 reactions with the solvent, and therefore reduce the solvent degradation.

NO_2 is the most reactive of all the NO_x present in the flue gas. NO_2 also reacts with MEA to form a thermally stable salt, causing degradation of the solvent. The flue gas NO_2 concentration from a pulverised coal fired power plant is approximately less than 10% of the total NO_x. This means degradation

of MEA due the presence of NO_2 is little compared to SO_2 degradation. NO_2 emission can be controlled by controlling the flame temperatures in the burners (Chapel et al., 1999, Rao and Rubin, 2002).

Other impurities in the flue gas that degrade the solvent and deteriorate the process and equipment are fly ash and soot. Fly ash could cause degradation of MEA through chemical and physical reactions. It can further lead to erosion, crevice corrosion and plugging of the equipment. Power plants are currently equipped with fly ash removals upstream of FGD. For the purpose of capture 99.7% removal of fly ash should be met (Chapel et al., 1999). Soot is present in flue gas from heavier fossil fuels. A stabilised MEA mist is formed with soot. The mist particles are not captured in the water wash zone of the absorber column. The micro-sized MEA mist particles must be captured by using a specialised mist absorber (Chapel et al., 1999).

The energy required for the process is primarily thermal energy, for regeneration of the solvent. Chapel et al. (1999) mentions that 36% of the total overall operating cost is the thermal energy required in the regenerator. The thermal energy which is supplied as steam is in the range of 3.0 – 4.2 GJ/tonne of CO_2 (Chapel et al., 1999, Singh et al., 2003, Alie et al., 2005, Abu-Zahra et al., 2007b). Electricity is consumed by flue gas blowers and solvent pumps, within the capture process. Electricity energy consumption is 0.06 – 0.11 GJ/tonne of CO_2 for post combustion capture from a coal fired power plant, and is within 0.21 – 0.33 GJ/tonne of CO_2 for post combustion capture from a natural gas fired powered plant (Metz et al., 2005). Post capture compression

of CO_2 to a pressure of 110 bar would require approximately 0.4 GJ/tonne of CO_2 (Metz et al., 2005).

Consumption of large amount of thermal energy in the regenerator is influencing the economic viability of the technology. In a study by Blomen et al. (2009) it was concluded that a 15% reduction in thermal energy (3.2MJ/kg CO_2 to 2.7MJ/kg CO_2) would see a process improvement of 20% reduction in capture cost (35-45 to 25-35 euro per tonne of CO_2). The study by the IPCC mentions that the thermal energy consumed is closely linked to the selection of solvents. It has been shown that mixture of amines from different groups, or novel solvent consume less energy to regenerate (Metz et al., 2005). Increasing the concentration of MEA in the solvent can decrease the thermal energy required for regeneration according to Blomen et al. (2009). A 33% increment to the concentration of MEA would reduce thermal energy by 5-8%. An increase in MEA concentration would increase corrosion as seen earlier. Inhibitors can be used to control corrosion of MEA as shown in the ECONAMINE process developed by Fluor Daniel (Metz et al., 2005). Using alternative novel solvents could reduce the thermal energy consumption. Sterically hindered amines developed by Kansai Electric Power Co, have shown to consume less energy with little solvent loss. These novel solvents are in their development phase and are currently too expensive to be implemented.

Capital costs for installation of the absorber and stripper column influences the economic feasibility of the technology. The flow rate of the flue gas determines the sized of the absorber column. Mass flow rate of the CO_2 captured defines the size of the stripper column and post capture compression.

It is mentioned by Metz et al. (2005) that it possible to achieve 80-90% of CO_2 recovery with the technology. Higher recovery would need taller absorption column with higher energy penalties, causing an increase in overall cost. An optimum recovery value needs to be evaluated during design of the technology. Process intensification by enhancing absorption and distillation can reduce capital costs. A rotating packed bed absorption column using the centrifugal force to boost gravity would increase the mass transfer of the solvent. An increased mass transfer would enable efficient reactions and enhance absorption (Wang et al., 2011).

2.2 Membranes

Capturing CO_2 using membranes has been conducted at high CO_2 partial pressures in natural gas processing (Metz et al., 2005). The technology is more suitable for capturing CO_2 from syngas or blast furnace top gas, which have a relatively high CO_2 partial pressure. The membrane technology is simple, compact and easy to operate. Chemical solvents are not used in its original form; therefore the technology is more environmental friendly. The compactness of the technology reduces capital investment. It can be easily scaled up to commercial levels. It also uses minimal equipment with no moving parts. It is very reliable and is flexible with the ability to incorporate new membrane developments (Lie et al., 2007, Ho et al., 2008a).

There are challenges in implementing the membrane technology for CO_2 capture. It requires a clean feed of gas with no particulates or moisture. It is still not proven at a larger scale. It requires high pressurised feed gas, therefore it is energy intensive (Lie et al., 2007). It is mentioned that the flue gas needs

to be compressed to 15-20 bar to provide the required driving force for the separation. This increases the overall cost of capture and is mentioned to be 30% more expensive than capturing CO_2 using amine scrubbing (Ho et al., 2008a). This is for conditions of low CO_2 partial pressure in the flue gas. An increase in CO_2 partial pressure in the flue gas will make it more cost effective than amine scrubbing (Lie et al., 2007).

The most popular membranes used for CO_2 separation are carbon membranes and polymer membranes. For the membrane to be efficient in capturing CO_2, it should have the following properties (Brunetti et al., 2010).

- CO_2 high permeability
- CO_2/N_2 or CO_2/H_2 high selectivity, depending on the feed gas.
- Resistance towards chemical reactions and thermal changes
- Plasticisation resistance
- Cheap to produce into different membrane modules
- Long life
- Cost effective CO_2 capture

It is mentioned by Brunetti et al. (2010) that the membranes available for CO_2 capture do not possess both high permeability and selectivity of CO_2. It was seen that only a few polymer based membranes had selectivity near to 100%, and the permeability on those membranes were low. Development of novel membranes with high permeability and selectivity through cheap

methods could be a driving factor for the technology to be commercialised. The work done by Lie et al. (2007) showed that novel membrane with incorporation of amine (facilitated transport membrane) has shown improvement in permeability and selectivity of CO_2. Other work by Ho et al. (2008a) has considered reducing the compression energy consumed in flue gas compression by using vacuum separation. Using vacuum separation, it was possible to achieve reduction in the overall cost of CO_2 avoidance. It is further mentioned that CO_2 purity was between 50-80% when using vacuum separation. This is not up to the levels of purity achieved by amine scrubbing. Using membranes with very high selectivity and permeability of CO_2 with vacuum separation could reduce cost and reach desired purity.

Another process improvement that is promising is the hybrid solvent/membrane technology. Membranes are employed to provide a high surface area to volume ratio for the contact of solvent and gaseous CO_2. The CO_2 reacts with the solvent and the cleaned gas diffuses out through the membrane. Advantages of this process include low capital investment from compact membranes used, less operational complexity and higher surface area.

In conclusion, membranes look promising and will compete with matured technology such as amine scrubbing, but there is still room for improvement. It is more suitable to be applied as a pre combustion technology. The uncertainties of the membranes reaction with chemicals and heat from flue or syngas is preventing it to be applied for large scale CO_2 separation.

2.3 Adsorption

CO_2 separation by adsorption involves a selective separation of the CO_2 molecules onto a sorbent. Depending on the bond formed between CO_2 and the sorbent the process can be categorised as either chemisorption or physisorption. Covalent strong bond are formed in the process involving chemisorption and it requires more energy for regeneration. Physisorption forms weak bonds and is more easily regenerated. The CO_2 molecules and other gaseous molecules are attracted to the surface of the sorbent through van de Waals forces. Both physisorption and chemisorption are exothermic; more heat is released during chemisorption than physisorption. Adsorption technology for CO_2 capture requires fast separation, therefore physisorption is more popular (Berger and Bhown, 2011).

Adsorption process has been used in CO_2 separation from syngas to produce H_2. The technology has not yet reached commercial scale demonstration of CO_2 capture for sequestration from flue or syngas. Molecular sieves and activated carbon (AC) can be used to adsorb CO_2.

2.3.1 Sorbents – zeolite 13X and activated carbon

Zeolite 13X has shown to have high CO_2/N_2 selectivity with good adsorption capacity. AC adsorption capacity increases with CO_2 partial pressures; at pressures above 1.7 bar AC has higher adsorption capacity than zeolite 13X (Choi et al., 2009). The work done by Chue et al. (1995) concluded that zeolite 13X are better performing sorbents for CO_2 separation when compared with AC. The CO_2 isotherm on zeolite 13X shows recovery of CO2 is achievable at pressures just above atmosphere. This would reduce the cost of

pressurisation the feed gas. Application of vacuum swing adsorption (VSA) or vacuum pressure swing adsorption (VPSA) with zeolite 13X would enable high recovery of CO_2 (Wilcox, 2012). Heat of adsorption of CO_2 on zeolite 13X is comparably more than that of AC, but Chue et al. (1995) mentions that the higher working capacity of zeolite 13X coupled with higher equilibrium selectivity makes zeolite 13X a better sorbent for bulk CO_2 separation.

The work done by Chue et al. (1995) has not incorporated effect of moisture on the sorbent. Wilcox (2012) mentions that water molecules would be more preferably adsorbed onto zeolite 13X than CO_2 by electrostatic forces. Activated carbon is resistant towards water molecules, but Choi et al. (2009) has identified humidity could have a long term detrimental effect on AC. Other impurities include SO_2 and NO_2 found in flue gas. SO_2 can react with adsorption sites on the sorbent, reducing CO_2 adsorption. NO_2 and other oxides of nitrogen have also shown reaction to reduce overall CO_2 adsorption capacity (Zhang et al., 2009a). Using layers of adsorbent to control pre-adsorbing impurities have been proven. It can be used to control and reduce SO_2, NO_2 and water molecules reaching the main CO_2 adsorbing layer (Zhang et al., 2009a).

2.3.2 Regeneration of sorbents

The regeneration of the sorbent involves desorbing the CO_2 on the sorbent. The regenerated sorbent is then used for adsorbing more CO_2. The technology uses cyclic processes to allow continuous adsorption and regeneration. The regeneration can be achieved by either a temperature increase or a pressure decrease. Pressure swing adsorption (PSA) uses higher pressures to adsorb CO_2

onto the sorbent and regenerates it at lower pressures. Desorbing at vacuum pressures is also practised and can be more efficient depending on the sorbent used. Temperature swing adsorption (TSA) uses higher temperatures to regenerate the bed (Thomas and Crittenden, 1998). Regeneration using heat is slower and is unpopular for CO_2 adsorption. TSA is considered to be a more expensive regeneration method and would require intercooling in between regeneration and adsorption (Metz et al., 2005). Hybrid processes using high pressure for adsorption and lower pressure with temperature increase for desorption can be used for CO_2 recovery and have been proven in pilot scale demonstrations (Ishibashi et al., 1996). Others have shown that more than one stage of capture would be required to get CO_2 purity over 95 mol% (Wang et al., 2013)

In adsorption technology the highest percentage of electricity is consumed by compressors/blowers and vacuum pumps. It is mentioned by Metz et al. (2005) that approximately 560 kWh/tCO_2 is consumed by the pumps blowers. This is approximately 21% of the electricity output of a power plant. Process improvements such as pressure equalisation, and waste heat regeneration can reduce the overall energy penalty. Other costs are contributed from installing large number of beds. The sorbents working capacity is low, therefore requiring many beds and stages for separation. Ho et al. (2008b) showed that a hypothetical sorbent with higher level of selectivity and capacity to recover CO_2 can reduce the overall cost by 11-35%. Further work by Gomes and Yee (2002) has shown that lowering the feed gas speed and increasing cyclic time could enhance CO_2 purity and recovery. With an increase in purity and recovery, the number of stages for separation can be reduced, therefore

reducing the overall cost. Conditions representing capture from pulverised coal-fired power plant or steel making produces large volume of flue gas. This requires continuous fast bulk separations.

Overall it can be concluded that adsorption technology is less energy consuming than amine scrubbing. Its continuous cyclic process can be utilised as a retrofit for steel making conditions. There is a requirement to effectively remove impurities before separation and this could be costly (Metz et al., 2005). Novel sorbents with higher working capacity and selectivity could make the technology competitive with matured amine scrubbing.

2.4 Physical Absorption

The technology has been proven to work at high CO_2 partial pressures. It is more suitable for capturing CO_2 from syngas or from processed gas from the water gas shift reaction. It follows Henry's Law to describe solubility of CO_2 onto the solvent. It therefore works at lower temperatures and higher pressures. The solvents used in the technology are organic that can physically absorb CO_2 rather than chemically reacting with it. The solvents are regenerated by lowering the pressure or increasing the temperature. Physical absorption display weak interactions between the solvent and CO_2, unlike amine absorption in which the CO_2 bond with the amine is stronger. Less energy is required to regenerate the solvent using physical absorption (Olajire, 2010, Rackley, 2010).

There are many different processes available that uses physical absorption for acid gas removal in commercial scale. They can be differentiated according

to the solvent used for separation. Selexol and Rectisol process are most popular and have decades of commercial experience in natural gas processing.

Selexol Process uses dimethylether or propylene glycol. Selexol is effective in capturing CO_2 at high pressures and can achieve bulk removal. Selexol absorbs at temperatures of 0-5^{o}C and the regeneration of the solvent can be achieved by lowering pressure or by using air to strip the CO_2 (Rackley, 2010). The solvent is less corrosive therefore equipment can be built with carbon steel, thereby reducing the overall cost. The process has low toxicity and can be operated at low pressure but is more efficient at higher pressures. The Selexol solvent has got a high affinity towards water molecules; therefore flue gas dehydration might be required (Olajire, 2010).

The Rectisol process uses chilled methanol to absorb CO_2 and the process can be configured in many different ways to suit various needs. It operates at very low temperatures -34 to -73^{o}C, increasing the cost of refrigeration. The process is non-corrosive and has high thermal and chemical stability. Equipment can be built with carbon steel, reducing installed cost. The solvent can be easily regenerated by low pressure flashing and does not require thermal heating as in amine scrubbing. Overall the Rectisol process is considered to have a high operating and installation cost due to the need of refrigeration (Olajire, 2010).

Other existing processes that use physical absorption are FLOUR and Morphysorb. The Morphysorb process is a relatively new technology. The FLOUR process uses propylene carbonate as the solvent since it is applied to conditions with high CO_2 partial pressure (> 4 bar). The FLOUR process

involves a higher solvent recirculation, therefore increasing the operational cost. The FLOUR solvent is considered to be expensive. The solvent regeneration can be achieved by lowering the pressure. The CO_2 solubility is high on the FLOUR solvent, therefore has enhanced CO_2 loading (Olajire, 2010).

2.5 Comparison of Separation Technologies

Table 2-1: The four technologies assessed with the design factors

	Chemical Absorption	Adsorption	Membranes	Physical Absorption
Maturity	High	Moderate	Low	High
Capital Cost	High	Moderate	Low	High
Reliability	Solvent loss, material corrosion	Few moving parts, but impurities can defect sorbents	Good if impurities are cleaned	Less corrosive
Recovery of CO_2	High recovery more than 90%	Moderate. 80% achievable with 2 stages	Low, but increases with pressure	High, but water molecules should be removed initially
CO_2 Selectivity	High selectivity, more than 90 mol% purity achievable	Moderate. Zeolite 13X has shown highest selectivity commercially	Low to moderate. Amine modified polymers could show better result	High values achievable at low temperature and high pressures
Operational Cost	Highest out of the four technologies, due to thermal regeneration	Moderate, VPSA is considered cheaper	Moderate to high. Cost rises with high feed pressure	High due to refrigeration
Environment Friendliness	Amine leakage to atmosphere	Very environment friendly	Polymers and carbon based membranes are environment friendly, but amine synthesized are not	Very environment friendly

Table 2-1 summarises the comparative study of this literature survey. It is clear that chemical absorption is the most mature technology. It has been proven in large scale CO_2 capture. There is a good understanding of the effect

of impurities and the performance of different amines. Technical and operational challenges such as corrosion and solvent degradation have been addressed and understood. The technologies impacts on the environment have also been outlined with results from pilot to medium scale projects. Economic evaluations have been studied widely with understanding of the design parameters that control the overall cost of CO_2 avoidance. There are commercial process modelling software like Aspen HYSYS, Aspen Plus and gPROMS that are able to model capturing of CO_2 using amines. Process modelling of chemical absorption has been conducted previously by Singh et al. (2003) and Abu-Zahra et al. (2007b), and the results are agreeing with real world CO_2 capture.

Membranes are the least developed technology of the four. The technology is suitable for capturing CO_2 with high partial pressures. It is still in a lab scale development phase. The process itself is simple and reliable and scaling up should be easy, but it is still not cost effective to be implemented at a large scale. There is very less understanding of the detrimental effects of flue gas impurities on the membranes. Hybrid novel technologies combining membranes with chemical absorption have been proposed. They are promising but are in early stages of development. Research on novel membranes with high CO_2 permeability and selectivity are being conducted globally. A research breakthrough could improve final CO_2 product purity and recovery to match with amine scrubbing. This could open doors for large scale CO_2 capture demonstrations.

Adsorption is also a technology that performs well with higher CO_2 partial pressures. The technology has been proven in large scale but not for CO_2 capture from flue or syngas for the purpose of sequestration. There are few pilot scale level demonstrations (Ishibashi et al., 1996, Wang et al., 2013). The theoretical understanding of the technology has developed throughout the last century. It is considered to have lower operating cost when compared with amine scrubbing. There is good understanding of the effect of impurities in the feed gas. At low CO_2 partial pressures, multiple stages of separation would be required to reach purity matching amine scrubbing. Feed gas pre-treatment such as dehydration and removal of impurities might be required, depending on the choice of sorbent. The two sorbents zeolite 13X and activated carbon are suitable for CO_2 separation, with zeolite 13X performing better at lower partial pressures of CO_2. A cyclic process can achieve continuous bulk removal of CO_2 with regeneration of the beds. Depending on the availability of waste heat, hybrid PTSA process can be more efficient than other processes such as PSA and VPSA.

Physical absorption separation technology has been proven at large scale to remove CO_2 form feed having high CO_2 concentration. The technology uses less energy to regenerate the solvent, because no thermal energy input is required during regeneration. It is less corrosive than amine absorption therefore equipment can be built using carbon steel. Working conditions are at low temperatures and the process performs better at elevated pressure. Depending on the process chosen, the solvent would need to be cooled to very low temperatures; therefore increasing operational cost. Dehumidification of the flue gas might be required depending on the solvent. Selexol process would

be more suitable for CO_2 separation when compared with FLOUR and Rectisol.

2.6 Capture Technologies for Steelmaking

In an integrated steel mill, there are multiple CO_2 emission points. The CO_2 concentration varies from one point to the other, and is between 7-27 vol% (Wiley et al., 2011). The works arising gases (top blast furnace gas, coke oven gas and basic oxygen furnace gas) are combusted in the on-site power station. The CO_2 concentration of the flue gas rising from the on-site power station is approximately 23 vol% (Wiley et al., 2011). If a single point retrofit CO_2 capture technology needs to be applied for the integrated steel mill, a post combustion technology after the power station would give the maximum decarbonisation of the mill. This conclusion is made after assuming no changes are made to the flow of the works arising gases. The flue gas properties of the on-site power station differ to that of a pulverised coal or natural gas fired power station. CO_2 concentration of the flue gas form the on-site power station from a steel mill is higher to that compared to a coal or natural gas fired power station. This higher concentration would make it suitable for separation technologies that are efficient with high CO_2 partial pressure.

Adsorption, membranes and physical absorption are all capable of recovering CO_2 from high CO_2 concentrated feed gas. Membrane technology is the least developed and would have high cost in pressurising the feed gas. Physical absorption is a mature technology but can have high operation costs due to cooling/refrigeration requirement. In conclusion adsorption, with its lower operating costs and medium level of maturity, would be the choice to be

applied for the integrated steel mill. As a benchmark study, chemical absorption will also be analysed in parallel to adsorption and the results will be compared.

2.6.1 Literature survey – chemical absorption for steelmaking

There a few published literature available that analyses CO_2 capture by chemical absorption for conditions of flue gas arising from steel making. The high concentration of CO_2 in the flue gas from steel making raises a question if amine scrubbing will be a suitable technology. Gielen (2003) mentions this in his work, and uses physical absoprtion for CO_2 capture. Gielen (2003) has used Selexol process after a water gas shift reaction, to capture CO_2 from blast furnace top gas. The cost for carbon dioxide captured is mentioned as \$18/tonne of CO_2. Farla et al. (1995) have also conducted a proccess modelling study on CO_2 capture from the blast furnace top gas. They have used post-blast furncace capture using chemical absorption and solvent MDEA (Methyl diethanolamine). The cost of CO_2 capture by Farla et al. (1995) is \$35/tonne of CO_2. The work by Ho et al. (2011) have also investigated a capture from the blast furnace top gas. They concluded that the cost of CO_2 avoidance is equal to \$68/tonne CO_2 using MEA scrubbing. Ho et al. (2011) mentions that the higher cost compared to that of Farla et al. (1995) is because of the exclusion of flue gas pre-treatment in Farla et al. (1995) work. It is also mentioned that Ho et al. (2011) has used CO_2 avoidance cost, where as the other has used CO_2 capture cost. Wiley et al. (2011) analysed different capture points within steelmaking and used MEA scrubbing. In their study it was concluded that the best place to apply a retrofit capture technology, in terms of financial ease, was

the blast furnace. Wiley et al. (2011) mentioned the cost of CO_2 avoidance is approximatley \$65/tonne of CO_2. Applying a CO_2 capture after the in-house power plant will cost approximatley \$71/tonne of CO_2 avoided (Wiley et al., 2011).

Technical analysis for CO_2 capture thorugh chemical absorption for conditions relating to steel making have been conducted through process modelling. Arasto et al. (2013) have modelled using a rate based process modelling software to capture CO_2 from an integrated steel mill. MEA was used as the solvent. They have considered capturing CO_2 from the flue gas arising from the in-house power station and the hot stoves. A 90% capture of CO_2 was achievable with a 50% reduction in the total CO_2 emissions from the steel mill. The reboiler duty was calculated as 3.4 MJ/kg of CO_2. Tobiesen et al. (2007) modelled CO_2 capture using MEA. The process was modelled to capture from the top gas of the blast furnace. The model calculated a reboiler duty of 3.77 MJ/kg CO_2 with 80% recovery.

2.6.1 Literature survey – adsorption for steelmaking

Published studies on large scale CO_2 capture using pressure swing adsorption (PSA) or vacuum swing adsorption (VSA) at high CO_2 concentration are little. Most of the studies are for conditions relating to flue gas from a coal fired or natural gas fired power plant. The study by Ho et al. (2008b) used a short cut mass balance calculation, to model post combustion capture from a coal fired power plant using PSA and VSA. Ho et al. (2008b) concluded that the cost of CO_2 avoidance were \$57/ton CO_2 and \$51/ton CO_2 for PSA and VSA respectively. They were only able to achieve a purity of 48

mol% with a recovery of 85% CO_2 for both sorbents. They used zeolite 13X in both their models.

A study by Wang et al. (2012a) investigated VSA using zeolite 13X in lab scale set up. The CO_2 concentration was 50 vol% in the feed gas. Wang et al. (2012a) was able to attain approximatly 84 vol% purity of CO_2 with a recovery of approximatly 78%.

Wang et al. (2013) conduted a pilot scale study to capture CO_2 from flue gas with CO_2 concnetration of 16 vol%. They used two succesive stages to attain a final CO_2 product purity of 98.8%. They achieved a recovery of 83.7%. The first stage in the lab study used zeolite 13X and the second used activaed carbon.

3 Cost Estimation Methods Used in this Study

An important part of this research was to investigate the economic feasibility of the separation technologies studied. Economic analysis starts with the estimation of installed costs of the equipment. It also includes operating cost per annum, which is made up of fixed and variable costs.

The most accurate way to obtain the installed costs is from the vendors. The second best approach is to use price information of previously purchased similar equipment, and apply it to price the designed equipment. Differences in equipment size, location, conditions of operation etc. might need to be considered when using the second approach (Karimi et al., 2011). An alternative approach is to use to proposed correlations data to calculate individual equipment cost. The latter approach estimate is considered to be ±30% accurate (Sinnott and Towler, 2009).

Process modelling software such as Aspen HYSYS, has an in-built embedded correlation for estimating the capital expenditure cost (CAPEX) and operational cost (OPEX). It is called the Aspen Process Economic Analyser. This research was process modelled on an older version of Aspen HYSYS, which did not include the add-on for economic analysis. This research uses the correlation proposed by Sinnott and Towler (2009) for economic analysis. The correlation would give an initial design phase estimate of the CAPEX and OPEX for CO_2 capture, with an uncertainty of ±30%. It is a reliable correlation because other peer reviewed published literature, such as the work done by Karimi et al. (2011), have used the proposition by Sinnott and Towler (2009).

3.1 Estimating the CAPEX using the Factorial Method

Sinnott and Towler (2009) use a factorial method to estimate the installed costs of the equipment. The correlation of cost estimation is dependent on equation 3-1. C_e is the purchased equipment cost of the equipment on US Gulf Coast basis as of January 2007. The constants a, b and the exponent n is found in the book by Sinnott and Towler (2009), and differs for each different equipment. S is a size parameter that defines the size of the equipment. S needs to be calculated from preliminary design details. The units of S are given in the book by Sinnott and Towler (2009).

Equation 3-1: Equipment purchase cost correlation equation

$$C_e = a + b \times S^n$$

S has a lower and upper limit, and if it falls out of the range equation 3-2 needs to be used to calculate the purchased cost. Equation 3-2 is the one sixth rule equation.

Equation 3-2: One sixth rule equation

$$C_2 = C_1 \times \left(\frac{S2}{S1}\right)^{0.6}$$

After calculating the equipment cost, C_e, it needs to be altered to match current year and location. The chemical engineering plant's cost index (CEPCI) published in the Chemical Engineering Journal annually can be used to calculate the cost for year 2013 (CEPCI., 2013). Location factors are given

in the book by Sinnott and Towler (2009), and they can be used to calculate equipment cost for specific location equipment is to be installed.

Table 3-1: CEPCI index (CEPCI., 2013)

Chemical Engineering Cost Index (CEPCI)	
2007	525
2013	567.3

Table 3-2: Location factor (Sinnott and Towler, 2009)

Location factor	
US Gulf Coast	1.0
UK	1.02

After calculating the installed cost, C_e, for the desired year and location equation 3-3 can be used to calculate the installed equipment cost. The factors in equation 3-3 contribute towards installing the equipment (Sinnott and Towler, 2009).

Equation 3-3: Factorial equation for calculating installed cost of equipment

$$C = \sum_{i=1}^{i=M} C_{e,i,CS} \left[(1 + fp)fm + (fer + fel + fi + fc + fs + fl)\right]$$

C = installed cost of equipment

$C_{e,\,i,\,CS}$ = purchased equipment cost of equipment i in carbon steel

M = total number of pieces of equipment

fp = installation factor for piping

fer = installation factor for equipment erection

fel = installation factor for electrical work

fi = installation factor for instrumentation and control

fc = installation factor for civil engineering work

fs = installation factor for structures and building

fl = installation factor for lagging, insulation or paint

fm = material factor if a material different to carbon steel is used

After calculating the installed cost for all equipment, the summation of all equipment cost will give the total installed cost of the plant. It is also known as the total installed ISBL (Inside Battery Limit) CAPEX.

An OSBL (Outside Battery Limit) investment includes contingency, design and engineering, changes to infrastructure etc. An OSBL cost needs to be added to the installed ISBL CAPEX, to calculate the total fixed capital investment (FCI) required. As part of this research it was assumed that OSBL cost is 60% of the fixed ISBL cost from information provided in the book by Sinnott and Towler (2009).

3.1.1 Annual fixed capital investment

It is common to calculate the FCI annual payments ($FCI_{annual)}$ or the amortized annual cost to understand annual cost of CO_2 capture or avoidance. The FCI_{annual} is given by equation 3-4. It is divided into equal annual payments

throughout the life of the plant in production. In equation 3-4, n represents the plant life time and i represents the interest rate at which the FCI is paid off (Sinnott and Towler, 2009, Karimi et al., 2011). This research has assumed a lifetime of 30 years for the capture and compression unit. It is also assumed that the interest rate is 10% for all calculations.

Equation 3-4: Fixed capital investment per annum calculation equation

$$FCI_{annual} = \frac{FCI}{((1+i)^n - 1) \Big/ (i \times (1+i)^n)}$$

3.2 Estimating OPEX made of Variable and Fixed Cost

In addition to the fixed capital investment calculated per annum, operation expenditure (OPEX) needs to be calculated per annum to understand the overall cost of CO_2 capture. OPEX is made of fixed and variable cost, and calculation of them varies in published literature (Singh et al., 2003, Abu-Zahra et al., 2007a, Sinnott and Towler, 2009).

3.2.1 Fixed operating cost

The fixed operating cost (FOC) per annum is required throughout the year to achieve continuous production. It can be made of different factors; the most common factors are outlined in Table 3-3. The estimation of the cost of each factor was adapted from (Sinnott and Towler, 2009) and (Karimi et al., 2011).

Table 3-3: Fixed operating cost factors

Costing Factor	Calculation
Labour Cost (LC)	$60000/year per shift position
Supervision Cost (SC)	25% of LC
Direct Salary Overhead (DSO)	40% of (SC+LC)
Maintenance (M)	3% of Total ISBL Fixed CAPEX
Property Taxes and Insurance	1% of Total ISBL Fixed CAPEX
Property Insurance	1% of Total ISBL Fixed CAPEX
General Plant Overhead	40% of (LC+SC+DSO+M)
Environmental Charges	1% of Fixed Capital Investment (FCI)

The direct salary overhead factor of the FOC includes payroll taxes, health insurances and other employee benefits. The general plant overhead factor includes R&D, IT, human resources, legal and finance.

3.2.2 Variable operating cost

The variable operating cost (VOC) is made up of costs due to using utilities and raw materials. It also includes waste disposal and landfill costs. As the name states, these costs are dependent on the yearly production. If annual production increases these costs will increase, and if it decreases the VOC will also decrease. The price of utilities, raw materials and waste disposal will also influence VOC. The price of utilities, raw materials etc. varies throughout the year and therefore the VOC will also change accordingly.

3.3 Estimating Cost of CO_2 Capture

After calculating the annual VOC and FOC, the total operating cost (TOC) per annum can be calculated. TOC is the summation of VOC and FOC. The total annual capture cost (TACC) is given by equation 3-5, and is the summation of FCI_{annual} and TOC.

Equation 3-5: Calculation of TACC from FCI_{annual} and TOC

$$\textbf{\textit{Total Annual Capture Cost (TACC)}} = FCI_{annual} + Total\ Operating\ Cost\ (TOC)$$

After calculating the TACC it can be used to calculate Cost of CO_2 capture and Cost of CO_2 avoidance given by equations 3-6 and 3-7 respectively.

Equation 3-6: Calculating cost of CO_2 capture

$$Cost\ of\ CO_2\ Capture\ (^{\$}/_{tonne\ of\ CO_2}) = \frac{Total\ Annual\ Capture\ Cost(\$)}{CO2\ captured\ annually\ (tonne)}$$

Equation 3-7: Calculating cost of CO_2 avoidance

$$Cost\ of\ CO_2\ avoided\ (^{\$}/_{tonne\ of\ CO_2}) = \frac{Total\ Annual\ Capture\ Cost(\$)}{Net\ CO2\ captured\ (tonne) annually}$$

It is good to understand both the cost of CO_2 capture and the cost of CO_2 avoidance. Cost of CO_2 capture does not include emissions emitted during the capture process, therefore would not be able to reflect the correct price for decarbonising. The cost of CO_2 avoidance includes the indirect CO_2 emissions from consuming utilities and raw materials. It uses the net amount of CO_2 captured as shown in equation 3-7. The net amount of CO_2 captured includes all the emission of CO_2 during the capture process (direct or indirect). Consumables such as steam and electricity are assumed to be obtained from outside the ISBL limits. They will emit CO_2 when and where they are produced. The net CO_2 captured removes these indirect emissions from the total amount of CO_2 captured.

4 CO_2 Mapping – Integrated Steel mill

The conventional method of steel making involves iron ore reduction (iron making) in the blast furnace (BF) to produce hot metal iron, followed by steelmaking using a basic oxygen furnace (BOF) (WSA, 2014b). Approximately 2.2 tonnes of CO_2 is emitted per tonne of steel produced through the conventional route of steel making (Orth et al., 2007). Carbon in the form of coke is used primarily for iron ore reduction in the BF. H_2 and charcoal from biomass, can also be used to covert iron ore into hot metal iron (WSA, 2014a).

A percentage breakdown of the CO_2 emissions arising from a conventional steel mill following the BF+BOS route for manufacturing steel is shown in Figure 4-1. Approximately 70% of the induced carbon, during the conventional steel making process flows through the BF (Kuramochi et al., 2012). 87% of CO_2 emissions are contributed from coke ovens, sinter plant and BF (Orth et al., 2007). It is to be noted that Figure 4-1 does not consider consuming the process arising gases, through an in-house power station to generate electricity and heat. The CO_2 emissions are therefore dedicated to each process within iron and steel making. In an integrated steel mill the low grade fuel will be consumed in the in-house power station as explained in Chapter 1 of this thesis.

Governments of industrialised nations have proposed at least 50% CO_2 emission reduction from current levels by the year 2050 (Allwood and Cullen, 2009). In response to this World Steel Association, representing the steel industry globally, has encouraged steel companies to decarbonise steel making (WSA, 2014a). Ultra low carbon steel making (ULCOS) is a consortium in

Europe made up of major steel companies, academia and engineering partners. ULCOS is investigating implementation of breakthrough technologies, which can decarbonise steelmaking. The technologies proposed by ULCOS are expected to achieve more than 50% CO_2 emission reduction but would require major changes to the BF (Kuramochi et al., 2012). As an alternative decarbonising route, carbon capture can be applied at other point sources in a steel mill as a retrofit technology. Mapping the CO_2 emissions arising from the steel mill studied in this research would give a clearer understanding of its different points of emissions.

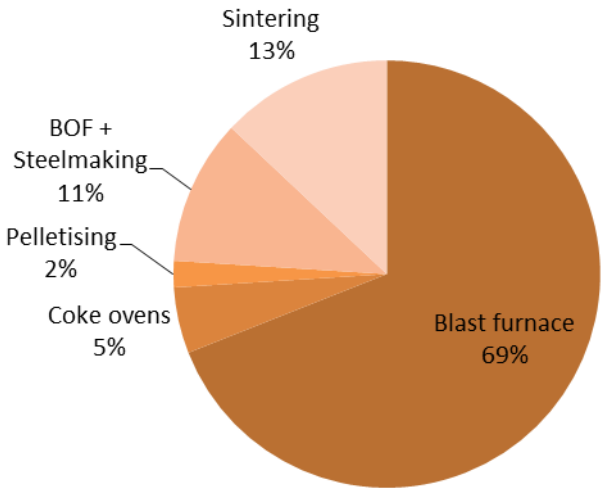

Figure 4-1: Breakdown of CO_2 emissions from a conventional steel mill (blast furnace + BOF route) (Orth et al., 2007)

4.1 CO_2 Emissions from the Studied Steel Mill

The steel mill chosen is located in the North East of England and is within close proximity to the North Sea. The captured CO_2 will be transported through pipelines to a deep-sea storage point in the North Sea. In similarity to the work done by Wiley et al. (2011) the steel mill in this study uses BF top gas, coke

oven gas and BOF gas as low grade fuel in other parts of the mill to generate electricity and heat. TATA Steel's in house CO_2 monitoring software was used to analyse CO_2 emissions from different point sources within the mill. The software is continuously updated with CO_2 emissions data. The CO_2 emission data for year 2011 was used as part of this research. Only direct CO_2 emissions were analysed as part of this research. Indirect emissions from consuming utilities or raw materials that emitted CO_2 is not included as part of this study. A similar approach has been used by Wiley et al. (2011).

The BF, coke oven and BOF gases are commonly known as works arising gases (WAGs), and have a fuel value as shown in Table 4-1. The composition of each WAGs is different, therefore the overall calorific value differs from one gas to the other. The flue gas from the sintering unit has zero calorific value, and is released to the atmosphere as a common practice (Wiley et al., 2011). The other three WAGs are combusted at different locations to generate electricity or heat as required.

Table 4-1: Compositions and calorific values of the works arising gases from steel mill, which are as used fuel adapted from (Arasto et al., 2013)

	Compositions (%vol)		
	Blast Furnace Gas	*Coke Oven Gas*	*Basic Oxygen Furnace Gas*
CO	23.1	5.1	69.0
CO_2	22.1	0.0	16.0
CH_4	0.0	23.1	0.0
C_2H_4	0.0	2.0	0.0
C_2H_6	0.0	0.7	0.0
O_2	0.2	0.0	0.0
H_2	5.3	57.9	0.0
N_2	45.1	6.9	15
H_2O	4.2	4.3	0.0
Heating Value (MJ/kg)	2.6	38.4	6.4

According to Arasto et al. (2013) the coke oven gas has the highest heating value of 38.4 MJ/kg, as shown in Table 4-1. Hydrocarbons and H_2 are present in the coke oven gas, therefore giving it the highest heating value. The BF gas has the highest concentration of CO_2 and has a heating value of 2.6 MJ/kg, due to the presence of CO and H_2. The BOF gas is highly concentrated with CO. Secondary steelmaking in the BOF unit converts carbon in the hot metal iron from the blast furnace into CO by blowing pure O_2, and therefore the BOF gas has a high concentration of CO (Kuramochi et al., 2012).

Figure 4-2 is the flow diagram of the WAGs flowing throughout the studied steel mill. WAGs are used as fuel in the sintering unit, secondary steelmaking, central power station and turbo blower house. Central power station (CPS) uses the fuel to generate electricity to use within the steel mill. The turbo blower house (TBH) uses the fuel to power the blowers that supplies air to the blast furnaces.

The largest volume of WAGs flowing through the mill is the BF gas. It has the lowest heating value of all three, but approximately 62% of it is used in the CPS and TBH. The blast furnace stoves use approximately 32% of the BF gas. Coke oven gas with the highest heating value of the all three WAGs, is used throughout the mill. Approximately 33% of the coke oven gas is used for firing coke ovens during coke production. The CPS and TBH uses approximately 30% of coke oven gas as shown in Figure 4-2. With a large volume of WAGs flowing into the CPS and TBH a carbon capture technology after these two units can recover a high volume of CO_2 emitted. In the steel mill studied the

two units (CPS and TBH) are within close proximity to one another so additional complexity of pumping flue gas will be reduced.

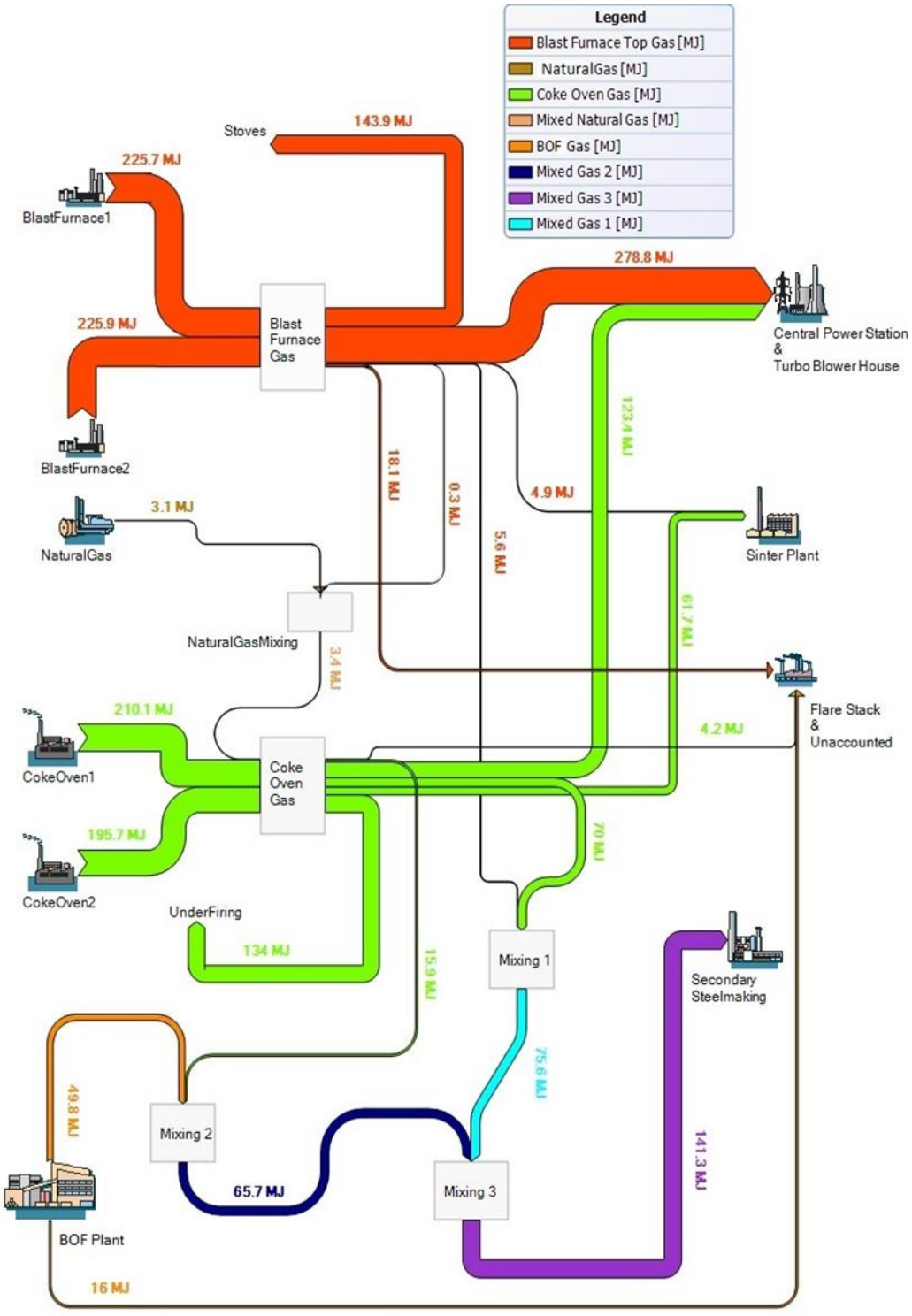

Figure 4-2: Sankey diagram of energy flow of works arising gases within the steel mill (based on measured data from studied steel mill)

Figure 4-3 shows the percentages of CO_2 emissions from different units within the steel mill. It is to be noted that this mill has not got an iron ore pelletising unit. A pelletising unit can also contribute to a large percentage CO_2 emissions as shown in Figure 4-1. It is clear from Figure 4-3 that point source CO_2 emission from this mill is highest from the CPS and TBH. Approximately 44% of CO_2 is emitted to the atmosphere by these two units. This clearly indicates that the best location for a post-combustion capture technology for the steel mill is after the CPS and the TBH. Applying a capture unit with the ability to recover 80% or more of CO_2 from the flue gas, will ensure 35% or more CO_2 emission reduction from the steel mill.

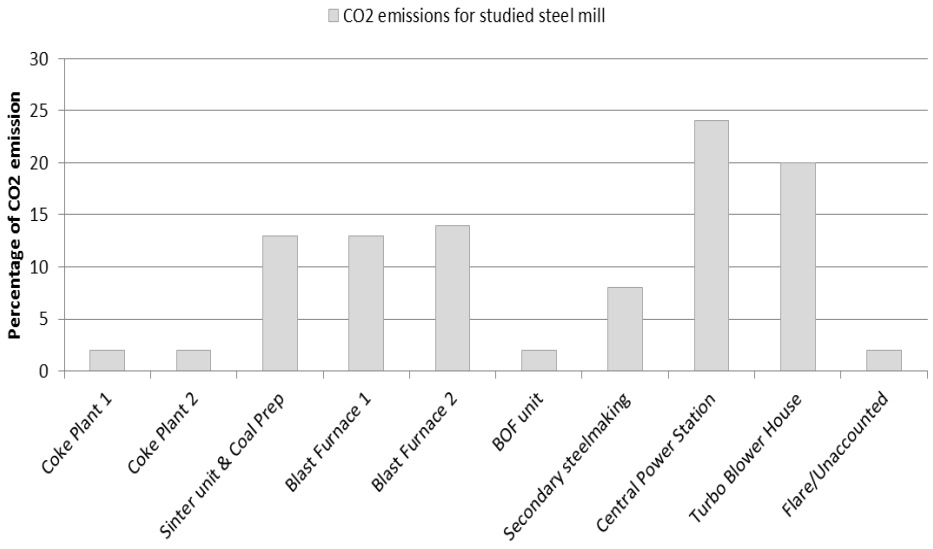

Figure 4-3: Percentage breakdown of point source CO_2 emissions from each unit in the studied steel mill (based on measured data)

4.1.1 Flue gas conditions from CPS and TBH

The studied steel mill has a total of nine boilers within the CPS and TBH units. The conditions and the compositions of the flue gas from these boilers are shown in Table 4-2. The flue gas from TBH boiler 3 has a lower flow rate

when compared with the rest. At the time of investigation TBH boiler 3 was under maintenance, therefore had a low output. The other boilers were working at full capacity. It can be seen from Table 4-2 that the flue gases from WAGs combustion at the CPS and TBH have a CO_2 concentration in the range of 23-25 vol%. These values are higher than that of pulverised coal fired or natural gas fired power plant (Singh et al., 2003). Chemical absorption using amines have been mentioned by Metz et al. (2005) to perform well at lower CO_2 partial pressures conditions in the flue gas. Membranes and adsorption technologies are more efficient at higher CO_2 partial pressures in flue gas (Chue et al., 1995, Ho et al., 2008a). The CO_2 composition in the flue gas from CPS and TBH makes it attractive to be used with adsorption or membrane separation technologies.

Table 4-2: Flue gas conditions and compositions from CPS and TBH (based on measured data from studied steel mill)

Boilers	*Flue gas temperature (°C)*	*Stack flow (Nm^3/h) (wet)*	*Compositions (%vol)*			
			O_2	*CO_2*	*N_2*	*H_2O*
CPS boiler 1	186	110000	1.2	23.1	67.7	8.0
CPS boiler 2	194	118000	1.6	22.4	68.0	7.9
CPS boiler 3	192	56300	2.9	26.2	68.1	2.81
TBH boiler 1	160	33100	3.56	25.6	68.5	2.35
TBH boiler 2	176	36300	4.99	23.5	69.3	2.13
TBH boiler 3	83.4	1260	9.85	3.95	73.7	12.5
TBH boiler 4	145	39000	5.27	22.3	69.6	2.8
TBH boiler 5	148	66800	4.79	24.1	69.2	1.96
TBH boiler 6	154	66300	4.46	24.5	69.0	2.02

When all the nine boilers of the CPS and TBH are working at full capacity the flue gas from them will have CO_2 concentration between 23-25 vol%. The temperatures of the flue gas will be in the range of 145-186^oC. Mixing these

gases and sending it to a single point post combustion capture unit would be feasible. A single point capture unit would have minimised operational cost and lower installation capital cost, then having multiple capture units.

4.2 Conclusions from the CO_2 Mapping Study

The largest two contributors to CO_2 emissions at the studied mill are from CPS and TBH. The emissions from these two units are approximately 44% of the total direct CO_2 emissions from the steel mill. Approximately 27% of the direct CO_2 emissions are emitted from the stoves of the blast furnace. The sinter and coal preparation are approximately 13% of the total direct CO_2 emissions.

Capturing and sequestering CO_2 using a post combustion unit after the CPS and TBH, can decarbonise the mill by at least 35% (assuming the capture unit can recover 80% of the CO_2 from CPS and TBH). To reach the target of 50% reduction to current emission levels by the year 2050, novel technologies proposed by ULCOS needs to be applied (Allwood and Cullen, 2009, Kuramochi et al., 2012, WSA, 2014a). The technologies proposed (Top gas recycling BF (TGRBF) and HIsarna) are in its developing phase. TGRBF and would require changes to existing BF and HIsarna would require changes to the conventional method of steel making (Kuramochi et al., 2012). Post combustion capture using a retrofit separation technology after CPS and TBH could act as an interim solution to reduce CO_2 emissions per tonne of steel produced. If HIsarna and TGRBF become techno-economically feasible it would replace the retrofit capture from TBH and CPS to achieve the target of 50% reduction in CO_2 emissions.

The concentration of CO_2 in the flue gas from CPS and TBH is approximately 23-25 vol%. Adsorption separation technology is suitable for these conditions (Metz et al., 2005). It needs to be technically analysed if more than one stage would be required to reach CO_2 product purity to meet transport by pipeline standard.

5 CO_2 Capture Using Chemical Absorption – Benchmark Study

As seen in Chapter 4, the flue gas from the Central Power Station (CPS) and Turbo Blower House (TBH) has a CO_2 concentration in between 23-25 vol%. This value is higher than that of flue gas from a pulverised coal fired power plant (13-15 vol%) or natural gas fired power plant (3-5 vol%) (Singh et al., 2003). Metz et al. (2005) has mentioned that amine scrubbing CO_2 separation is more suitable in capturing from low CO_2 concentrated flue gas.

Amine scrubbing is the most matured technology for CO_2 separation that has been proven at commercial scales. There is a good understanding on the technical feasibility of the technology. There is commercial software that is able to model large scale CO_2 separations from flue gas (Chapel et al., 1999, Singh et al., 2003, Metz et al., 2005). As part of this research, a benchmark study using MEA for CO_2 scrubbing was conducted. The results from the benchmark study will be compared with capture using adsorption, to evaluate the performance of using adsorption.

5.1 Process Modelling Chemical Absorption

The two film theory proposed by Whitman (1923) can be used to describe the mechanism of chemical absorption. Molecules are transferred in the bulk of the phases through convection current. It is assumed that there is a gas-liquid interface separating the bulk gas and bulk liquid. On either side of the interface is a stationary thin film for both gas and liquid, as shown in Figure 5-1. All mass transfer resistance is assumed to be concentrated in these two films. CO_2 from the bulk gas is transported by molecular diffusion through the gas film.

CO_2 then enters the liquid film and is absorbed by the liquid. Chemical reactions binding the amine with CO_2 starts in the liquid film. The bounded CO_2 diffuses through the liquid film onto the bulk liquid (Sinnott and Towler, 2009, Khan et al., 2011, Liu, 2014). It is mentioned by Khan et al. (2011) that the CO_2 reactions with amines is a fast reaction, therefore all chemical reactions takes place in the liquid film.

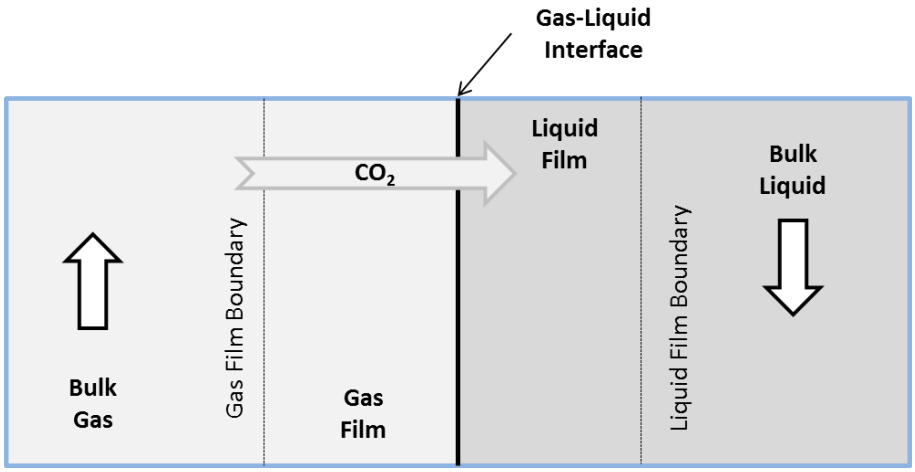

Figure 5-1: Two film model representing CO_2 mas transfer from gas to aqueous solution during chemical absorption (adapted from (Khan et al., 2011)

The chemical reactions occurring in the liquid film are complex and can be represented by five main reversible reactions for primary and secondary amines. Mono-ethanolamine (MEA) aqueous solution reaction with CO_2 is represented by equation 5-1 to 5-5 (Liu et al., 1999a, Abu-Zahra et al., 2007b).

Equation 5-1: Ionisation of water

$$H_2O \leftrightarrow H^+ + OH^-$$

Equation 5-2: Dissociation of CO_2

$$CO_2 + H_2O \leftrightarrow H^+ + HCO_3^-$$

Equation 5-3: Dissociation of MEA

$$MEA + H_2O \leftrightarrow MEAH^+ + OH^-$$

Equation 5-4: Formation of carbamate

$$MEA + CO_2 \leftrightarrow (C_2H_6NO)COO^- + H^+$$

Equation 5-5: Disassociation of carbamate

$$HCO_3^- \leftrightarrow H^+ + CO_3^-$$

Study of thermodynamic models to represent the vapour-liquid equilibrium (VLE) of aqueous amine with sour gas has gained large interest in the past two decades. A model by Kent and Eisenberg has been widely used and is considered as one of the simplest model (Kohl and Nielsen, 1997). The model assumes that the activity and fugacity coefficient are equal to one, considering ideal solutions and ideal gases. Equilibrium constants of equations 5-3 and 5-4 representing the amine disassociation and carbamate formation are regressed on experimental data of carbon dioxide solubility on aqueous amine solution. Similar set of equations could be used for secondary amines; the MEA in equations 5-3 and 5-4 needs to be replaced by the secondary amine. Kent-Eisenberg model is capable of modelling primary amines, secondary amines or a mixture of them both (Kohl and Nielsen, 1997).

Even though the Kent-Eisenberg thermodynamic model is simple, there have been discrepancies found in VLE calculations when the model is used for very low or very high acid gas loadings. There is also an argument that the

model does not represent accurately, the mixed acid gas systems (Kohl and Nielsen, 1997).

Further works to improve the Kent-Eisenberg model have been conducted in the past. Details of such works can be found elsewhere (Kohl and Nielsen, 1997). Li-Mather thermodynamic model is considered to be a better representation of the vapour-liquid equilibrium than the Kent-Eisenberg model. It is defined in a similar way to the Kent-Eisenberg model but the activity and fugacity coefficient is not equated to one (non-ideal solvent and gas) (Kohl and Nielsen, 1997).

Commercially available chemical process modelling software is equipped with thermodynamic models to represent sour gas and aqueous amine solvent vapour liquid equilibrium. Aspen HYSYS is an example of one such software. Kent-Eisenberg and Li-Mather models are integrated within the software to represent equilibrium based separation of acid gas using alkanolamines (Øi, 2010).

A more complex model to represent VLE is the model presented by Austgen et al. (1989), which uses electrolyte-NRTL model (electrolyte-Non Random Two Liquid). The model accounts for rigorous chemical equilibria and mass balance. In this model the activity coefficient in the liquid phase are represented by electrolyte-NRTL. The fugacity coefficients in the vapour phase are represented by Redlich-Kwong equation of state. This model is particularly suitable for rate based separation (Liu et al., 1999a).

The mass and heat transfer in absorber and distillation column can be represented by equilibrium based separation or non-equilibrium separation

(rate based) model. The equilibrium model assumes vapour-liquid equilibrium at each stage of the column. The variation from equilibrium is represented by tray efficiency for tray columns or height equivalent of a theoretical plate (HETP) for packed columns. The rate based simulation model assumes that vapour-liquid interface only occurs in the interface (Liu, 2014). In considers material and energy balance, mass and energy transfer rate, vapour-liquid equilibrium and liquid phase reactions with reaction rates for each stage (Liu et al., 1999a). A more detailed comparison of the equilibrium and rate based separation model is given elsewhere (Taylor et al., 2003). Rate based separation is considered to be thermodynamically rigorous, but a more accurate representation of sour gas and aqueous solvent chemical absorption according to Taylor et al. (2003). Currently available versions of Aspen HYSYS have the capability of modelling rate based separation in columns. This research was modelled with an older version of Aspen HYSYS, which did not have the add-on for modelling columns using rate based separations.

The study by Zhang et al. (2009b) compared rate based separation and equilibrium based separation by mimicking a pilot scale demonstration. It was concluded that the rate based model performs better than the equilibrium based model. Others like (Øi, 2010) have shown that the equilibrium model is also capable of representing practically sound results with correct utilisation of steady state operational unit. This research is an investigation by comparing different CO_2 capture technologies to fit into steel making. An equilibrium based separation model, therefore would be sufficient for this study. If further sensitive analysis is to be conducted, a rate based model is recommended. Li-

Mather thermodynamic model was chosen for modelling CO_2 absorption due to its better accuracy than the Kent-Eisenberg model.

5.2 Modelling CO_2 Capture using Aspen HYSYS

CO_2 capture using chemical absorption involves two main process; absorption and desorption. Desorption is sometimes termed as regeneration. The absorption process involves acid gas diffusion followed by the chemical reactions with the alkanolamines. The absorber column is operated in a counter-current manner where the CO_2 rich flue gas is fed to the bottom of the column, while the lean amine enters the column from the top. The temperature profile in the column is influenced by; heat transfer between the two phases due to the temperature difference, heat released from chemical reactions, heat released or absorbed due to water condensation or vaporisation, and heat released to the atmosphere (Kvamsdal et al., 2009). When CO_2 is absorbed by the down-coming solvent, the solvent's temperature will increase. This will cause water to be vaporised. Towards the top of the column, the colder solvent will cause water to condensate (Kvamsdal and Rochelle, 2008). The resulting temperature profile will show a distinct temperature bulge. It is mentioned by Kvamsdal and Rochelle (2008) that the temperature bulge is commonly located near to the column midpoint. The regenerating process involves regeneration of the solvent by splitting the CO_2 from it. This is an energy intense endothermic process. The energy is supplied to the stripper column as steam generated by a re-boiler. A simple illustration of the chemical absorption flowsheet is shown in Figure 5-2.

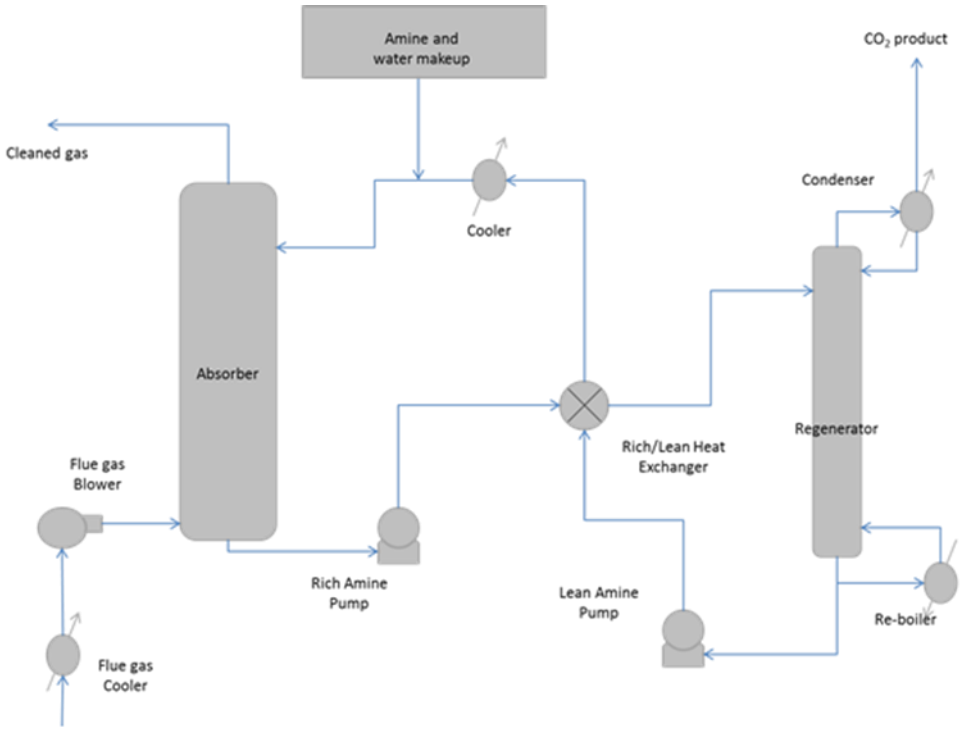

Figure 5-2: Chemical absorption simple flow sheet (adapted from (Øi, 2007))

The pre-treated flue gas is cooled and blown into the bottom of the absorber column. The rising up flue gas interacts with the counter flowing solvent, which has been recycled back to absorber column through the top of the absorber column. The decarbonised gas leaves the absorber through the top of the absorber. In reality a water wash would be incorporated to the top of the absorber column to reduce amine slippage. The rich amine stream, which contains the absorbed CO_2, is pumped through the heat exchanger to the regenerator by the rich amine pump. An additional pump between the heat exchanger and regenerator column might be needed, depending on the height of the column.

The rich amine enters the regeneration column at one of the top stages and is heated by the steam generated by the re-boiler. The vaporised portion of the rich amine is directed towards the condenser. The condenser is a reflux

condenser, in which the condensate is returned back to the top of the regenerator. The lean amine stream, which has lost most of its CO_2, leaves the regenerator column through the bottom end.

The lean amine stream is then pumped across the heat exchanger. The heat exchanger provides the surface area for heat exchange from the lean amine stream to the rich amine stream. Heating of the rich amine stream before it enters the regenerator column using the cross heat exchanger, is energy efficient. A minimum temperature approach of $10^{o}C$ was set when modelling in Aspen HYSYS with accordance to work done by Fisher et al. (2005). The lean amine exiting the heat exchanger is cooled down further and is mixed with make-up amine and water. There is amine slippage with the decarbonised gas and amines would be lost due to salt formation and oxidation. The cleaned gas and CO_2 product stream would contain a small percentage of water. Loss of amines and water requires continuous make-up streams, which is mixed with the lean amine before it is recycled back to the absorber.

5.2.1 Process modelling CO_2 capture using ASPEN HYSYS

The literature (Øi, 2007) was used as a reference to set-up a model of chemical absorption in HYSYS. Initially it was necessary to build a model for chemical absorption and validate the results against published data. The paper by Tobiesen et al. (2007) published by SINTEF was used for validation. SINTEF is a research organisation with expertise in research into chemical absorption. The work by Tobiesen et al. (2007) has considered CO_2 capture from blast furnace (BF) top gas, and used SINTEF's own coded software for

modelling CO_2 capture. Tobiesen et al. (2007) has considered two scenarios for CO_2 capture; top gas from a conventional BF and top gas from a nitrogen free BF. The nitrogen free BF produces a top gas richer in CO_2 and carbon monoxide. It also contains lesser amount of nitrogen. The model representing the conventional BF was replicated in Aspen HYSYS and the obtained results were compared with the work by Tobiesen et al. (2007).

5.2.1.1 Model setup in Aspen HYSYS to replicate SINTEF study

The BF top gas specifications mentioned by Tobiesen et al. (2007) is shown Table 5-1. There are two models mentioned in the paper; one a simple absorber column and the other has an inter-cooler to increase absorption. The simple, one absorber model was used for validation. The tray sizing utility available in Aspen HYSYS was used to model packed columns in similar to the work by Tobiesen et al. (2007).

Table 5-1: BF top gas compositions and conditions from SINTEF study (Tobiesen et al., 2007)

Pressure (bar)	1.43				
Temperature (^{0}C)	55				
Flow rate (kg/h)	4.819×10^5				
Mole (%)	N_2 + Ar	CO_2	CO	H_2	H_2O
	43.62	20.47	20.47	4.46	10.98

The design requirements of the capture unit are mentioned in Table 5-2. It is to be noted that the thermodynamic model in Aspen HYSYS does not incorporate chemical reactions of carbon monoxide with alkanolamines, but physical absorption would cause carbon monoxide to diffuse onto the solvent. This could result in carbon monoxide slippage through the top of the

regenerator column. Only a small quantity of carbon monoxide is lost due to physical absorption, therefore the second design requirement was ignored when modelling in Aspen HYSYS. The full completed flowsheet in Aspen HYSYS is shown in Figure 5-3.

Table 5-2: Design requirements of SINTEF model (Tobiesen et al., 2007)

CO_2 slippage in decarbonised gas	<10% mole
CO recovery in decarbonised gas	85% mole

Tobiesen et al. (2007) mentions that the absorber and regenerator columns are packed with Intalox Metal Tower Packing (IMTP) 50mm. Aspen HYSYS contain a library of packing materials in its directory. The closest match to one mentioned in the paper is the Intalox Saddles (Metal) 2 inch (Perry's) packing material (HYSYS, 2007). The absorber and regenerator were therefore filled with Intalox Saddles (Metal) 2 inch (Perry's) in the model created in Aspen HYSYS. SINTEF mentions of use of mono-ethanolamine (MEA) aqueous solvent with 30% in mass of the amine. Aspen HYSYS allows simulating with conditions of 1-29% mass of MEA in the solvent; therefore the simulations were conducted with MEA 29% mass in the HYSYS model.

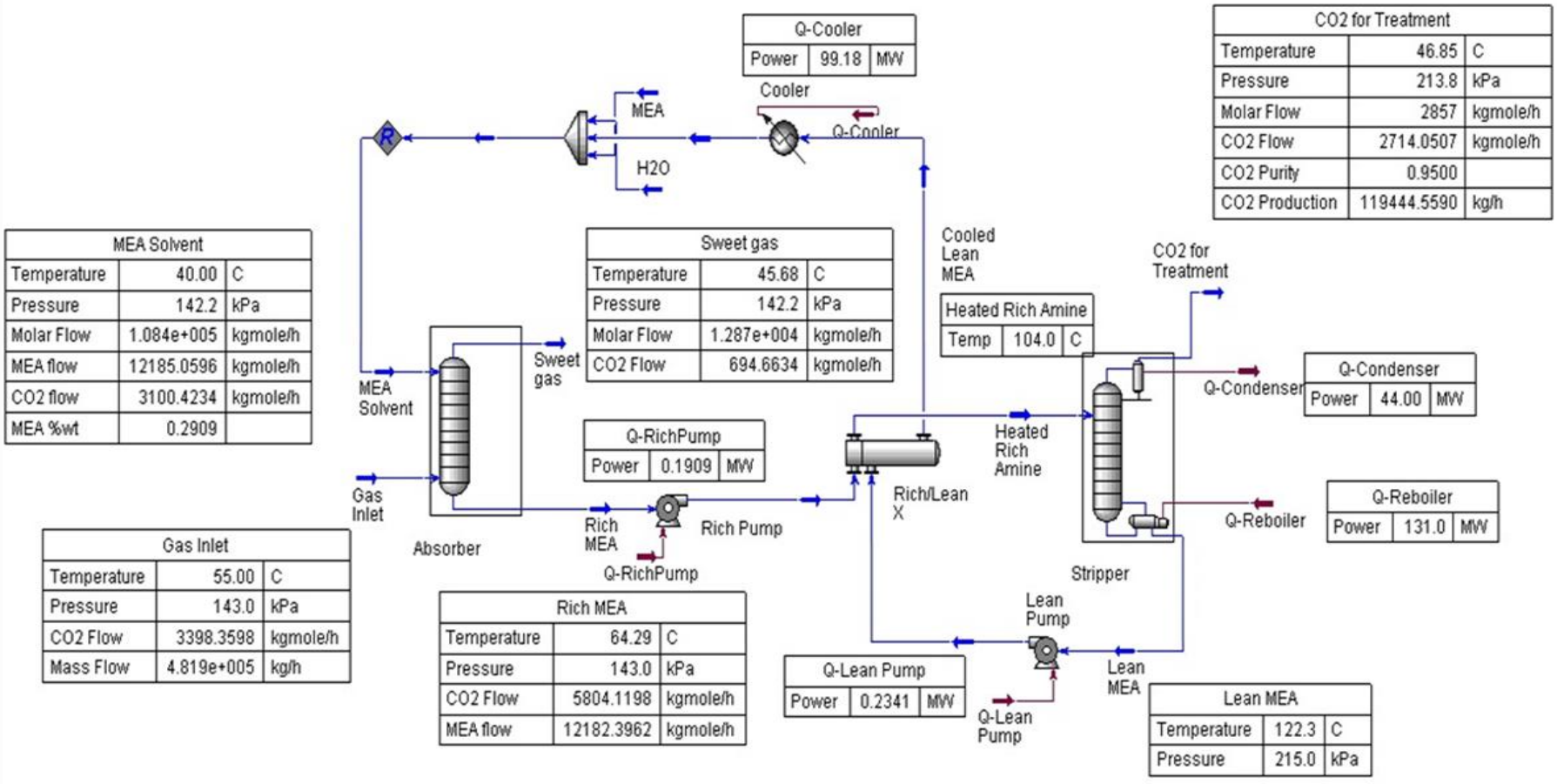

Figure 5-3: Flowsheet in Aspen HYSYS representing SINTEF chemical absorption model

5.2.1.2 Results and discussion of the SINTEF model validation

The converged simulation in ASPEN HYSYS using the thermodynamic model Li-Mather was compared with results mentioned by SINTEF. Table 5-3 summarises the comparison between them. Aspen HYSYS has got an in-built tray sizing utility, which is capable of sizing converged packed or trayed columns. A converged column in HYSYS can be modelled in the tray sizing utility to calculate the pressure drop, column diameter and column height. The design parameter, flooding percentage for the column needs to be entered into the tray sizing utility. The Sherwood-Leva-Eckert (SLE) general pressure drop correlation is used by the tray sizing utility, to calculate the column pressure drop and cross sectional area. Further details of the correlation and procedure to calculate pressure drop and cross sectional area can be found elsewhere (Kister et al., 2007). The packing factor and the HETP (height equivalent to theoretical plate) for different packing material are obtained from vendors and are in-built with HYSYS (HYSYS, 2007). These values are then used to calculate the column height, diameter and pressure drop.

Aspen HYSYS was simulated with design criteria of 80% capture giving a CO_2 production of approximately 120,000 kg/h. The regenerator was set with a design criterion to work with steam at about 122^{o}C. A temperature approach of 10^{o}C was set for the rich lean cross heat exchanger. The sizings of the columns were performed using a flooding design criterion of 60% maximum flooding in one stage of the columns.

Table 5-3: Summary of the comparative study between SINTEF model and HYSYS model

Simulation with MEA	SINTEF 30%wt MEA	HYSYS 29%wt MEA
%CO_2 removed	80.0	79.9
CO_2 production (kg/h)	119470	119445
Steam cons. (MJ/kg CO_2)	3.77	3.95
Liquid circulation (m^3/ton CO_2)	16.53	20.78
Absorber Performance		
Lean loading (mol CO_2/mol MEA)	0.21	0.25
Rich loading (mol CO_2/mol MEA)	0.48	0.48
Liquid load (m^3/m^2h))	51.4	67.4
Diameter (m)	7.0	7.5
Liquid outlet temp (^oC)	75.6	64.3
Gas outlet temp (^oC)	50.6	45.7
Max column liquid temp (^oC)	100.3	66.8
Desorber Performance		
Diameter (m)	5.7	5.8
Reboiler temp (^oC)	122.2	122.3

Table 5-3 compares the results obtained from the Aspen HYSYS model with the SINTEF model. The model in ASPEN HYSYS is able to recover 79.9% of CO_2 from the flue gas. When compared with the SINTEF model this is 0.13% less. CO_2 production is also less by 0.02%, for the model in Aspen HYSYS. The rich loading for both models are equal to 0.48 mol CO_2/mol MEA. The model in HYSYS is showing an increase of 4.77% steam consumption when compared with SINTEF.

HYSYS is calculating a higher reboiler duty than SINTEF. This is due to the outlet temperature of rich amine from the absorber column. According to SINTEF the rich amine is exiting the absorber at a temperature 15% more than that calculated by HYSYS. There is no information about the temperature approach of the cross heat exchanger used by the SINTEF model (Tobiesen et al., 2007). If assumed that the temperature approach is 10^oC for the SINTEF model, to match the temperature approach set in HYSYS. The SINTEF model

will have a rich amine entering the regenerator column at a comparatively higher temperature to that of the model in HYSYS. In HYSYS the rich amine enters the regenerator column at 104^{o}C, and SINTEF will have a temperature higher than 104^{o}C for the rich amine when it enters the regenerator column. This will allow the model by SINTEF to have a lower reboiler duty (lesser volume of steam) than the model by HYSYS.

The lean loading is lower in the model representing SINTEF, when compared with HYSYS. It is to be noted that in the SINTEF uses MEA mass of 30% in the solvent. The HYSYS model uses MEA mass of 29% in the solvent. This discrepancy will mean that the HYSYS model will have a solvent with a larger concentration of water. This would also mean that lean loading will be lower in the case of the SINTEF model when compared with the HYSYS model. The comparatively higher lean loading within HYSYS would result a higher liquid loading and circulation on the absorber column. This can be observed in Table 5-3. The relatively higher liquid loading on the absorber column would require an absorber with a larger diameter as shown in Table 5-3.

The conclusions from the comparative study shows that the model in Aspen HYSYS can be adjusted to achieve the required CO_2 capture rate and recovery, with an increase of 4.77% steam consumption in the regenerator. Solvent lean loading in HYSYS is lower than that of SINTEF. The variation of the MEA concentration in the solvent for the two models can give different lean loadings. HYSYS is showing an increased liquid circulation throughout the flowsheet, due to the higher concentration of water in the solvent. A higher

liquid load on the absorber column would require more surface area for solvent gas contact. This would require a larger diameter for the absorber column. To understand and investigate the discrepancy in heat of absorption in HYSYS a basic calorimeter experiment needs to be modelled and compared with published data.

5.2.1.3 Investigating the heat of absorption in HYSYS

As explained in the previous section, there is a discrepancy in the heat of absorption calculated by Aspen HYSYS and the model published by SINTEF. The exothermic reactions occurring during the absorption process disperses heat. It is necessary for thermodynamic models to represent the heat dissipated accurately, since a costly input of heat is supplied in the regenerator column to reverse the reactions. As a further investigation, a model was created to replicate experiment conducted using calorimeter to study the heat of absorption.

According to the stoichiometry for MEA-carbon dioxide absorption, half a mole of CO_2 is absorbed by one mole of MEA. The literature by Mathonat et al. (1997) mentions that this limit could be exceeded if physical absorption and hydrolysis is considered. Physical absorption and hydrolysis is small when compared to the chemical reactive absorption. It is therefore expected for the heat of absorption to reduce once the saturation stoichiometry is reached.

A model in HYSYS was setup to represent the experimental set-up of the work done by Mathonat et al. (1997) and Kim and Svendsen (2007). Figure 5-4 shows the schematic for the model set-up in HYSYS. The inlet temperature and pressure were set to 40^{o}C and 2MPa respectively, to copy experimental

conditions. An absorber unit with one stage was set to represent the reaction calorimeter. The Li-Mather thermodynamic model was used in the absorber column. The adaptive damper in HYSYS column solver was activated to overcome problems with convergence.

The experiments conducted by Kim and Svendsen (2007) and Mathonat et al. (1997) measures the change in enthalpy due to absorption using a reaction calorimeter. Change in enthalpy (ΔH_{abs}) can represent the heat dispersed due to chemical absorption if the system is assumed isothermal. In order to calculate the enthalpy change, the absolute enthalpies of all the streams mentioned in Figure 5-4 needs to be obtained from HYSYS. It is complicated to obtain the absolute enthalpies of the streams through Aspen HYSYS since it had different offset references for each component (HYSYS, 2007). The offset references are confidential data and is not accessible. A modified model with coolers was set-up to obtain heat duties in outlet streams. Figure 5-5 shows the modified model flowsheet in HYSYS. The cooler duties were then used to calculate the change in enthalpy, using equation 5-6.

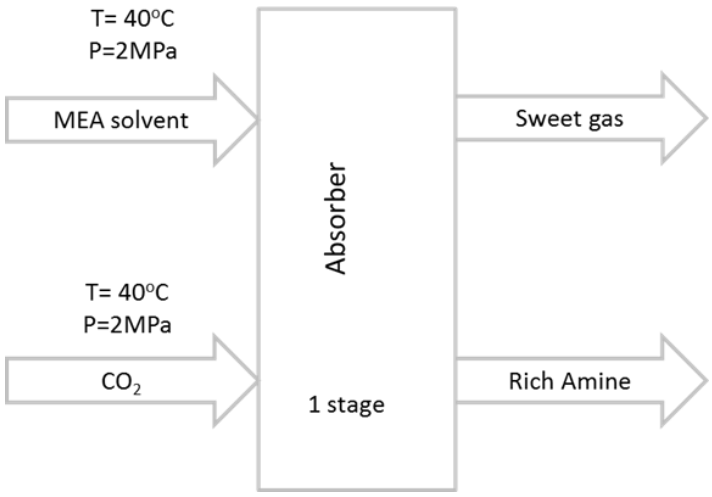

Figure 5-4: Schematic of the calorimeter experiment setup in HYSYS

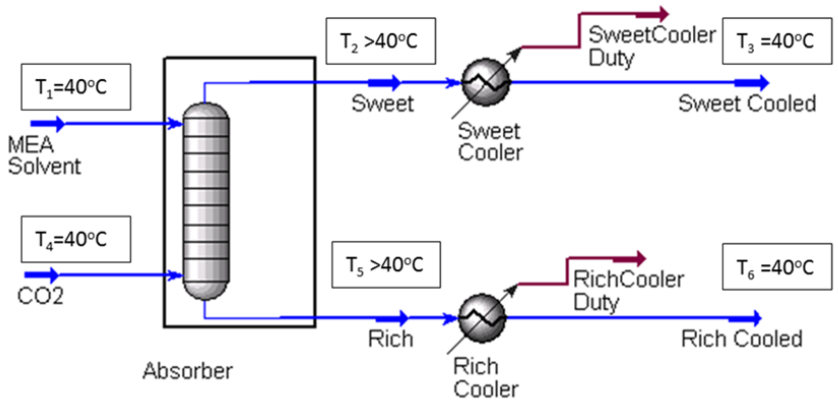

Figure 5-5: Modified flowsheet in HYSYS to calculate change in enthalpy

Equation 5-6: Change in enthalpy due to heat of absorption

$$\Delta H_{abs} = \frac{Sweet\ Cooler\ Duty + Rich\ Cooler\ Duty}{Molar\ flow\ of\ CO2\ absorbed}$$

It is mentioned by Aresta (2003) that the heat of reaction of carbon dioxide with MEA is approximately -84.46kJ per kmol of CO_2 absorbed. The calculated results of heat of absorption from HYSYS were compared with published experimental results from (Kim and Svendsen, 2007). Figure 5-6 is a comparative graph of the results obtained. It is clear from the graph that once the stoichiometric saturation point is reached there is dramatic reduction in enthalpy change for the calorimeter experiment. This drop in ΔH_{abs} is not shown in the HYSYS model.

It is clear from the enthalpy study that the Li-Mather model in HYSYS is a good approximation for MEA-CO_2 absorption for the leading loading below 0.5. The model is not capable of representing for higher inlet loadings since it does not incorporate saturation of solvent. The data representing Figure 5-6 is attached to the Appendix.

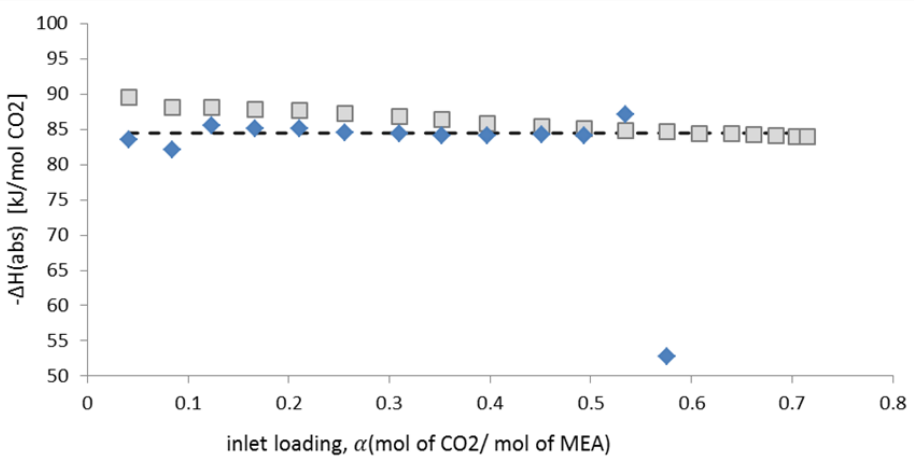

Figure 5-6: Comparison of change in enthalpy for MEA-CO_2 absorption with published experimental results (□) Aspen HYSYS; (◊) published experimental results (Kim and Svendsen, 2007) (-) textbook (Aresta, 2003)

5.3 CO_2 Capture from CPS and TBH using Chemical Absorption

It was concluded from Chapter 4 that approximately 44% of total direct CO_2 emissions of the studied steel mill are emitted to the atmosphere through the flue gas of the CPS and TBH. This research is investigating the techno-economic performance of CO_2 separation technologies suitable for conditions representing post combustion capture from the flue gas of CPS and TBH. As a benchmark study amine chemical absorption using MEA, was modelled in HYSYS. CO_2 separation using MEA chemical absorption has been proven in large scale, and there is vast knowledge on the challenges with technology (Chapel et al., 1999, Metz et al., 2005). Process modelling the separation process with economic evaluation has been widely studied, and the final results obtained are similar to results from real world capture using MEA (Singh et al., 2003, Abu-Zahra et al., 2007b, Abu-Zahra et al., 2007a)

5.3.1 Technical evaluation of MEA chemical absorption on HYSYS for CPS and TBH

The inside boundary limit (ISBL) enclosing the units investigated in this research is shown in Figure 5-7. This is a comparative study investigating the most suitable CO_2 separation than can be applied for the CPS and TBH of the studied mill. Flue gas pre-treatment and the desulphurisation unit have not been modelled as part of this study. It is assumed that the flue gas from the CPS and TBH are cleaned off from particulates, SO_2 and NO_2 to the relevant recommended values mentioned by Chapel et al. (1999) and Rao and Rubin (2002). With the above assumption the ISBL was drawn to include the capture and post-capture compression units as shown in Figure 5-7.

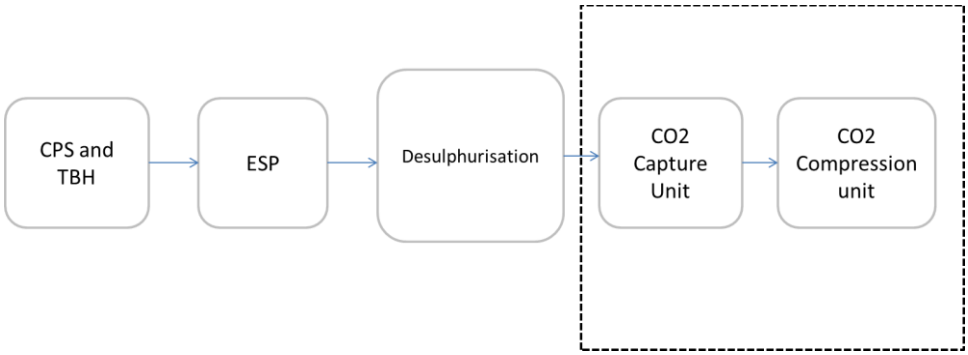

Figure 5-7: ISBL boundary line enclosing the units investigated in this research

The flue gas from the CPS and TBH goes through an electrostatic precipitator (ESP) to get the particulates removed. It then enters the desulphurisation unit, where the flue gas is desulphurised to have less than 10ppm SO_2 concentration (Chapel et al., 1999). The flue gas then exits the desulphurisation unit and is assumed to have a temperature of 50^{o}C and atmospheric pressure. The 10ppm level of desulphurisation would allow lessened degradation of the solvent and enhance absorption in the column

(Chapel et al., 1999). The flue gas from the desulphurisation unit is blown to a pressure of 110 kPa and cooled to a temperature of 50.4^{o}C and enters the absorber column. The flow diagram of the units within the ISBL is shown in Figure 5-8.

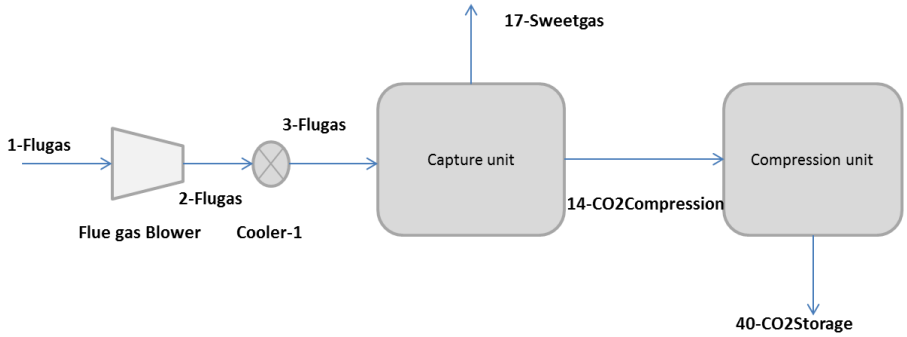

Figure 5-8: Flow diagram inside the ISBL boundary for chemical absorption post combustion capture

5.3.1.1 Modelling and assessment of the capture unit

The capture unit was setup on HYSYS with a similar layout to the flowsheet shown in Figure 5-3. The flowsheet in Figure 5-9 details the model of the capture with names for equipment and streams. A water wash was modelled separately to ensure that the decarbonised gas has less than 3 ppm amine leakage (Karimi et al., 2011). In real-world scenario the water wash would be incorporated on to the top of the absorber column. It is also to be noted that the model in Figure 5-9 is in its simplest form to understand techno-economic feasibility. If it is to be implemented onto the industrial site more pumps would be required throughout the flowsheet, to overcome pressure drops and to pump the solvents/utilities to higher elevations.

The flue gas enters the ISBL boundary through the stream *1-Flue Gas* from the desulphurisation unit. It is blown to higher pressure by the Flue Gas Blower

and is cooled by Cooler-1, before it enters the absorber column through the stream *3-Flue Gas*. The stream *3-Flue Gas* enters the absorber column and is contacted with the recycled solvent *12-Amine Mixed*. The streams *13-Cleaned Gas* and 14 *CO_2 for Compression* are the outlet streams of the capture unit, they are sent for water wash and compression units respectively. The streams *10-H_2O Makeup* and *11-Amine Makeup* are additional inlet streams contributing to the loss of water and amine through the top of the absorber and regenerator column. Detailed conditions and compositions of the streams with in the capture unit are mentioned in Table 5-4.

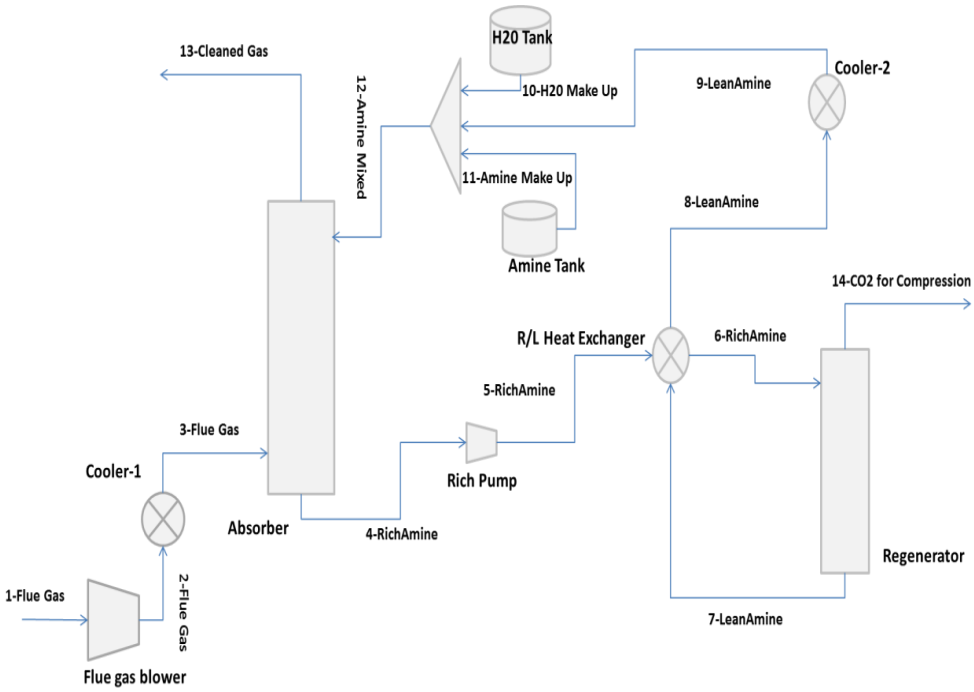

Figure 5-9: Detailed flowsheet of MEA chemical absorption capture unit

It is assumed that water for cooling, make-up and water wash is obtained from an existing source on-site at 20^{o}C. Cooler-1, cooler-2 and the condenser of the regenerator were modelled as shell and tube heat exchangers that used water as the cooling utility. The re-boiler of regenerator column was modelled

as a kettle re-boiler, which used low pressure steam as the heating utility. It was also assumed that steam at 500 kPa pressure is generated on-site to be used for the capture process.

Table 5-4: Conditions and compositions of the streams in the capture unit (compositions in mole fraction)

Stream Name	Pressure (kPa)	Temp (°C)	Mass flow (kg/h)	CO2	N2	H20	O2	MEA
1-Flue Gas	101.3	50.0	7.51×10^5	0.24	0.68	0.05	0.03	0.0
2-Flue Gas	110.5	59.9	7.51×10^5	0.24	0.68	0.05	0.03	0.0
3-Flue Gas	110.0	50.4	7.51×10^5	0.24	0.68	0.05	0.03	0.0
4-RichAmine	107.0	54.0	3.93×10^6	0.06	0.0	0.83	0.0	0.11
5-RichAmine	262.0	54.1	3.93×10^6	0.06	0.0	0.83	0.0	0.11
6-RichAmine	212.0	104.0	3.93×10^6	0.06	0.0	0.83	0.0	0.11
7-LeanAmine	215.0	123.3	3.71×10^6	0.03	0.0	0.86	0.0	0.12
8-LeanAmine	152.0	64.5	3.71×10^6	0.03	0.0	0.86	0.0	0.12
9-LeanAmine	101.0	40.0	3.71×10^6	0.03	0.0	0.86	0.0	0.12
10-H20MakeUp	101.0	40.0	5.84×10^4	0.0	0.0	1.0	0.0	0.0
11-AmineMakeUp	101.0	40.0	1132.0	0.0	0.0	0.0	0.0	1.0
12-AmineMixed	101.0	40.0	3.77×10^6	0.03	0.0	0.86	0.0	0.12
13-CleanedGas	101.0	61.4	5.93×10^5	0.04	0.74	0.19	0.03	0.0
14-CO2Compression	212.0	46.6	2.19×10^5	0.95	0.0	0.05	0.0	0.0

A design threshold of 85% or more recovery and purity of 95% or more in mole of carbon dioxide in stream *14-CO_2 for Compression* was set as design target. This was achievable with the model with a total absorber volume of 1252 m^3 and a total regenerator volume of 601m^3. The capture unit was modelled to have four columns each for absorption and regeneration. As an initial assumption it proposed that the absorber and stripper columns are

manufactured by third party on-site, therefore reducing problems with logistics. The performance of the capture unit is summarised in Table 5-5.

Table 5-5: Summary of the performance of chemical absorption capture unit

Capture Unit Performance	
%CO2 removed	85.71
CO2 production (kg/h)	214000
CO2 purity (mole%)	95
Steam cons. (MJ/kgCO2)	3.45
Liquid circulation (m3/ton CO2)	17.80
Absorber	
Lean loading (mole CO_2/mole MEA)	0.228
Rich loading (mole CO_2/mole MEA)	0.494
Liquid load (m3/m2h)	35.77
Diameter (m)	5.71
Packed height (m)	10.38
Pressure change (kPa)	3.94
Liquid outlet temp (^{0}C)	60.69
Gas outlet temp (^{0}C)	54.73
Max column temp (^{0}C)	80.04
Maximum flooding (%)	59.74
Internal	Structured metal packing
Number of columns	4
Regenerator	
Diameter (m)	3.73
Packed height (m)	13.71
Maximum flooding (%)	58.85
Pressure change (kPa)	2.86
Re-boiler temperature (^{0}C)	123.3
Reflux ratio	1.00
Internal	Structured metal packing
Number of columns	4

5.3.1.1.1 Modelling the water wash for the absorber column

The cleaned gas (sweet gas), *13-CleanedGas,* is further processed through a water wash to remove the MEA before it is released to the environment. It is mentioned by Karimi et al. (2011) that the cleaned gas should have less than 3ppm amines according to environmental good practice. Munasinghe (2011) has showed, through process modelling, that if the sweet gas could be cooled to temperatures less than 60^{o}C through a water wash, the vaporised amines could be reclaimed. Using this design factor, a water wash column was modelled for the sweet gas *13-flue gas.*

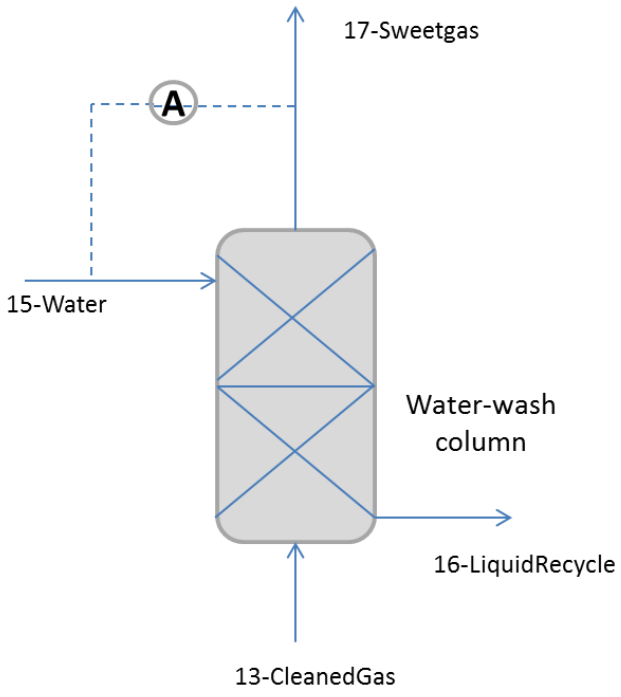

Figure 5-10: Flowsheet of water wash column

To achieve a temperature of less than 60^{o}C an adjuster was used in HYSYS to control the inlet flow rate of the water for the water wash as shown in Figure 5-10. The stream *13-CleanGas* from the top outlet of the absorber contains approximately 800ppm of MEA, which needs to be reduced to less than 3ppm.

This was achievable with a water flow rate of approximately 37.8tonne/h. The final overhead vapour, *16-Sweetgas,* is the final stream released to atmosphere had 2.99 ppm MEA. The details of the streams within the water wash are shown in Table 5-6. The water wash column was modelled as absorption column to understand the sizing and water requirement. It was assumed that there is no significant pressure drop across the column. The column was modelled to have two sections and had internal structured metal packing.

Table 5-6: Conditions and compositions of the streams within the water wash section

				Mole fraction				
Stream Name	Pressure (kPa)	Temp (°C)	Mass flow (kg/h)	CO2	N2	H20	O2	MEA
15-Water	101.3	40.0	$3.78x10^5$	0.0	0.0	1.0	0.0	0.0
16-LiquidRecylce	101.8	58.6	$3.89x10^5$	0.0	0.0	0.97	0.0	0.03
17-Sweetgas	101.8	58.1	$5.89x10^5$	0.04	0.75	0.18	0.03	0.0

The design properties of the water wash was calculated using the tray sizing utility in HYSYS. To achieve the required solvent recovery, the water wash column needed to have a diameter of 7.6 m and height of 1.83 m. This allowed the process to achieve less than 3 ppm solvent leakage in the sweet gas with a maximum flooding of less than 40%.

CAPEX costing of the water wash was not calculated separately. It was assumed that the water wash would be combined with the absorber column as demonstrated by the patent (Mimura et al., 2008) and the work published by Munasinghe (2011). This meant that the final height of the absorber packed column was 1.83 m more than the value shown in Table 5-5.

5.3.1.2 Modelling and assessment of the compression unit

The stream *14-CO2Compression* enters the compression unit with a pressure of 212 kPa and a temperature of 46.5^{o}C. It is in vapour phase and requires to be converted into dense liquid at high pressure suitable for transport. A method proposed used by Karimi et al. (2011) to achieve final pressure of $1.1x10^{4}$ kPa in a two stage process was used. The first stage compresses the inlet stream with a series of compressors. The maximum pressure ratio in each compressor was set as 2; this therefore required a seven stage compression to reach $0.75x10^{4}$ kPa. The first six compressors were set at a pressure ratio of 2 and the seventh used a lower pressure ratio. Inter-stage coolers were required, to cool the gas to 30^{o}C in between the compressors. The critical temperature of CO_2 is 31.1^{o}C and critical pressure is $0.74x10^{4}$ kPa (Karimi et al., 2011). The second stage pumps the CO_2 product stream to a dense liquid at 30^{o}C and pressure of $1.1x10^{4}$ kPa. The schematic for the compression unit is shown in Figure 5-11. The final CO_2 stream can be transported by pipelines to designated storage point. The final product stream properties and compositions are illustrated in Table 5-7. It is to be noted that the *40-CO2Storage* stream increases in CO_2 mole purity by approximately 5%, when compared to the inlet stream into the compression unit (14-CO2Compression). This is because the inlet stream had a percentage of steam, which was condensed in the first stage of the compression unit. The condensed steam was removed gradually in between the compressors.

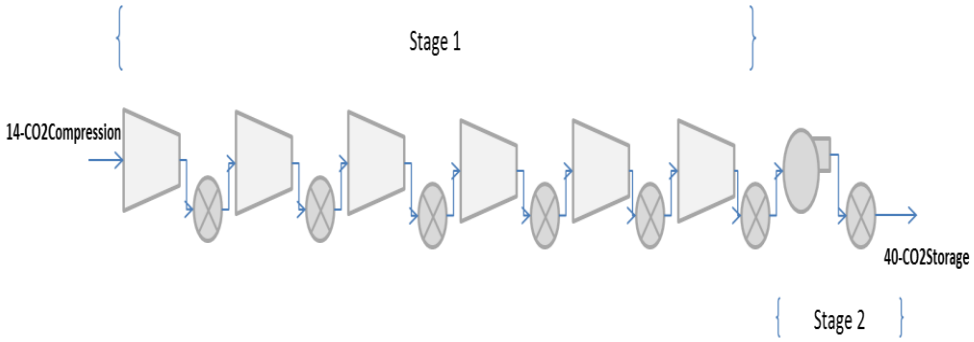

Figure 5-11: Multi-section compression followed by pumping in the compression unit

Table 5-7: Stream conditions and compositions of the final CO_2 product stream (compositions in mol fraction)

Stream Name	Pressure (MPa)	Temp (°C)	Mass flow (kg/h)	CO2	N2	H20	O2	MEA
40-CO2Storage	11.0	30.0	2.14×10^5	0.99	0.0	0.01	0.0	0.0

5.3.2 Economic evaluation of MEA absorption on HYSYS for CPS and TBH

Economic analysis of the benchmark study was evaluated using the equations given in Chapter 3. All costs were calculated in US dollars.

5.3.2.1 CAPEX analysis

The equipment mentioned in Figure 5-9 were cost estimated individually using equations 3-1 to 3-3. Detailed parameters used for each equipment is mentioned in Appendix, while a summary of each equipment costing is mentioned in Table 5-8. The total installed cost for the units in the base case is $64.34 million. The offsite cost (OSBL) includes offsite work, design and engineering and contingency and is estimated as 60% of the total installed cost according to Sinnott and Towler (2009). This results in a fixed capital investment (FCI) requirement of $102.95 million.

The life-span of the capture unit and compression unit is assumed to be 30 years. If the FCI will be paid out annually though out the life-span of the plant, equation 3-4 can be used to calculate the annual fixed capital investment (FCI_{annual}). The FCI_{annual} is $10.92 million to pay for 30 years.

Table 5-8: Fixed Capital Investment for the equipment in benchmark study using MEA scrubbing

Equipment	*Cost($M)*
Compression Unit	30.7
Absorber	11.0
Regenerator	6.00
Rich/Lean Heat Exchanger	4.58
Flue gas blower	3.12
Lean Amine Cooler	2.8
Regenerator – reboiler	1.94
MEA start-up	1.68
Regenerator – condenser	0.97
Water Tank	0.59
Rich Amine Pump	0.49
Flue gas cooler	0.31
Amine tank	0.12
Water start-up	0.001
Total Installed ISBL CAPEX	64.34
OSBL Factor	1.60
Fixed Capital Investment (FCI)	102.95

5.3.2.2 OPEX analysis

The total operating cost per annum (TOC) is equal to the sum of variable operating cost (VOC) and Fixed Operating Cost (FOC).

5.3.2.2.1 Variable operating cost

It is assumed that the site is operational for a total of 8000 hours per annum to ensure more than 90% operation throughout the year. The main five variable operation costs are

- Degradation and evaporation of solvent
- Electricity cost
- Steam cost
- Cooling water makeup treatment cost
- Waste disposal cost

The MEA degradation is equal to 1.5kg of MEA per tonne of CO_2 in the flue gas according to Abu-Zahra et al. (2007b). In addition to degradation some of the solvent is lost through the top of the absorber column. The total loss of MEA annually is calculated as 3025 tonnes by HYSYS. The cost of MEA is assumed as $1500/tonne MEA (Karimi et al., 2011). Therefore the annual cost of MEA replacement is equal to $4.54 million.

Electricity is consumed by pumps, blowers and the compression unit. The total power consumed in the benchmark model is equal to 19.32MW (obtained from HYSYS). The plant is operated for a total of 8000 hours per annum. Therefore the total consumption of electricity is 1.55×10^8kWh. Sinnott and

Towler (2009) has mentioned that the average price for wholesale electricity is equal to $0.07 per kWh, therefore the total cost of electricity consumption per annum is equal to $ 10.9 million.

Steam at 0.6 MPa pressure and 160^{o}C is required by the re-boiler of the regenerator. It costs $8.9/tonne of steam at this quality to be produced (Sinnott and Towler, 2009). The total steam used annually is equal to 2.8 x10^{6} tonnes. Therefore the total cost of steam used is equal to $24.92 million per annum.

The cooling water makeup and treatment cost is mentioned as approximately $0.0042/tonne of water circulated (Sinnott and Towler, 2009). The base case circulates 1.751x10^{7} kg/h of water. Therefore the total annual cost for cooling water make-up and treatment is equal to $0.59 million.

The disposal of degraded solvents is assumed to be sent to the landfills and the cost for this is mentioned by Sinnott and Towler (2009) as approximately $50/tonne. The total loss of solvent annually due to degradation is equal to 2990 tonnes. The cost of waste disposal to landfill therefore is equal to $0.15 million per annum.

Table 5-9: Variable operating cost annually for benchmark model using MEA

VOC annually	Cost ($M)
Electricity usage	10.9
Steam consumption	10.4
Degrading and loss of solvent	4.54
Cooling water	0.59
Waste to landfill	0.15
Total VOC	26.58

The total VOC per annum is equal to $41.08 million. Individual VOC with their cost and the total VOC is summarised in Table 5-9.

5.3.2.2.2 Fixed operating cost (FOC)

The factors contributing towards the overall FOC per annum is mentioned in Table 3-3. The labour cost is estimated by calculating the number shifts required for operating the units. Sinnott and Towler (2009) mentions that a chemical processing site would require three shift positions; a shift position costs approximately $60,000 per annum. It is assumed that the capture unit and compression unit would require a total of five shift positions, resulting in annual labour cost of $0.3 million.

The individual FOC were calculated using the information provided in Table 3-3. The summarised FOC for the benchmark MEA model with total overall FOC is shown in Table 5-10.

Table 5-10: Annual fixed operating cost for benchmark model using MEA

Costing Factor	Cost($M/year)
Labour Cost (LC)	0.3
Supervision Cost (SC)	0.075
Direct Salary Overhead (DSO)	0.15
Maintenance (M)	1.93
Property Taxes and Insurance	0.64
Property Insurance	0.64
General Plant Overhead	0.98
Environmental Charges	1.03
Total (FOC)	5.75

5.3.2.3 Cost of capturing CO_2 – MEA benchmark model

The total operating cost (TOC) annually is a summation of VOC and FOC; therefore TOC is equal to $46.83 million per annum. To calculate the total

annual capture cost (TACC), TOC and FIC_{annual} needs to be added together. The summary of the cost for base case using MEA is shown in Table 5-11.

Table 5-11: Total cost for capturing CO_2 benchmark study

	Cost ($M/year)
Fixed Capital Investment (FCI)	10.92
Total Operating Cost (TOC)	46.83
Total Annual Capture Cost (TACC)	57.75

For the benchmark model using MEA the total annual CO_2 captured is equal to 1.71 million tonnes. Using equation 3-6 the cost for capturing CO_2 was calculated and is equal $33.77/tonne of CO_2.

The cost of capturing CO_2 does not include the additional emissions during the capture and compression process. Much of the literature (Rao and Rubin, 2002, Abu-Zahra et al., 2007a, Ho et al., 2008b) has used the term "cost of carbon dioxide avoided" to include the influence of emissions during capture. The net amount of CO_2 captured includes the emission of CO_2 during capture process. The consumables such as steam and electricity have been assumed to be obtained from outside the ISBL limits, but they emit CO_2 when they are generated. The net CO_2 captured is the exclusion of these indirect emissions from the total amount of CO_2 captured from CPS and TBH.

This study assumes that indirect CO_2 emission is only contributed from consuming steam and electricity. The operational cost of consuming cooling water and waste to landfill is less than 2% of the total variable operational cost, therefore the indirect CO_2 emission from these are ignored. The emissions for generating steam and electricity are $0.219kgCO_2/kWh_{th}$ and $0.491kgCO_2/kWh_e$

respectively (DECC, 2011). Using these values and the total steam and electricity consumed per annum, the net CO_2 captured was calculated, the results are summarised in Table 5-12. Using equation 3-7 the cost of CO_2 avoided was calculated to be equal to $44.92/tonne of CO_2.

Table 5-12: Summary of net CO_2 captured MEA benchmark model

	CO_2 per annum (Mtonnes)
Total amount of CO_2 captured	1.71
CO_2 emitted form electricity usage	0.06
CO_2 emitted from steam usage	0.36
Net CO_2 captured	1.29

5.3.2.3.1 Comapring CO_2 avoidence with published Litrature

The cost of CO_2 avoidence have been calcualted by many authors (Rao and Rubin, 2002, Singh et al., 2003, Abu-Zahra et al., 2007a, Ho et al., 2008b). It is quoted to be between $50-$60/tonne of CO_2 avoided. The benchmark model created in HYSYS as part of this research has not included the desulphurisation unit. Work by other authors, mentioned above, have considered the desulphurisation unit and used it calcuate the final cost of CO_2 avoidence.

To include a desulphurisation unit for final cost of CO_2 capture, a similar approach to that of (Singh et al., 2003). In his work Singh et al. (2003) calculates the size of the desulphurisation using the one sixth rule (equation 3-2) and data from a pilot scale MEA scrubbing CO_2 capture plant. Operational costs for desulphurisation unit were assumed to be a percentage of the installed desulphurisation unit. For this reserch, data from (Singh et al., 2003) was used to size a desulphurisation unit and calculate the variable operational cost. The

calculated results of installation cost and operating cost are summarised in Table 5-13.

Table 5-13: ISBL installed cost ad variable operating cost for a desulphurisation unit

	ISBL installed cost_UK (2013) ($M)	*Variable Operating Cost/ ($M/year)*
Desulphurisation unit (this study)	14.40	4.78

The amended cost of capture with inclusion of a desulphurisation unit is \$51/tonne CO_2 avoided. This result is within the range of other published work mentioned above. The result from this study is compared with published results as shown in Figure 5-12, and is within the lower-range of the capture cost.

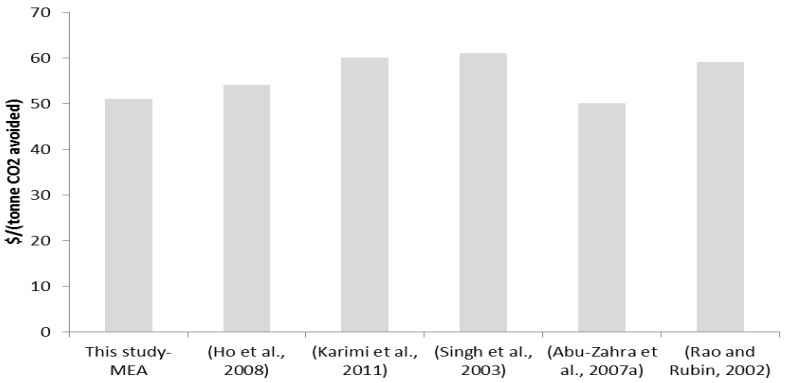

Figure 5-12: Comparison of CO_2 avoided cost with published literature

6 CO_2 Capture Using Physical Adsorption

This chapter has considered using adsorption as the separation technology to capture CO_2 from the flue gas of the central power station (CPS) and turbo blower house (TBH) of the studied steel mill. It was concluded from Chapter 2 and Chapter 4 the condition of the flue gas from CPS and TBH has high CO_2 partial pressure. At high CO_2 partial pressures, adsorption technology is expected to perform well (Chue et al., 1995). Therefore a techno-economic performance analysis for capturing CO_2 from CPS and TBH is covered in this chapter.

6.1 Process Modelling of Physical Adsorption

The selective separation that occurs when gas mixtures come in contact with porous material can be used to describe the adsorption phenomena. The gas mixture would contain different molecules with different strength of interaction with the solid surface. Some molecules have a stronger interaction than the others; this is used to favour the adsorption of the strongly interactive molecules onto to the solid surface. A bond is formed between the porous solid material (sorbent) and the molecule in adsorbed phase (adsorbate). This bond can be either a weak intermolecular bond or strong covalent bond. If the molecule is held by intermolecular forces, it is termed as physisorption. The latter is called chemisorption (Richardson et al., 2002, Wilcox, 2012).

Chemisorption involves activated electron transfer leading to a slow process, which in many cases is irreversible. It also contributes to high heat of adsorption with restriction to a monolayer specific site adsorption. Physisorption has low heat of adsorption compared to chemisorption and

involves rapid, non-activated reversible bonds. In some cases polarization can occur. It is also non site specific and can cover mono or multi-layer adsorption (Ruthven, 1984).

Physisorption is more preferred for CO_2 capture than chemisorption, due to the above mentioned reasons (Metz et al., 2005). This research focusses on CO_2 separation by physisorption. Physisorption is an exothermic process. Ruthven (1984) explains this as follows. The entropy change in the adsorbed molecule is negative, since the degree of freedom of the molecule in the gas phase is reduced from three to a maximum of two. Therefore ΔS in equation 6-1 should also be negative.

Equation 6-1: Entropy equation

$$\Delta S = S_{ads} - S_{gas}$$

The main forces contributing to the intermolecular bond in physical adsorption are the van der Waals forces (dispersion and repulsion). In some systems there are additional electrostatic forces in addition to van der Waals forces; these systems contain a charge or surface disruption. Metal organic frameworks and zeolites are two sorbents known to have an ionic structure and therefore demonstrate electrostatic forces (Ruthven, 1984, Wilcox, 2012). It is mentioned by Ruthven (1984) that the van der Waals forces are dominant in many systems but if the sorption involves adsorbing smaller dipolar molecules, such as H_2O, electrostatic forces shows dominance.

6.1.1 Adsorption equilibria

6.1.1.1 Adsorption equilibria of single components

Adsorption isotherms can define the equilibrium relationship of the sorbate in the gaseous phase and the adsorbed phase at given temperatures. If a quantity, q of the sorbate is adsorbed onto the sorbent, the relationship between the amounts adsorbed is a function of partial pressure and temperature (equation 6-2). The plot of amount adsorbed (q) versus the equilibrium partial pressure (P) at constant temperature is known as the adsorption isotherm curves (Yang, 1997).

Equation 6-2: Amount of sorbate adsorbed as a function of partial pressure and temperature

$$q = f(P, T)$$

There are five main forms adsorption curves can take, as shown in Figure 6-1. Type 1, 2 and 4 are the most common forms. Type 1 defines a sorbent with micro-porous nature and adsorption is controlled by the saturation of micro-pores. In this setting the pore sizes are similar to the gas/liquid molecules diameter. This gives a mono layer adsorption when the pores are completely filled. Sorbents with a wide range of pore size will display a type 2 isotherm. Type 2 is a multilayer adsorption isotherm, after completion of the first layer an inflection point is reached in the curve which than will be followed by multi layers of adsorption. Type 2 is displayed for sorbents having macro pores. Type 4 isotherm is common in sorbent containing meso-pores. It is similar to type 2 but the adsorption stops when the relative pressure reaches unity. The relative pressure is the ratio of absolute pressure and the saturation

pressure. Type 5 isotherms is similar to type 3 isotherm in conditions of low relative pressure (Ruthven, 1984, Yang, 1997, Thomas and Crittenden, 1998, Wilcox, 2012). At higher relative pressures saturation can be seen. CO_2 adsorption on zeolite 13X and activated carbon (AC) will show a type 1 isotherm relationship (Chue et al., 1995).

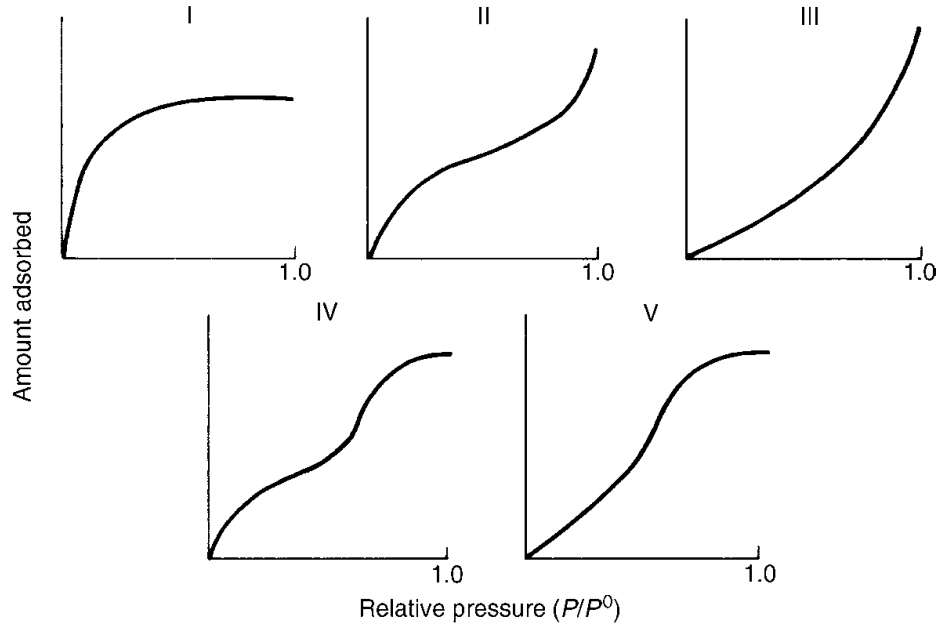

Figure 6-1: Classification of Isotherms into five types (Richardson et al., 2002)

Many equations have been proposed to define the isotherm curves of different types. The equations are either theoretically based or based on empirical data. Most of the equations define the isotherm curves well in low pressures and fail in higher pressures (Thomas and Crittenden, 1998). In his book, Yang (1997) has mentioned many theories to represent the isotherm curves. The Langmuir isotherm theory is one of them. The Langmuir theory and the Langmuir isotherm proposed in 1918 is still one of the most common equilibrium principle used today. The Langmuir isotherm was derived on the basis of dynamic equilibrium between the adsorbed phase and the gaseous

phase. It was suggested that the adsorption was directly proportional to the pressure, p, and a fraction of empty space or available adsorbent site (1-θ). Desorption was said to be proportional to the fractional coverage (θ). Finally Langmuir's theory mentions that adsorption and desorption are in equilibrium. The equilibrium relationship is represented by equation 6-3 (Thomas and Crittenden, 1998). It is very common to represent the Langmuir relationship as shown in equation 6-4. Where b is k_a/k_d and q_m is monolayer adsorbed capacity. The constants k_a and k_d adsorption and desorption constants. At low pressures equation 5-4 is in a linear form, which is analogous to the Henry's law equation. This represents the initial part of the type 1 isotherm curve. The Henry's isotherm model is based on this principle (Yang, 1997).

Equation 6-3: Langmuir adsorption and desorption equilibria relationship

$$k_a p(1-\theta) = k_d \theta$$

Equation 6-4: Langmuir isotherm

$$\theta = \frac{q}{q_m} = bP/(1+bP)$$

The Langmuir isotherm in its simplest form is based on the following assumptions (Yang, 1997, Thomas and Crittenden, 1998)

- Mono-layer adsorption only
- The adjacent molecules in the surface do not interact with one another.
- Molecules only accommodate one adsorption site and do not migrate.
- The heat of adsorption is constant and is not influenced by the coverage of the surface.

The Langmuir principle has been developed further to overcome the above assumptions, details of it is found elsewhere (Yang, 1997). One such model is the BET model. This model incorporates the necessity to consider multilayer adsorption. The type 1 isotherm is the only isotherm curve to represent monolayer adsorption; all other isotherm curves show the possibilities of having multilayer adsorption. The BET isotherm model derivation is explained elsewhere (Thomas and Crittenden, 1998, Richardson et al., 2002). It is mentioned that BET model is a rigid model able to represent types 2-5 of the isotherm curves. The BET model is widely used to determine the surface area of porous material.

Much of the published literature has shown that adsorption of CO_2 on zeolite 13X and activated carbon (AC) can be successfully represented by the Langmuir isotherm model (Kikkinides et al., 1993, Chue et al., 1995, Gomes and Yee, 2002, Ko et al., 2002). This research is focussing on adsorption of CO_2 from flue gas using zeolite 13X and AC, therefore the Langmuir model was used to represent the equilibrium model.

6.1.1.2 Multicomponent adsorption equilibria

The importance of considering the effect of other components in gaseous phase is emphasised for post combustion capture. The flue gas will contain the desired sorbate CO_2. Other components such as nitrogen and oxygen will also be present in the flue gas. Flue gas will also contain impurities of unburned fuel and water vapour (Gomes and Yee, 2002). The single component isotherm models presented in the previous section can be adjusted to include the influence from other components. There are many theories present to represent

multicomponent adsorption. Detailed explanation of such theories can be found in (Ruthven, 1984) and (Thomas and Crittenden, 1998).

The Extended Langmuir isotherm is the most stable and reliable model in ASPEN ADSIM for multicomponent adsorption (Aspentech, 2004). The derivation of the Extended Langmuir isotherm can be found in the following (Yang, 1997). Its final form, to represent loading of component i, is shown in equation 6-5.

Equation 6-5: Extended Langmuir Isotherm

$$q_i = \frac{q_{mi} b_i P_i}{1 + \sum_{j=1}^{n} b_j P_j}$$

The Extended Langmuir isotherm is a popular multi-component equilibrium model for CO_2 and nitrogen mixtures to be adsorbed on zeolite 13X and AC. Extended Langmuir is one of the available multi-component equilibrium models in ADSIM. It has also been used widely in research and published data has shown high stability and reliability in modelling carbon dioxide/nitrogen adsorption (Kikkinides et al., 1993, Chue et al., 1995, Gomes and Yee, 2002, Ko et al., 2002, Chou and Chen, 2004).

6.1.2 Adsorption kinetics

In earlier years it was assumed that the adsorption was controlled only by equilibrium, therefore the adsorption took place instantly. This simplified process calculations but in reality this is false. Various resistances are present that control the speed and limit the flow of the sorbate from the bulk gas to the adsorption site. A sorbate in the turbulent bulk gas surrounding the pellet and

experiencing a concentration gradient will diffuse through a laminar boundary layer around the exterior of the pellet. The sorbate then diffuses through further regions of mass transfer resistances to reach an adsorption site. During desorption this process is reversed. Since adsorption is exothermic and the adsorbed sorbate releases heat, the heat is dispersed out of the particle and it undergoes somewhat similar resistance to mass transfer. The rate of heat dispersion is vital in deciding the capacity of the sorbent (Richardson et al., 2002).

The modelling of adsorption requires the coupling of the adsorption isotherm with the mass and heat balance equations. This research assumes that the adsorption process for carbon dioxide capture is isothermal for simpler process modelling; therefore the mass transfer resistance will only be discussed. More details on heat transfer rate and resistance can be found elsewhere (Ruthven, 1984, Yang, 1997, Thomas and Crittenden, 1998).

Wilcox (2012) in her book has categorised the resistances, which a sorbate undergoes from bulk gas to its final destination of the porous adsorbent site into three. They are as follows.

- The resistance due to the thin layer of laminar fluid (boundary film) surrounding the pellet.
- The resistance in the macro-pores (the space encompassing the pellet surrounding micro-pores)
- Inter-crystalline resistance in the micro-pores.

The laminar film surrounding the pellet is known as the external mass transfer region while the macro-pores and the inter-crystalline region is referred as the internal mass transfer region.

6.1.2.1 External mass transfer resistance

The rate of mass transfer from the bulk gas to the solid surface of the pellet is limited by the layer of laminar fluid. This mass transfer rate can be expressed in accordance of Fick' law and is given by equation 6-6. It can be seen that the rate of mass transfer is proportional to concentration difference ($C_s - C_b$) across the boundary film and the external surface area of the pellet, a_s. The mass transfer coefficient k_f has the unit ms^{-1} (Thomas and Crittenden, 1998).

Equation 6-6: Mass transfer rate in the boundary film region

$$\frac{dq}{dt} = k_f a_s (C_s - C_b)$$

It is mentioned by Richardson et al. (2002) that the boundary film does not contribute to a large amount of mass transfer resistance, unless in exception of unsteady conditions when the pellet is first introduced to the bulk gas. Unlike mass transfer the boundary film is said to contribute largely to heat transfer.

With correlated data from experiments it has been proposed that the boundary layer mass transfer coefficient can be expressed using dimensionless Sherwood number (Sh) given by equation 5-7.

Equation 6-7: Film mass transfer coefficient expressed in terms of Sherwood number

$$Sh = 2k_f R_p / D_m = 2.0 + 1.1 Sc^{0.33} Re^{0.6}$$

In equation 6-7; k_f is the film mass transfer coefficient, R_p is radius of the particle, D_m is the molecular diffusion, Sc is Schimdt number and Re is the Reynolds number. The relationship between Sherwood number and film transfer coefficient in backed beds is correlated by equation 6-7 for Reynolds number in range of $3\text{-}10^4$ (Yang, 1997)

6.1.2.2 Internal mass transfer resistance

6.1.2.2.1 Single straight cylindrical pore diffusion

The diffused sorbate from the boundary layer enters the pellet, which consists of a complex network of pores. As mentioned by Wilcox (2012) the diffusion through the network of micro/macro pores is the internal mass transfer. The pores can be categorised to macropores ($d_p > 50$ Å), mesopores (20 Å $< d_p < 50$ Å) and micropores ($d_p < 20$ Å) where d_p is the pore diameter (Yang, 1997). For simplicity mesopores are considered as micropores, when calculating pore diffusion. As an initial step of understanding pore diffusion, the pore diffusion through a single cylindrical pore is considered which then would be elaborated to understand the whole of the pellet (Yang, 1997).

The diffusion in pores is defined by the sorbate molecules collision. They collide with one another, the pore wall or both. In relatively large diameter pores the collision between molecules will prevail more than the collision between molecules and the wall. This therefore results in molecular diffusion (D_m). When the pore diameter decreases there is an increase in collision between molecules and the pore wall, resulting in a diffusion mechanism known as the Knudsen diffusion (D_k) (Richardson et al., 2002)

The mean free path of gas molecules is used in deciding which of the above diffusion mechanism is more dominant. As a rule of thumb it is considered that Knudsen diffusivity will show dominance if the mean free path is ten times the pore diameter. If not molecular diffusivity will show dominance in the pore diffusivity (Richardson et al., 2002, Yang, 1997).

Knudsen diffusivity (D_k) is given by equation 6-8 and it relates to the loss in momentum due to the gas molecules colliding with the pore wall.

Equation 6-8: Knudsen diffusivity

$$D_k = 9.7 \times 10^3 r_p \left(\frac{T}{M}\right)^{\frac{1}{2}}$$

Where r_p is the pore radius in centimetres, T is the temperature in Kelvin, and M is the molecular weight of the sorbate. The calculated Knudsen diffusivity is in cm^2s^{-1}.

Equation 6-9: Chapman-Enskog to calculate molecular diffusivity of binary gases

$$D_m = \frac{(1.858 \times 10^{-7})\, T^{3/2}}{P\sigma_{AB}{}^2 I}\left(\left(\frac{1}{M_A}\right)+\left(\frac{1}{M_B}\right)\right)^{1/2}$$

Molecular diffusivity can be calculated using the Chapman-Enskog equation as shown in equation 6-9. Where P is pressure in Nm^{-2}, T is temperature in K, σ_{AB} is the collision diameter nm, I is the dimensionless collision integral and M_A and M_B is molecular weight of the gases A and B. The calculated D_m has the unit ms^{-1}. The values of the collision diameter and collision integral have been published in many literature and they can be found in (Cussler, 2009). Cussler (2009) obtained a similar expression to equation 6-9

proposed using empirical data. It is equation 6-10, and does not require estimation of σ_{AB} and I.

Equation 6-10: Molecular diffusivity equation from empirical data

$$D_m = \frac{1.013 \times T^{-7}\left(\frac{1}{M_A} + \frac{1}{M_B}\right)^{1/2}}{P[(\sum_A v_i)^{1/3} + (\sum_B v_i)^{1/3}]^2}$$

Where T is temperature given in K, M_A and M_B are the molecular weights of the two gases. P is pressure in bar and $\sum v_i$ is the summation of the diffusion volume of component A and B.

In is mentioned by Yang (1997) and Wilcox (2012) that when the mean free path and pore diameter are of the same order of magnitude or if the mean free path is not known an approximation to the net diffusion, D, from both molecular and Knudsen can be made using equation 6-11. It is assumed that the molecules diffusing experience equimolar counter diffusion, during adsorption and desorption (Thomas and Crittenden, 1998).

Equation 6-11: Net diffusivity from Knudsen and Molecular

$$\frac{1}{D} = \frac{1}{D_m} + \frac{1}{D_k}$$

6.1.2.2.2 Diffusion in porous sorbent

The net diffusion in equation 6-11 is derived from the assumption of a single cylindrical pore, but in reality the sorbent has a highly complex pore network. Therefore in reality the sorbate diffusing through a porous sorbent will have an effective diffusivity less than the net diffusivity calculated in

equation 6-11. Yang (1997) has mentioned that the sorbate travelling through the porous pore would have tortuous pathway. There is also free space in the pore, which is not available for diffusion. Therefore the tortuosity factor, τ, and the inter-pellet void fraction, ϵ_p are used to calculate the effective diffusivity D_e as shown in equation 6-12.

Equation 6-12: Effective diffusivity

$$D_e = \frac{\epsilon_p D}{\tau}$$

6.1.2.3 Mass balance in the pellet

The mass balance within a spherical pellet controlled by macropore resistance is shown in equation 6-13. Where c is the concentration of sorbate in the fluid phase, ϵ_p is the pellet porosity, q is the concentration of sorbate in adsorbed phase and R is the particle radius (Ruthven, 1984, Wilcox, 2012).

Equation 6-13: Mass balance in a spherical particle with macro pore controlled resistance

$$(1-\varepsilon_p)\frac{\partial q}{\partial t} + \varepsilon_p \frac{\partial c}{\partial t} = \varepsilon_p D_e \left(\frac{\partial^2 c}{\partial R^2} + \frac{2}{R}\frac{\partial c}{\partial R}\right)$$

It is mentioned by Yang (1997) that some systems display dominance in micropore resistance. If assumed that the micro particle crystals can be considered as identical spheres surrounded by a uniform sorbate concentration throughout the pellet. The mass balance equation within micropores is given by equation 6-14. Isothermal conditions are assumed, since heat transfer is rapid when compared to sorption.

Equation 6-14: Mass balance equation for micro-pore crystal

$$\frac{\partial q}{\partial t} = \frac{1}{r^2}\frac{\partial}{\partial r}\left(r^2 D_c \frac{\partial q}{\partial r}\right)$$

Where r is the micro particle crystal radius and D_c is the inter-crystalline diffusivity. If D_c is constant equation 6-14 can be represented by 6-15.

Equation 6-15: Micro-pore crystal mass balance with constant inter-crystalline diffusivity

$$\frac{\partial q}{\partial t} = D_c\left(\frac{\partial^2 q}{\partial r^2} + \frac{2}{r}\frac{\partial q}{\partial r}\right)$$

In molecular sieve sorbents the internal resistance is a combination of micropore and macropore resistance. Simultaneous equations covering both resistances needs applied and solved for such systems. A simplified approach is to eliminate the mass balance in the particle. It is called the linear drive force (LDF) approximation (Yang, 1997). LDF was proposed by Glueckauf (1955) and it relates the overall sorption rate to the bulk concentration of the sorbate. Equation 6-16 is the linear drive force equation for a spherical pellet. The R_p in the equation is the pellet radius, D_e is the overall diffusivity in the pellet, and k is the mass transfer coefficient. D_e can be by micro-pore effective diffusivity, macro-pore effective diffusivity, or a combination of both. The LDF gives a linear function, relating the equilibrium amount of sorbate adsorbed (q^*) with the amount adsorbed in the sorbent. The LDF equation coupled with the isothermal equilibrium equation can be used to calculate the mass transfer in a pellet.

Equation 6-16: Linear Driving Force approximation for mass transfer in a pellet

$$\frac{\partial q}{\partial t} = \frac{15 D_e}{{R_P}^2}(q^* - q) = \mathrm{k}(q^* - q)$$

It is mentioned by Yang (1997) that the validity of the LDF approximation is limited to conditions representing $D_e t/R_p^2 > 0.1$. It is also only valid for conditions following a linear or slightly curved equilibrium isotherm. CO_2 and N_2 and adsorption on zeolite 13X and AC display a type 1 isotherm and will be separated using cyclic process. Therefore the LDF approximation can be applied for CO_2 separation using adsorption.

This research assumes that the mass transfer resistance in the pellet is controlled by Knudsen and molecular diffusivity. Therefore the overall effective diffusivity was calculated using equations 6-8 to 6-12. Other published work, such as the work done by Ko et al. (2005), has used the same assumption to define the mass transfer rate in a pellet for a system with CO_2 and N_2.

6.1.2.4 Mass balance in the bed

With the definition and understanding of the mass balance transfer in the pellet the mass balance for the overall bed under isothermal conditions can be defined by equation 6-17. In reality axial mixing causing axial dispersion can occur in the bed. It is desired to reduce axial dispersion to increase efficiency in the adsorption (Wilcox, 2012). The first term on the left of equation 6-17 represents axial dispersion, where D_L is the axial dispersion coefficient. If the condition in the bed is axial pug flow, the first term on the left can be omitted (Richardson et al., 2002, Wilcox, 2012). The second term on the left of

equation 6-17 represents the convective flow in the bed. The interstitial velocity, u_o which is equal to the fluid superficial velocity divided by the bed cross sectional area is assumed constant. The third term represents the accumulation of the adsorbate in the fluid phase. The fourth term represents the rate of adsorption onto the solid sorbent.

Equation 6-17: Mass balance equation in the bed

$$-D_L \frac{\partial^2 c}{\partial L^2} + u_o \frac{\partial c}{\partial L} + \varepsilon_p \frac{\partial c}{\partial t} + (1 - \varepsilon_p)\rho_p \frac{\partial q}{\partial t} = 0$$

Dynamic results are obtained when equation 6-17 is coupled and solved with equation 6-16 for given boundary conditions. In the presence of multi-component in the fluid, equations 6-16 and 6-17 must be solved for all components separately. The final overall mass balance continuity for all components must be satisfied (Thomas and Crittenden, 1998).

6.2 Modelling CO_2 Capture using ADSIM

There was a necessity to investigate the isothermal equation and the pellet mass transfer rate in ADSIM. ADSIM does not have an in-built library to represent the parameters defining mass transfer and equilibrium. The equilibrium parameters and the mass transfer coefficients for CO_2 and N_2 adsorption was investigated from literature and was adapted to match ADSIM's input requirement.

6.2.1 Equilibrium isotherm parameter investigation

The extended Langmuir isotherm equation can be used to represent CO_2 and N_2 adsorption onto a solid sorbent. The extended Langmuir equation in ADSIM has the format shown in equation 6-18 (Aspentech, 2004). The loading, w_i, of the sorbate i onto the sorbent is proportional to the partial pressure P_i of the sorbate i. The isotherm variation at different temperatures is included in equation 6-18 using the temperature of the sorbent (T_s). Equation 6-18 has included the influence of other molecules (competitive adsorption) and k represent the total number of components in the system.

Equation 6-18: Format of the extended Langmuir equation in ADSIM

$$w_i = \frac{(IP_{1i} - IP_{2i}T_s)IP_{3i}e^{IP_{4i}/T_s}P_i}{1 + \sum_k (IP_{3k}e^{IP_{4k}/T_s}P_k)}$$

The extended Langmuir equation is popular for modelling CO_2 adsorption on zeolite 13X and AC. Authors have used different relationships to define the isotherm parameters (IP_1-IP_4). Kikkinides et al. (1993) has used a similar representation to equation 6-18. Chue et al. (1995) and Chou and Chen (2004) have used an exponential dependency for the isotherm parameters. Ko et al. (2005) has used a dual site Langmuir equation. Wang et al. (2012a) has used a multi-site extended Langmuir equation.

6.2.1.1 Correlation and calculation of the isotherm parameters IP1-IP4

The parameters IP1-IP4 were correlated and calculated by interpolating data from (Chue et al., 1995). The single component isotherm equation 6-4 was reorganised to the linearised format shown in equation 6-19. The saturated

loading (q_m) and Langmuir isotherm parameter (b) were obtained from the plots created. The gradient of and the intercept of the plot p/q versus p was used to calculate q_m and b.

Equation 6-19: Linearised Langmuir equation

$$\frac{p}{q} = \frac{1}{bq_m} + \frac{p}{q_m}$$

The saturated loading (q_m) and the Langmuir isotherm parameter b were obtained for different temperatures. Using equations 6-20 and 6-21 the isotherm parameters of the extended Langmuir equation (IP_1-IP_4) were calculated. The calculation was done for all gaseous molecules in the system (CO_2 and N_2). The calculated extended Langmuir equation isotherm parameters (IP1-IP4) are shown in Table 6-1.

Equation 6-20: Equation to calculate the saturated loading to IP1 and IP2

$$q_{mi} = IP_{1i} - IP_{2i}T_s$$

Equation 6-21: Equation to calculate the Langmuir isotherm parameter to IP3 and IP4

$$b_i = IP_{3i}e^{IP_{4i}/T_s}$$

Table 6-1: Isotherm parameters for extended Langmuir equation (AC-activated carbon)

	IP1 (kmol/kg)	IP2(kmol/kg)	IP3(bar^{-1})	IP4(K)	Sorbent
CO2	0.0119	2.34×10^{-5}	0.0142	1982.25	Zeolite 13X
N2	0.0067	1.88×10^{-5}	0.0166	1195.93	Zeolite 13X
CO2	0.0212	6.04×10^{-5}	0.6726	312.85	AC
N2	0.0045	1.01×10^{-5}	0.0030	1201.74	AC

To validate the isotherm parameters calculated, equation 6-18 was used to create isotherm curves for CO_2 and N_2 at different temperatures. The isotherm curves were then compared with published literature data. Figure 6-2 shows the curves representing isotherms for CO_2 and N_2 on zeolite 13X compared with experimental results from (Cavenati et al., 2004). Figure 6-3 compares isotherm curves created for CO_2 and N_2 on AC compared with experimental data from (Dreisbach et al., 1999).

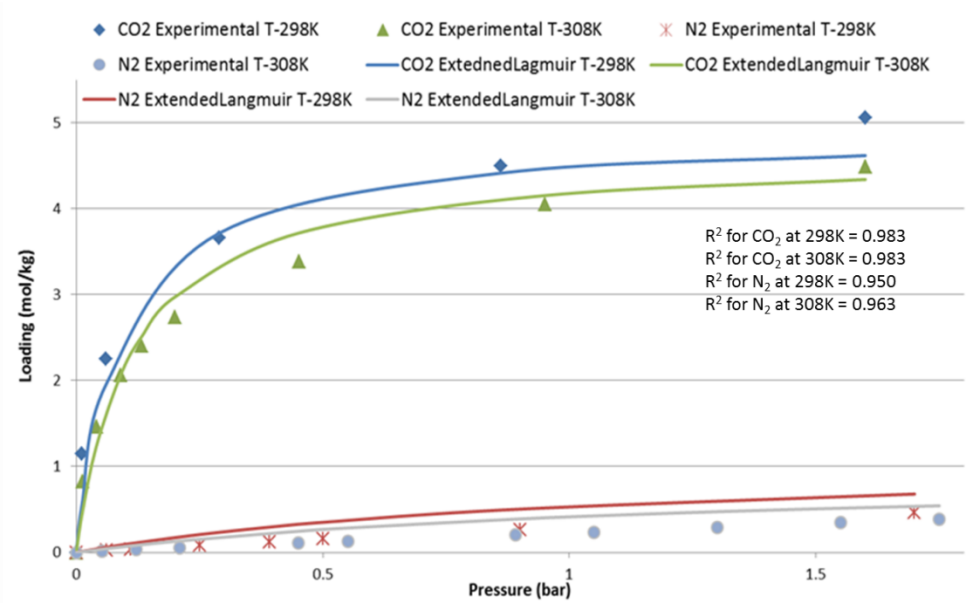

Figure 6-2: Isotherm comparison of experimental data versus model in this study (zeolite 13X)

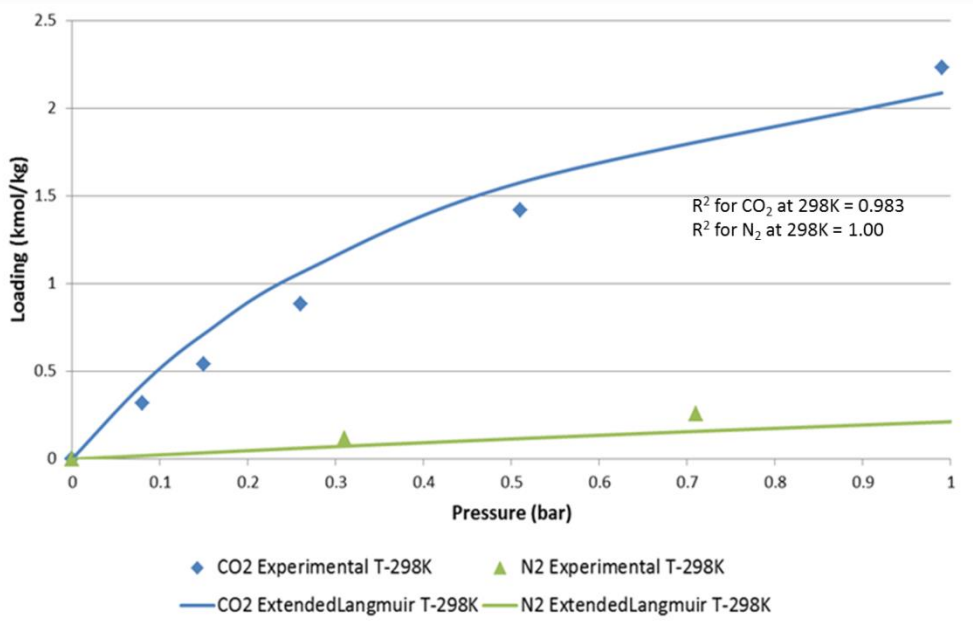

Figure 6-3: Isotherm comparison of experimental data versus model in this study (AC)

It can be seen that the coefficient of determination (R^2) for the plots is more than 0.95 for all six curves. R^2 indicates how well a curve fits data points. If the value of R^2 is equal to 1, it means that the regression line is a perfect fit. If the value of R^2 moves towards zeros the regression line fit is not fitting data points. Further details of calculation and explanation of R^2 can be found elsewhere (Johnson, 2009). This means that the isotherm parameters (IP1-IP4) and the extended Langmuir equation is able to represent CO_2 and N_2 equilibrium on zeolite 13X and activated carbon.

The sorbent zeolite 13X has a higher CO_2 loading than AC according to Figures 6-2 and 6-3. At higher pressures the loading capacity on AC gradually overtakes the loading capacity of zeolite 13X. Siriwardane et al. (2001) and Zhang et al. (2010) have proved this in their works. Siriwardane et al. (2001) has shown that zeolite 13X performs better at pressures below 340 kPa. AC out performs zeolite 13X at pressures above 340 kPa. This is explained as the

effect of higher surface area and total pore volume in AC when compared with zeolite 13X (Zhang et al., 2010). The physical characteristics of the two sorbents are shown in Table 6-2.

Table 6-2: Sorbent physical properties (Zhang et al., 2010)

Sorbent	Bet surface area (m^2g^{-1})	Average pore diameter (nm)	Total pore volume (cm^3g^{-1})
Activated Carbon	2829	2.19	1.55
Zeolite 13X	400	1.00	0.21

It is also clear from Figure 6-2 increase in temperatures has got an adverse effect on CO_2 and N_2 loading on the zeolite 13X. This is also true for sorbent AC and has been shown elsewhere (Zhang et al., 2010).

6.2.2 Mass transfer coefficient investigation

The LDF representation for mass transfer (equation 6-16) in the pellet can be used in ADSIM. ADSIM allows the user to enter a value for the mass transfer coefficient, k in equation 6-16. ADSIM also has the option to calculate micro-pore and macro-pore resistance using properties of the sorbent and sorbate entered by the user (Aspentech, 2004). The previous method is known as the lumped resistance and is simple to compute. It requires the user to enter the mass transfer coefficient, k, and solves the LDF equation in parallel to the mass balance equation of the bed. An option to choose a quadratic driving force (QDF) for the representation of the mass transfer rate in the pellet is also available in ADSIM (Aspentech, 2004). QDF is a modification to LDF to

represent less favourable isotherms, and more details can be found in (Ruthven, 1984).

6.2.2.1 Calculating the mass transfer coefficient for the LDF

To use the LDF, the overall mass transfer coefficient (lumped mass transfer coefficient) needs to be calculated. Assuming that the sorbent is spherical, the mass transfer rate can be written as follows in equation 6-22. The unit of k is given as s^{-1}.

Equation 6-22 Mass transfer coefficient

$$k = \frac{15 D_e}{{R_p}^2}$$

For zeolite 13X assuming that the pore diffusivity is dominant in the pellet. The effective diffusivity, D_e, can be calculated using equations 6-8 to 6-12. A similar approach has been used by Ko et al. (2005). Kikkinides et al. (1993) and Chue et al. (1995) have assumed equilibrium based separation of CO_2 and N_2 on AC. Therefore k is set as $1s^{-1}$ for both CO_2 and N_2 adsorbed on AC.

The properties of zeolite 13X and the sorbate CO_2 and N_2 shown in table 6-3, and were used to calculate the effective diffusivity of the sorbate.

Table 6-3: Properties of zeolite 13X and sorbate for calculation of effective diffusivity

		Reference
Particle radius Rp (m)	1×10^{-3}	(Ko et al., 2005)
Pore radius (m)	5×10^{-10}	(Ko et al., 2005)
Porosity	0.38	(Ko et al., 2005)
Tortuosity	2.2	(Wang et al., 2012a)
Molecular weight, M_i CO_2 : N_2	44 : 28	
Diffusive Volume, V_i CO_2 : N_2	26.9 : 17.9	(Cussler, 2009)

Table 6-4: Effective diffusivity and mass transfer coefficient of CO_2 and N_2 on zeolite 13X

	Effective Diffusivity , D_e (m^2/s)	Lumped Mass Transfer Coefficient , k (s^{-1})
CO_2	2.18×10^{-8}	0.33
N_2	2.73×10^{-8}	0.41

The calculated mass transfer coefficient for zeolite13X is shown in table 6-4. It can be entered onto ADSIM to be used with the LDF equation. As it is assumed earlier, the mass transfer of CO_2 and N_2 on AC is instantaneous (Kikkinides et al., 1993). The LDF equation for AC will be simplified and will be represented by equation 6-23.

Equation 6-23: LDF equation for CO_2 and N_2 on activated carbon

$$\frac{\partial q}{\partial t} = \frac{\partial q^*}{\partial t}$$

6.2.3 Work done by the blower and vacuum pump

It is necessary to define and calculate the work done by the vacuum pump and the blower, to evaluate the economics of CO_2 capture using adsorption.

The work can then be converted to power to calculate the electricity consumed by the capture unit. Equation 6-24 has been used by others to calculate the work done by the blower and vacuum pump (Wang et al., 2012a).

Equation 6-24: Equation to calculate the work done by blower and vacuum pump

$$W = f_{molar} R_g T \frac{1}{\eta} \frac{\gamma}{1-\gamma} \left[\left(\frac{P_{high}}{P_{low}} \right)^{\frac{\gamma-1}{\gamma}} - 1 \right] t$$

The term W is the work done by the blower or vacuum pump and has the unit Joules (J). The term f_{molar} (mol/h) is the flow rate of the gas. R_g (J/mol-K) is the universal gas constant, T (K) is the absolute temperature and η is the efficiency. Efficiency of 75% has been used as part of this research. The term P_{high}/P_{low} is the pressure ratio. ϒ is the ratio of specific heats and is used as 1.4 in this study. The term, t represents the time in hours.

6.2.4 Modelling breakthrough study in ADSIM

As part of the full scale setup for modelling of CO_2 adsorption, the initial requirement was to model a breakthrough study and validate the results against published literature. A simple bed setup was modelled in ADSIM as shown in Figure 6-4. The same model was used to validate breakthrough curves for zeolite 13X and AC, but the bed properties and flow conditions were varied to match the literature used.

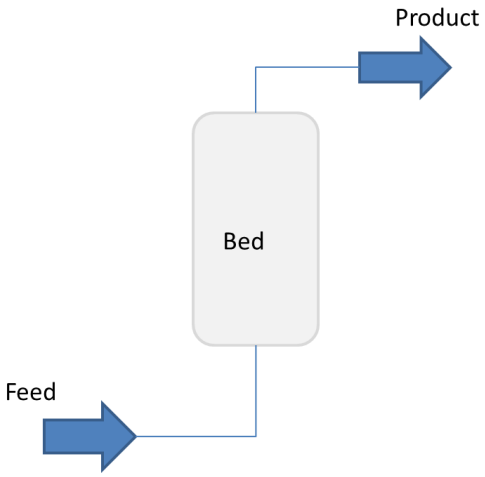

Figure 6-4: Simple model flowsheet for breakthrough analysis

6.2.4.1 Modelling activated carbon breakthrough study

The work by Shen et al. (2011) was used to validate breakthrough curves for AC in ADSIM. Shen et al. (2011) has used a fixed bed to conduct an experiment to understand the breakthrough behaviour of CO_2 on AC. The AC used in the experiments is a synthesised pitch based activated carbon. The sorbent has been produced in State Key laboratory in China and the preparation method is detailed elsewhere (Liu et al., 1999b). The sorbent has a specific area of 845.87m^2/kg. According to Shen et al. (2011) the sorbent is a small pored AC, therefore the simulation used in the paper considers inter-crystalline diffusivity combined with pore diffusivity. In ADSIM the proposition made by Kikkinides et al. (1993), which said that adsorption on AC is equilibrium based separation, was used. The mass transfer coefficient k was set to 1s^{-1}, and the lumped mass transfer model was used in ADSIM.

The properties of the bed and the sorbent are detailed in Table 6-5 and 6-6 respectively. These properties were replicated in ADSIM to study the breakthrough behaviour of CO_2 on AC. The feed flow conditions used in

ADSIM, to replicate the work conducted by Shen et al. (2011) is shown in Table 6-8.

Table 6-5: Properties of the bed for activated carbon breakthrough analysis

	Bed Properties
Bed height (m)	0.557
Bed diameter (m)	0.025
Bed porosity	0.32
Bed bulk density (kg/m^3)	670.6

Table 6-6: Properties of the pellet for activated carbon breakthrough analysis

	Pellet Properties
Diameter of pellet, D_p (m)	$1x10^{-3}$
Pellet density (kg/m^3)	984.3
Pellet porosity	0.506
Pellet tortuosity	2.0

Table 6-7: Feed flow conditions for activated carbon breakthrough study

CO2 mole fraction	0.15
N2 mole fraction	0.85
Flow rate (mmol/s)	1.49
Feed temperature (K)	303
Feed pressure (kPa)	130

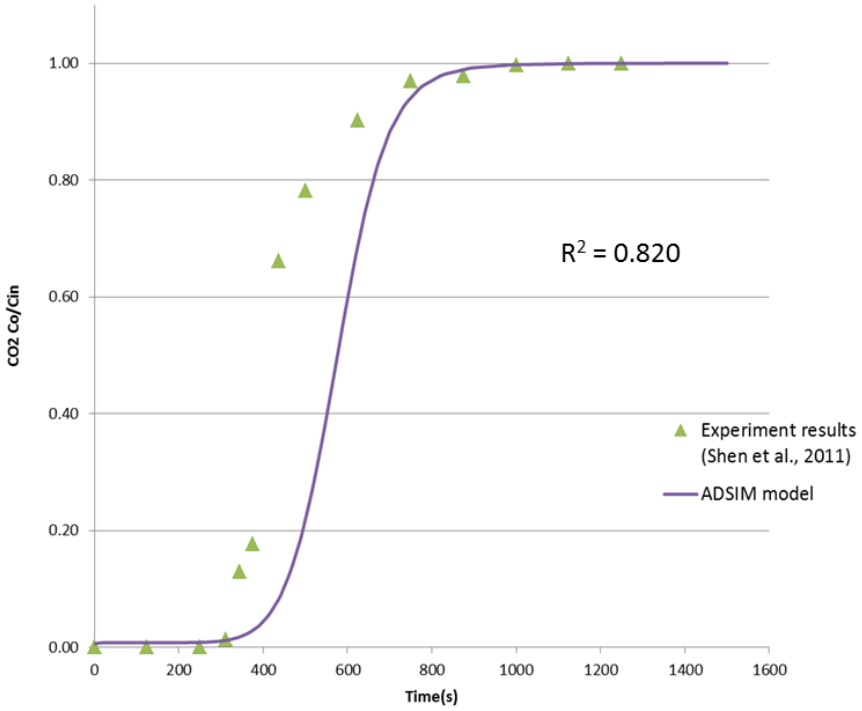

Figure 6-5: Comparison of breakthrough curves for AC

6.2.4.1.1 Analysis of the breakthrough study for activated carbon

Figure 6-5 shows the comparison of the breakthrough curves for AC, of the model created in ADSIM and the work done by Shen et al. (2011). The coefficient of determination (R^2) for the curve is 0.820. The two plots start to differ after 300s when the bed is starting to get saturated. In reality the bed will see a temperature increase with adsorption, therefore reducing the loading capacity of the sorbent. In ADSIM it is assumed that the conditions are isothermal, therefore no temperature change is experienced. With no temperature change in the bed the ADSIM model will not experience a decrease to the loading capacity. This can be seen in Figure 6-5. The curve representing the work by Shen et al. (2011), shows that the bed reaches saturation a little bit earlier than the curve for the model represented by ADSIM.

Another variation in the breakthrough curves is seen towards end when the bed is getting fully saturated. The breakthrough curve for Shen et al. (2011) is showing a less steeper curve at the end compared to the ADSIM model. Shen et al. (2011) has mentioned that the synthesised AC has small pores and has considered inter-crystalline diffusivity combined with pore diffusivity. ADSIM model uses a simple equilibrium based separation model proposed by Kikkinides et al. (1993). The small pores in the AC will cause micro-pore diffusion. Micro-pore diffusion will cause a slower saturation, producing a less steep curve at the end. The breakthrough curve of Shen et al. (2011) displays this, but this phenomena is visible for the breakthrough curve from ADSIM model.

It can be concluded that the model created in ADSIM has a bed saturation point at approximately 300s. The breakthrough curve of Shen et al. (2011) has also got a bed saturation point at approximately 300s. The model is ADSIM is not able to replicate the breakthrough curve after the bed saturation point. The assumptions; isothermal adsorption and equilibrium based separation in ADSIM is causing this difference. This research investigates process modelling of cyclic bulk separation of CO_2. The adsorbent bed will only be used up to the saturation point ($t < 300s$). As soon the bed starts saturating, the bed will be purged and regenerated making it ready for the next cycle. Therefore the assumption of equilibrium based separation with isothermal conditions would be sufficient for this research.

6.2.4.2 Modelling zeolite 13X breakthrough study

The breakthrough study by Wang et al. (2012b) was used and replicated in ADSIM to model breakthrough of CO_2 on zeolite 13X. Wang et al. (2012b) has used zeolite 13X-APG sorbent, which has been provided by the UOP company in China. It is mentioned that the sorbent used is similar to the commercially available zeolite 13X sorbent. The properties of the bed and the pellet used by Wang et al. (2012b) for fixed bed breakthrough modelling is shown in Tables 6-8 and 6-9 respectively. The conditions of the feed are shown in Table 6-10.

Table 6-8: Properties of the bed for zeolite 13X breakthrough study

	Bed Properties
Bed height (m)	0.35
Bed diameter (m)	0.025
Bed porosity	0.39
Bed bulk density (kg/m^3)	666.5

Table 6-9: Properties of the pellet for zeolite 13X breakthrough study

	Pellet Properties
Radius of pellet, R_p (m)	0.00135
Pellet density (kg/m^3)	1099.5
Pellet porosity	0.30
Pellet tortuosity	2.0

The model in ADSIM has used the assumption that mass transfer rate is controlled by pore diffusivity. Therefore Knudsen and molecular diffusion define the overall effective diffusivity. The LDF approximation was used to

represent the mass transfer rate in the pellet. The mass transfer coefficient shown in Table 6-4 was used in ADSIM. The extended Langmuir equation (equation 6-18) was used to represent equilibrium conditions. The breakthrough curve of Wang et al. (2012b) was compared with ADSIM model's breakthrough curve, and is shown in Figure 6-6.

Table 6-10: Feed flow conditions zeolite 13X breakthrough study

CO2 mole fraction	0.15
N2 mole fraction	0.85
Flow rate (mol/h)	5.904
Feed temperature (K)	303
Feed pressure (bar)	1.33

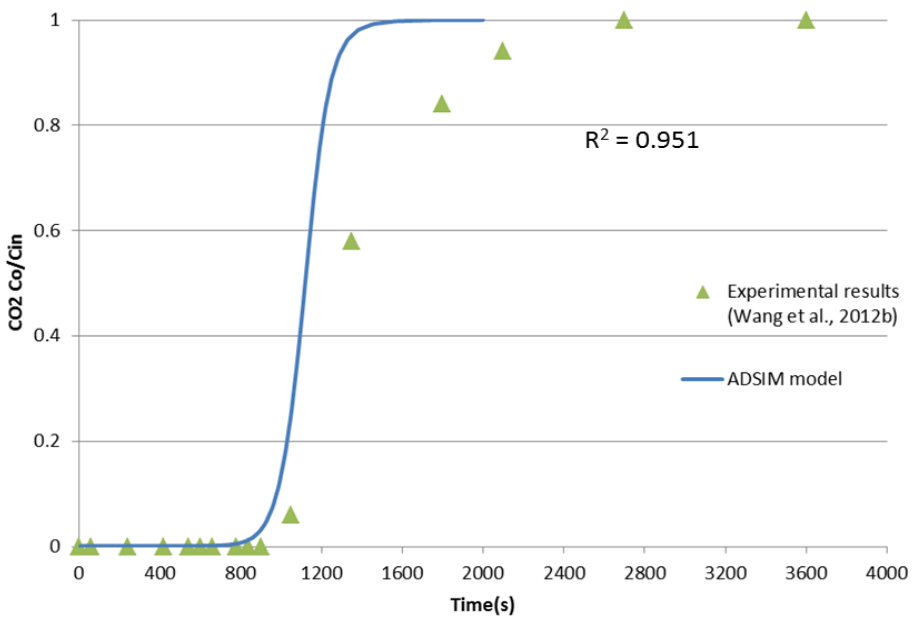

Figure 6-6: Comparison of breakthrough models for zeolite 13X

6.2.4.2.1 Analysis of the breakthrough study for zeolite 13X

According to Figure 6-6, the bed for ADSIM model starts saturating at approximately 800s. The breakthrough curve from the work by Wang et al. (2012b) also has a bed saturation point at approximately 800s. After the 800s the curves for the ADSIM model and model by are showing differences. ADSIM breakthrough curve shows a steeper curve after 800s. The work by Wang et al. (2012b) is showing a breakthrough curve, that is damped towards full bed saturation. According to Figure 6-6 the breakthrough curve for the ADSIM model is showing that it takes approximately 1500s to fully saturate the bed. The other breakthrough curve is showing approximately 2700s to fully saturate the bed.

Wang et al. (2012b) have used a multi-site Langmuir isothermal equation. ADSIM model uses the simpler extended Langmuir equation that assumes single site competitive adsorption. The model by Wang et al. (2012b) will have more adsorption sites, therefore the bed takes more time to get fully saturated. ADSIM model, with its fewer adsorption sites, experiences the bed to fully saturate at a lesser time.

It can be concluded that the ADSIM model is able to replicate the breakthrough curve by Wang et al. (2012b) for conditions where the bed has not started to saturate. In similarity to AC, this would be sufficient for this research. This research is investigating cyclic bulk CO_2 removal, and therefore will work in conditions before the saturating point ($t < 800s$). When the bed starts to saturate it will be purged and regenerated, making it ready for the next cycle.

6.2.5 Lab scale CO_2 capture using ADSIM

Skarstom 4 steps cycle is a simple 2 bed continuous pressure swing adsorption cycle. The cycle involves two beds working alternatively to adsorb and regenerate the bed. The layout of the system involves two beds connected by valves. The process involves four steps as shown in figure 6-7.

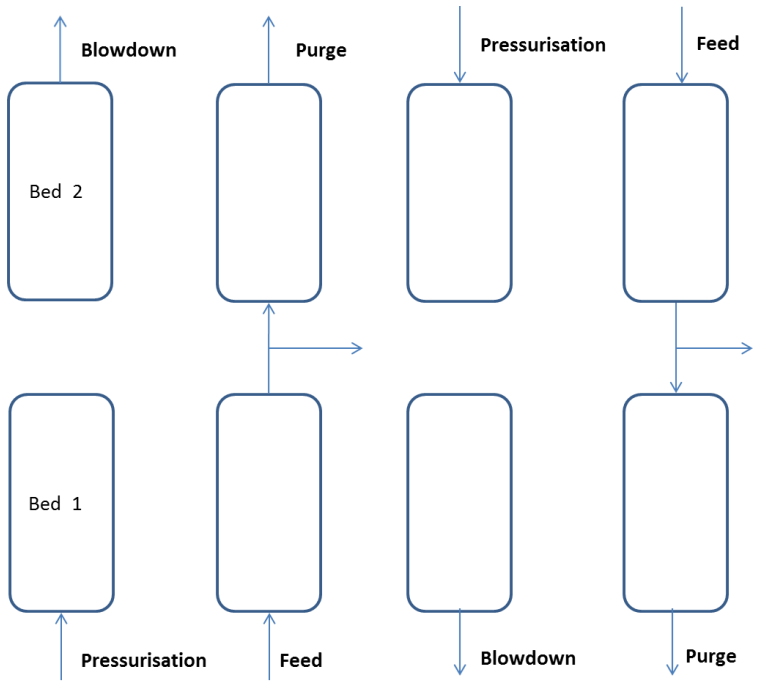

Figure 6-7: Skarstom cycle with four steps illustrated adapted from (Thomas and Crittenden, 1998)

The four steps of the Skarstom cycle are as follows:

- Step 1: the bed is initially pressured with feed to the required adsorption pressure. Some layouts can include pressurisation with the outlet gas.

- Step 2: Is the adsorption step where the bed is continuously fed by the feed gas at adsorption pressure. The gas leaving the other end of the bed has the less adsorptive gas molecules. In capture of CO_2 from flue gas the outlet gas will be concentrated with N_2.

- Step 3: involves a counter-current depressurisation known as the blowdown. This step decreases the bed pressure causing the adsorbed CO_2 molecules to desorb and exit the bed.

- Step 4: is the purge step, which uses the less adsorptive N_2 molecules in counter-current direction to push back the adsorbed CO_2 molecules out of the bed.

The two beds work out of phase by 180^o, therefore enabling one bed's N_2 to be used as purge for the other bed in a continuous process. If the system works in a way that adsorption takes place at pressure much higher than atmospheric pressure and blowdown is applied at atmospheric pressure, the process is called a pressure swing adsorption (PSA). If adsorption is applied at pressures near to atmospheric and if the desorption is carried out at pressures below atmospheric, the process it is known as vacuum swing adsorption (VSA). The selection of pressure range varies from one system to the other as chosen from isotherms for specific sorbents. It is also possible to use temperature increment during desorption (Thomas and Crittenden, 1998, Wilcox, 2012).

The full layout of the 4 step Skarstom cycle is shown in Figure 6-8. In ADSIM it is possible to model the two bed 4 steps Skarstom cycle with a single bed and an interaction unit. Setting up such a model is explained in the Aspen ADSIM reference guide (Aspentech, 2004). This setup on ADSIM is shown in Figure 6-9. The interaction unit D1 shown in Figure 6-9 records the purge flow conditions during the adsorption step, it then uses the recorded purge details as the purge stream during the purge step. The step times and

valve conditions during each steps is defined in the cycle organiser. The cyclic organiser runs the model until the defined numbers of cycles are completed or until the model reaches cyclic steady state. Cyclic steady was set to be achieved with an error tolerance of $1x10^{-3}$ for all models.

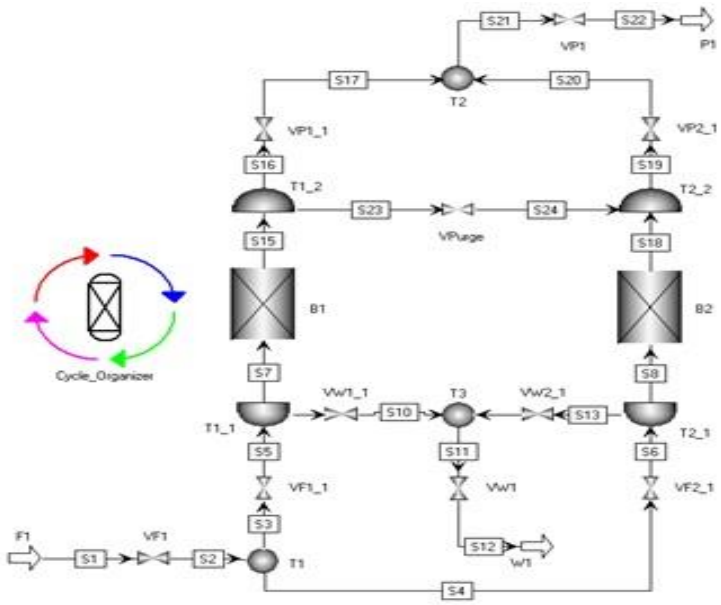

Figure 6-8: 4 step Skarstom cycle model layout in ADSIM

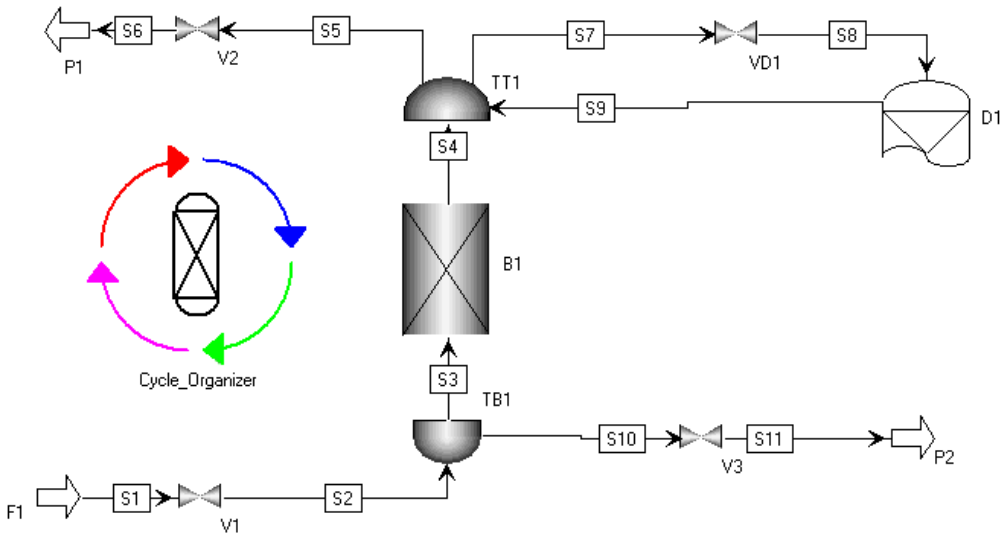

Figure 6-9: Simplified layout of the model in ADSIM using the interaction unit D1

6.2.5.1 Modelling lab scale CO_2 capture using activated carbon

Shen et al. (2011) have performed lab-scale vacuum pressure swing adsorption (VPSA) for conditions relating to flue gas from a coal fired power plant (CO_2 composition > 15 mol %). The flue gas has been created, in the lab, by mixing CO_2 (15-50 mol %) with N_2. In their work Shen et al. (2011) have used one bed and applied the four steps shown in Figure 6-7. During purge step pure N_2 has been used as the purge gas. This is a variation to the 4 step Skarstom cycle in which the bed's top decarbonised gas is used as purge gas.

The work by Shen et al. (2011) was replicated in ADSIM with the bed sizing and pellet properties shown in Tables 6-5 and 6-6. The extended Langmuir isotherm (equation 6-18) was used with the parameters shown in Table 6-1. Kinetics was modelled using LDF representation with a lumped mass transfer resistance ($k = 1\ s^{-1}$).

6.2.5.1.1 Analysis of the lab scale study for activated carbon

The lab scale model was conducted to check the validity of the ADSIM model at different design parameters such as feed flow rate, feed pressure, desorption pressure, temperature and feed composition. The results from ADSIM, compared with the results from (Shen et al., 2011) is shown in Table 6-11. For the cases 1 to 7, ADSIM is showing a higher recovery and purity of CO_2, compared to the results by Shen et al. (2011). If we consider case 1 it can be seen that the ADSIM model is showing, 13.22% higher CO_2 purity then that of (Shen et al., 2011). Recovery of CO_2 is also 2.60% more in the ADSIM model. Therefore an increase in productivity can be seen in Table 6-11 for the ADSIM model.

Table 6-11: Lab scale activated carbon in ADSIM compared with work of (Shen et al., 2011)

Case	Q_{feed} (mol/h)	Temp (K)	P_{feed} (bar)	P_{low} (bar)	CO_2 mol%	CO_2 purity %	Purity Diff. %	CO_2 recovery %	Recovery Diff %	CO_2 Productivity (mol/kgh)
VPSA 1	5.35	303	1.31	0.1	15	48.56		55.35		1.64
ADSIM						54.98	13.22	56.79	2.60	1.68
VPSA 2	8.03	303	1.31	0.1	15	50.35		40.7		1.76
ADSIM						56.92	13.05	41.7	2.46	1.83
VPSA 3	5.35	303	1.31	0.05	15	53.75		66.03		1.59
ADSIM						58.84	9.47	69.05	4.57	1.65
VPSA 4	5.35	303	1.31	0.03	15	54.06		69.05		1.54
ADSIM						60.03	11.04	69.05	0.00	1.61
VPSA 5	5..35	303	1.31	0.1	25	67.79		55.81		2.63
ADSIM						73.41	8.29	61.06	9.41	2.87
VPSA 6	5.35	303	1.31	0.1	50	90.06		57.8		4.64
ADSIM						90.58	0.58	63.41	9.71	5.08
VPSA 7	5.35	313	1.31	0.1	15	47.89		49.81		1.53
ADSIM						54.17	13.11	55.41	11.24	1.7
VPSA 8	5.35	303	3.24	0.1	15	63.04		96.16		2.42
ADSIM						52.01	-17.50	85.07	-11.53	2.3
VPSA 9	5.35	303	2.03	0.1	50	93.70		78.23		5.56
ADSIM						90.78	-3.12	75.95	-2.91	5.39

It was expected for the ADSIM model to output a higher purity and recovery of CO_2, compared to (Shen et al., 2011) for the following reasons.

- The purge gas used in the experimental study by Shen et al. (2011) is pure N_2. The ADSIM model used the decarbonised gas from the top of the bed. The decarbonised gas will have un-adsorbed CO_2 molecules. Purging with gas containing un-adsorbed CO_2 will increase recovery and purity in CO_2 product stream.

- The experimental work by Shen et al. (2011) would have experienced an increase in temperature, therefore having an adverse effect on CO_2 loading. Isothermal conditions were assumed in ADSIM; therefore CO_2

loading would have been constant throughout the cycle in the ADSIM model.

It was also noted that the ADSIM model had a low recovery of CO_2 for cases 8 and 9 when compared to the experimental work. The cases 8 and 9 represent conditions of the feed gas having very high CO_2 partial pressure. A reasonable explanation for this variation can be rooted back to how the isotherm parameters (IP1-IP4) in equation 6-18 were interpolated. The data used for interpolation was obtained from (Chue et al., 1995). The CO_2 loadings presented by Chue et al. (1995) is only up to 100 kPa. Therefore the equation 6-18 interpolated from that data is not able to accurately define adsorption at partial pressures more than 100 kPa.

It is mentioned by Siriwardane et al. (2001) that AC shows a high selectivity of CO_2 at high partial pressures, even more than zeolite 13X. This research concentrates on capture of CO_2 at lower pressure and desorption at vacuum, for economically favourable reasons (Metz et al., 2005). Therefore the correlated extended Langmuir isotherm using data from (Chue et al., 1995) is sufficient.

6.2.5.1.2 A sensitive study on effect of purge/feed ratio on CO_2 purity and recovery

Purge/feed ratio is defined as the ratio of the flow rate of the purge stream and the flow rate of the feed. The lab-scale study shown in Table 6-11 uses a purge/feed ratio of 7.5% for case 1. A sensitive study, by varying the purge/feed ratio was modelled in ADSIM. The purity and recovery of CO_2

obtained at different purge/feed ratio was analysed and is shown in Figure 6-10.

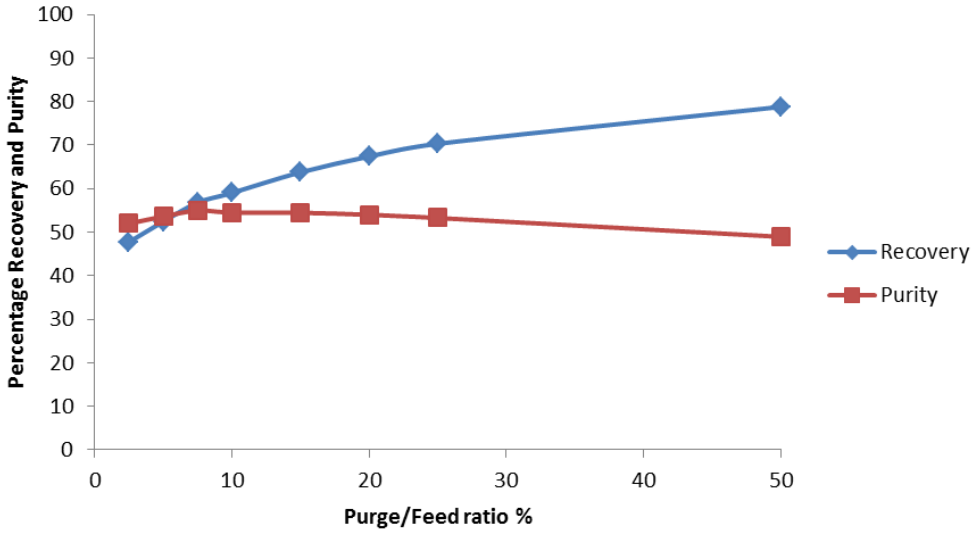

Figure 6-10: Activated carbon purge/feed ratio sensitive analysis

It is clear from Figure 6-10 an increment on purge to feed ratio has a positive impact on CO_2 recovery, but purity has a maximum value somewhere around 8% purge to feed ratio. The purity then declines with an increment of purge to feed ratio.

6.2.5.2 Modelling lab scale CO_2 capture using zeolite 13X

Shen et al. (2011) work on AC was easy to reproduce in ADSIM because all design parameters were given. There is limited literature with experimental data for a simple 4 step Skarstom cyclic process, involving CO_2 separation using zeolite 13X. The two published works (Wang et al., 2012a, Wang et al., 2012b) have results of experimental data for a 4 step Skarstom cycle but there is no clear explanation of the design parameters used.

Wang et al. (2012b) has used a single bed experimental configuration and applied the 4 step Skarstom cycle in similar procedure to the work of Shen et al. (2011). Wang et al. (2012b) has mentioned the achievement of CO_2 product purity of 65% and recovery of more than 57%. The experiments were started with CO_2 15 mol% in the feed gas and pure N_2 was used as purge gas. Even though Wang et al. (2012b) mentions that the desorption pressure is 10 kPa, vital information such as feed pressure and times for each steps is not given. This is causing limitation to replicate this experiment on ADSIM, to validate and prove that such recovery and purity is achievable.

The other work by Wang et al. (2012a) details a second stage 4 step Skarstom cycle used to increase purity after an initial cyclic process. The work therefore has involved a feed with CO_2 of 50 mol% or more. Experimental work has been conducted by Wang et al. (2012a) with a single bed configuration and the 4 steps of the Skarstom cycle were continuously run one after the other. In similar to Shen et al. (2011) a purge gas of pure N_2 was used.

The properties of the bed and zeolite 13X pellet in the experiment are same as shown in Tables 6-8 and 6-9. The feed flow conditions used in the experiment is not mentioned in the paper by Wang et al. (2012a); therefore reverse calculation was used to determine the feed flow rate. For example for run 1 shown in table 6-12, the productivity of CO_2 is given this with the recovery of CO_2 can be used to determine the total moles of CO_2 fed into the bed. Using the inlet mole fraction of CO_2 in the inlet feed and the overall time of pressurisation and feeding, the overall feed flowrate was calculated.

6.2.5.2.1 Analysis of the lab scale study of zeolite 13X

Table 6-12 shows the results obtained from modelling lab scale CO_2 capture replicated from the work by Wang et al. (2012a). In comparison to the experimental results the ADSIM model is showing a higher CO_2 purity and recovery. The reasonable explanations for this difference are similar to that given AC lab scale analysis. They are as follows

- Experimental work has used pure N_2 to purge, but the ADSIM model uses decarbonised gas from the top of the bed. The decarbonised gas is not pure N_2 it will have CO_2 molecules, that would increase the purity and recovery of CO_2 in the product stream

- In reality there will be an increase in temperature in the bed, causing the CO_2 loading per kilogram of sorbent to reduce. This phenomenon is not modelled in ADSIM, because it is assumed isothermal conditions in the bed.

- Mass transfer resistance in the zeolite 13X are complex in reality. In includes diffusion through pores and crystals. In ADSIM it is assumed that pore diffusion is dominant in zeolite 13X. Therefore mass transfer rate in the experiment would be slower than that of the model created in ADSIM.

Table 6-12: Lab scale zeolite 13X in ADSIM compared with work of (Wang et al., 2012a)

Run	Q_{feed} (mol/h)	Temp(K)	P_{feed} (bar)	P_{low} (bar)	CO_2 mol%	CO_2 purity %	Purity Diff %	CO_2 recovery %	Recovery Diff %	CO_2 Productivity (kg/kgh)
1	2.47	300	1.34	0.1	50	84.26		77.73		0.164
ADSIM						86.02	2.09	82.12	5.65	0.205
2	2.00	300	1.34	0.1	60	84.44		84.27		0.177
ADSIM						85.49	1.24	90.41	7.29	0.214
3	1.86	300	1.33	0.1	70	85.02		91.47		0.208
ADSIM						87.01	2.34	95.34	4.23	0.231

6.3 CO_2 Capture from CPS and TBH using Adsorption

As it was concluded from the chapter 2 and chapter 4 the conditions of the flue gas rising from the CPS and TBH of the studied mill would be suitable for CO_2 capture using adsorption. This section of the thesis will look at applying CO_2 separation using zeolite 13X and AC.

6.3.1 Technical evaluation of adsorption using ADSIM for CPS and TBH

In similarity to process modelling using HYSYS for chemical absorption in Chapter 5, the ISBL boundary starts after the desulphurisation unit and finishes after the CO_2 post capture compression. The ISBL boundary for the models considering CO_2 capture using adsorption is shown in Figure 6-11.

If the sorbent used for adsorption is zeolite 13X the models needs to include a dehumidifier. For the models using AC a dehumidifier will not be required.

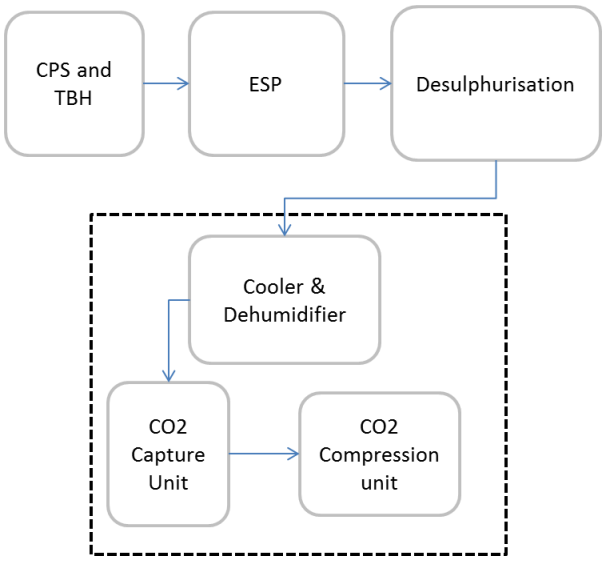

Figure 6-11: ISBL boundary with the units for physical adsorption capture (CPS-Central Power Station, TBH –Turbo blower house, ESP-Electrostatic precipitator)

Three studies were considered and they are as follows

- Capture using zeolite 13X with a desorption pressure of 5 kPa (adsorption benchmark model)
- Capture using zeolite 13X with a desorption pressure of 10 kPa
- Capture using activated carbon (AC) with a desorption pressure 5 kPa

The model representing capture using zeolite 13X and a desorption pressure of 5 kPa will be used as the benchmark model for the other two.

The dehumidified cooled flue gas entering the capture unit is assumed to be a binary mixture, consisting only N_2 and CO_2. This is a valid assumption since any oxygen present in the flue gas will behave like N_2, within the adsorption bed. The flue gas conditions and properties are given in Table 6-13. As it can be seen from Table 6-13 the volume of flue gas entering the capture

unit is large. The flue gas will be split and directed towards trains of capturing beds. This is necessary to reduce capturing step times and bed sizes, and will reduce the overall capital cost of equipment.

Table 6-13: Conditions and properties of flue gas entering the adsorption capture unit

Stream Name	Pressure (bar)	Temp (°C)	Mass flow (kg/h)	CO2	N2
Flue Gas	1.013	25	7.14×10^5	0.23	0.77

As understood from the lab scale study there is a necessity to have two or more stages to attain a CO_2 product with purity of more than 95 mol%. The first stage will concentrate CO_2 while maintaining a high recovery, and the following stages will increase purity to the level required. The ratio of predecessor stages to subsequent stages is 2:1 as shown in Figure 6-12.

Intermediate tanks will be present in between the stages to maintain the required flow rate into the succeeding stages. This is not illustrated in Figure 6-12. If two sections in a stage are controlled precisely with the required time lags, intermediate tanks will not be required. A detailed study of the impact of having tanks or sophisticated complex control systems will be discussed in the following sections of costing.

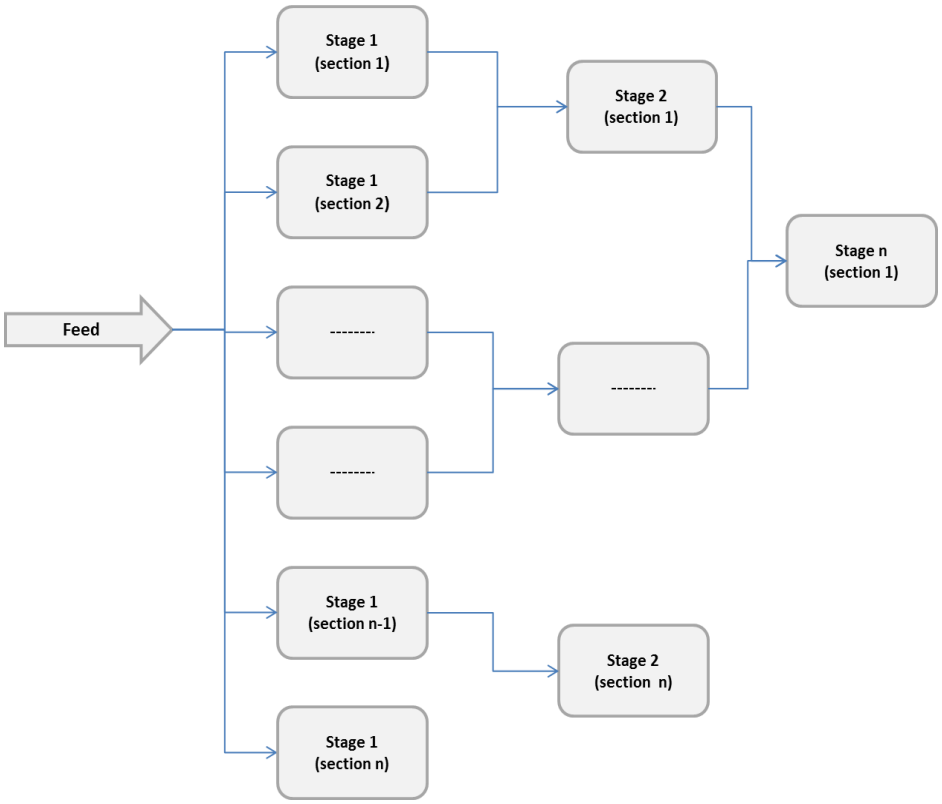

Figure 6-12: Flue gas split and sent into different stages in the capture unit

6.3.1.1 Application of CO_2 capture for CPS and TBH using zeolite 13X adsorption

6.3.1.1.1 Capture using zeolite 13X – desorption pressure 5 kPa

Capturing of CO_2 using zeolite 13X was conducted at a desorption pressure of 5 KPa. The flue gas entering the capture unit was split and sent into forty six sections in the first stage. The average flow rate of the flue gas entering one section of stage 1 is approximately 491.7 kmol/hr. The flue gas conditions are shown in Table 6-13.

A layout of the beds and valve settings in one section of stage 1 is shown in Figure 6-13. Stream 1 is the feed stream with varying flowrate, during pressurisation and adsorption. Stream 6 consists of the CO_2 product, released from the bed during blowdown and purge of the beds. Stream 11 will contain a

higher purity of nitrogen and would be sent out through the stack or used for purging the alumina beds in the dehumidification unit. Details of the dehumidification unit are given later in this chapter in section 6.3.2.1.1.

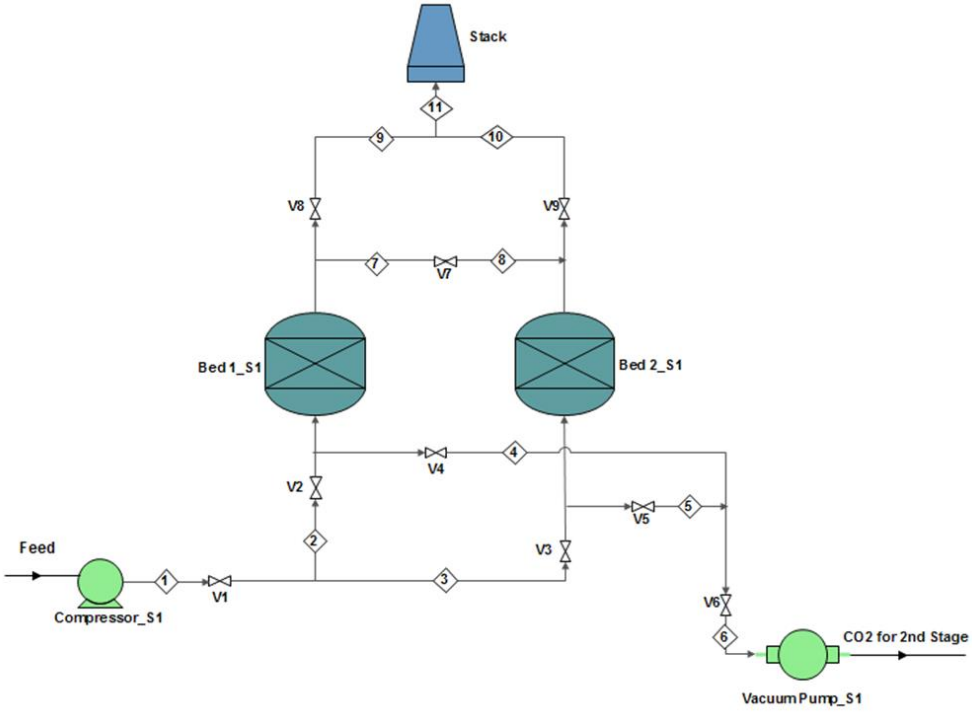

Figure 6-13: Beds and valve layout for 4 step Skarstom cycle (stage 1)

It is mentioned by Wilcox (2012) a bed's length defines the capital cost and separation capability due to pressure loss along the bed. The pressure change in a bed for laminar and turbulent flow is defined by the Ergun equation. According to the Ergun equation the pressure change in a packed bed is proportional to the length (or height) of the bed. Taking this into consideration the full scale models were simulated with smaller length beds. The beds were said to have a height of 1m, while the diameter of the beds were increased to accommodate the high flow rate.

The first stage desirable design outcome was to achieve a concentrated product stream of CO_2 with a high recovery. This was achieved with a high purge to feed ratio. The purge/feed ratio of was set as 15% for stage 1. The first stage has a total cyclic time of 900s, of which adsorption and purge is twice that of blowdown and pressurising.

The first stage for zeolite 13X is able to achieve a recovery of 93.4% CO_2 with a purity of 0.58 mole fraction. A further second stage was modelled to increase purity to above 0.95 mole fraction. The second stage was modelled with many different purge/feed ratios to obtain the desired purity. The change in purity and recovery in the second stage for different purge to feed ratio is shown in Figure 6-14.

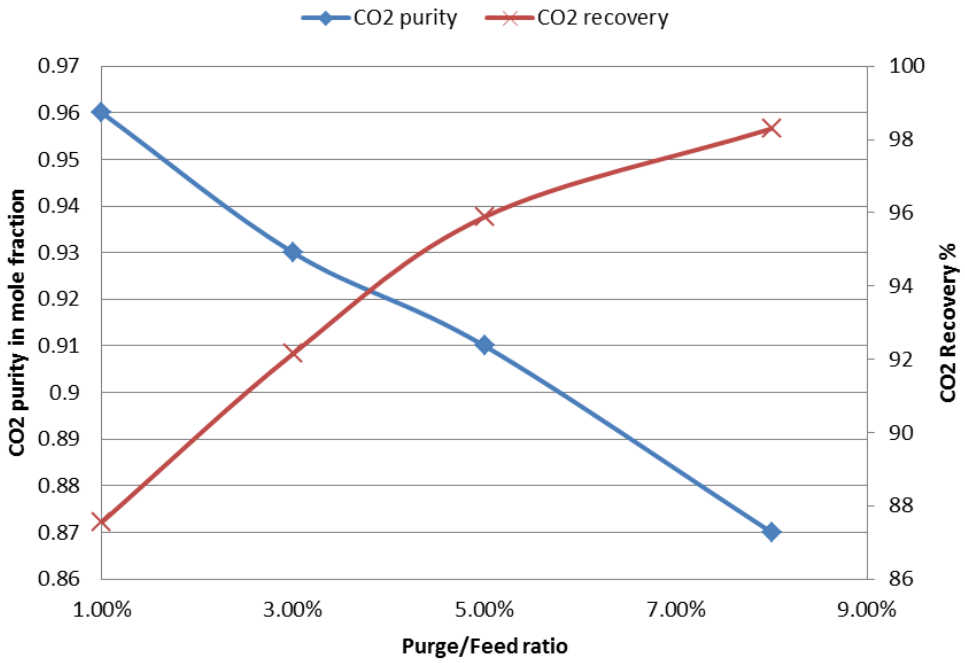

Figure 6-14: Variation of CO_2 purity and recovery for different purge to feed ratio in second stage of the capture unit (zeolite 13X -5 KPa)

The second stage has a total cycle time of 600s; in which the times for adsorption and purge is twice that of blowdown and pressurisation. It is clear that an increase of purge/feed ratio is giving a higher recovery of CO_2, but has the adverse effect of lowering the purity. If the purge/feed ratio is set at 1% it is possible to attain a purity of 0.96 mole fraction CO_2 with a recovery of 87.56%. The overall recovery of CO_2 is equal to 81.8%. This is within comparable levels, with the results obtained for capturing using MEA chemical absorption.

The overall mass balance for the two interacted stages is shown in Figure 6-15. Stage 2 has a total of twenty three sections; therefore the overall CO_2 production is equal to 4434.4 kmol/h (1.92×10^5 kg/h). The captured CO_2 product stream is then sent into the post-capture compression unit. The CO_2 compression unit is similar to the one for chemical absorption as explained in Chapter 5. The only difference is an extra compressor in the compression stage. The final condition of the CO_2 product stream has a pressure of 11MPa with a purity of 96 mol% CO_2. The mass flow rate is equal to 1.92×10^5 kg/h.

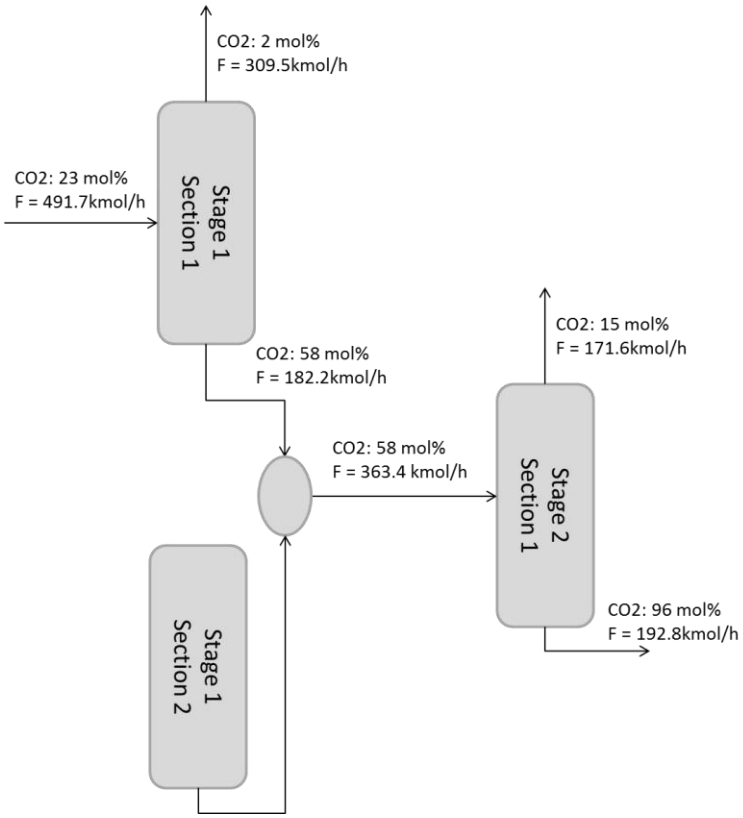

Figure 6-15: Mass balance of the two interacting stages for zeolite 13X capture (5 kPa)

6.3.1.1.1.1 Sensitive analysis of adsorption at different temperatures

For the adsorption benchmark model, a sensitive analysis on the effect of temperature change on CO_2 purity and recovery was conducted. Stage 2 of the adsorption benchmark model was simulated at two more different temperatures. They were 59.85^{o}C and 69.85^{o}C (333K and 343K). The benchmark model at 25^{o}C (323.15K) was compared with the other two. The sensitive analysis was done at two different purge/feed ratios. The results are summarised in Table 6-14.

Table 6-14: Temperature increment sensitive study for on purity and recovery of CO_2 (zeolite 13X-5 kPa)

	T = 25^{0}C	T = 59.85^{0}C	T = 69.85^{o}C
		Purge/Feed = 1%	
CO_2 Purity (mol%)	96.00	96.00	96.00
CO_2 Recovery (%)	87.56	82.08	77.72
		Purge/Feed = 8%	
CO_2 Purity (mol%)	87.00	88.00	88.00
CO_2 Recovery (%)	98.30	93.87	88.60

At higher temperatures the amount of CO_2 adsorbed onto zeolite 13X is decreased. This gives a lower recovery of CO_2 in the product stream as shown in Table 6-14.

The purity of CO_2 does not change much with an increase in temperature. An explanation for this in the considerably large flow rates in the CO_2 product stream. This is the second stage of separation and the bottom product from the bed is of a large quantity. This can be seen in Figure 6-15. The purge stream has relatively much lesser flow rate than the product stream, so it does not influence the purity by much. It can be seen for purge/feed ratio of 1% the purity remains the same for all temperatures. At purge/feed ratio of 8% increases the CO_2 purity to 88 mol% from 87 mol%. This is because the purge flow rate at 1% purge/feed ratio is much lesser than that of 8% purge/feed ratio. Therefore the 1% purge/feed ratio has not got enough gas molecules to change the CO_2 product purity stream.

6.3.1.1.2 Capture Using Zeolite 13X – desorption pressure 10 kPa

As a further technical sensitive analysis capturing using zeolite 13X, with a desorption pressure of 10 kPa was modelled. Its techno-economic performance

needs to compared with the adsorption benchmark model that used 5 kPa desorption pressure. Similarly to the adsorption benchmark model it was assumed that stage 1 would have forty sections with an average flue gas inlet flow rate of 491.7 kmol/h. Different purge to feed ratio was used in the first stage to understand its effect on the CO_2 purity and recovery. A plot representing the first stage purity and recovery versus the purge/feed ratio is shown in Figure 5-15.

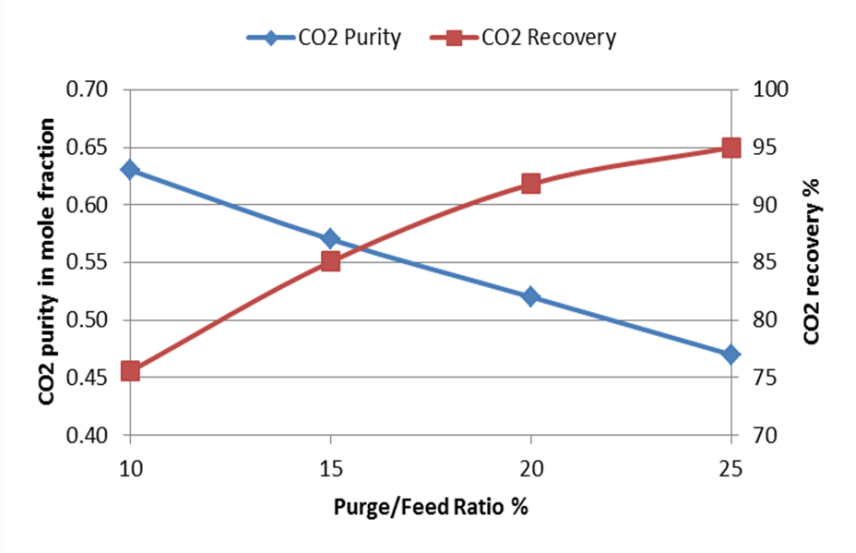

Figure 6-16: Variation of CO2 purity and recovery for different purge to feed ratio in first stage of the capture unit (zeolite 13X -10 KPa)

The total cycle time of the first stage was set as 900s, with adsorption and purge steps having twice the time to that of desorption and pressurisation. As mentioned earlier the first stage requirement is to attain a high recovery of CO_2 with reasonably good level of CO_2 purity. At purge/feed ratios of 20% and 25%, the recovery of CO_2 is 91.80% and 94.98% respectively. The purity of concentrated CO_2 stream is less than 55 mol% in both of those ratios. This could mean an extra third stage requirement to attain final CO_2 product purity of more than or equal to 95 mol%.

At 15% purge/feed ratio a purity of 0.57 mole fraction CO_2 is achievable with a recovery of only 85.08%. This is the cross-over point at which the purity and recovery of CO_2 is reasonably good according to Figure 6-16. Therefore the product stream, from the first stage representing 15% purge/feed ratio, was used as the feed stream to the second stage 2 of separation.

The second stage has a total of twenty three sections each accepting an inlet flow rate of 337.6 kmol/h with CO_2 mole fraction of 0.57. The total cycle time is set to 600s with adsorption and purge being twice the time of pressurisation and blowdown in a 4 step Skarstom cycle. The final CO_2 product stream from the stage 2 of the capture unit has got an ultimate purity of 0.95 mole fraction CO_2. This purity was only achievable with a purge/feed ratio set at 1% in stage 2. The recovery of CO_2 in stage 2 is equal to 72.84%. Therefore the overall recovery of CO_2 using a 10 kPa desorption pressure is 61.97%. The mass balance of the two stages for capturing using a 10 kPa desorption pressure is shown in Figure 6-17.

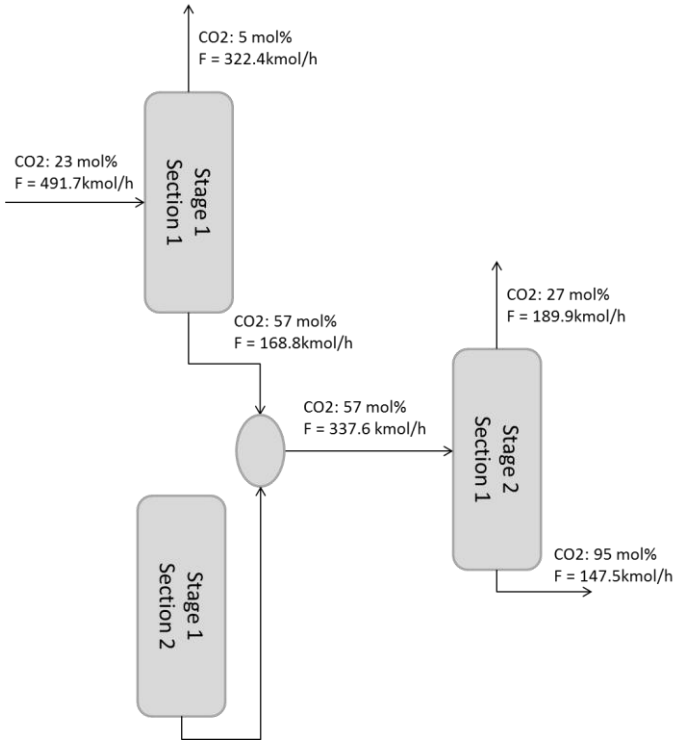

Figure 6-17: Mass balance of the two interacting stages for zeolite 13X capture (10 kPa)

One section of stage 2 produces a CO_2 product stream with a flow rate of 147.5 kmol/h; therefore the total flow rate of the CO_2 production is 3392.5 kmol/h ($1.47x10^5$ kg/h). The CO_2 product stream is then compressed to attain an overall pressure of 11 MPa with purity of 0.95 mole fraction CO_2. This fits the requirement for storage of captured CO_2; therefore it could be transported to required destination.

6.3.1.2 Application of CO_2 capture for CPS and TBH using activated carbon adsorption

6.3.1.2.1 Capture using activated carbon – desorption pressure 5 kPa

Models representing beds with the sorbent AC were modelled to compare with zeolite 13X. As mentioned earlier AC has a low affinity towards water molecules (Sinnott and Towler, 2009). At a temperature of 293K and pressure of 1.23 kPa, the saturated adsorbed amount of H_2O on activated carbon is equal

to 0.253 mol/kg (Kim et al., 2005). Therefore it is assumed that capture using AC would not require a dehumidifier in the pre-capture unit. The flue gas from the CPS and the TBH will be cooled down to 25^{o}C and directed towards the capture unit. Assuming that the water molecules and oxygen will behave similarly to N_2 in the bed, it is fair to consider a binary gas flue gas consisting N_2 and CO_2. The flue gas entering the capture unit will have the compositions and conditions shown in Table 6-13. Similar to the adsorption benchmark model the flue gas will be split into forty six sections in the first stage of capture. In the capture unit for each stage the compressor will pressurise the flow gas to 110kPa before it enters the beds.

As understood from the breakthrough curves the separation using AC is a fast kinetic separation. This required the total cycle time to be set to a lower value than the adsorption benchmark model. This will allow the beds to regenerate after a quick saturation. The total cyclic time for stage was set as 450s, with the time for the adsorption and purge twice to that of pressurisation and blowdown.

The effect of purge/feed ratio on purity and recovery of CO_2 in stage 1 is shown in Figure 6-18. It is clear that the cross-over point for high purity and recovery is at about 14% purge/feed ratio. At this purge/feed ratio the purity of the concentrated CO_2 stream is less than 55 mol% of CO_2. It is necessary for the first stage to concentrate the CO_2 stream to a value of more than or equal to a mole fraction of 0.55 in CO_2. If this is not the case an additional third stage would be required to get an ultimate CO_2 purity of 95 mol% (to meet storage specification).

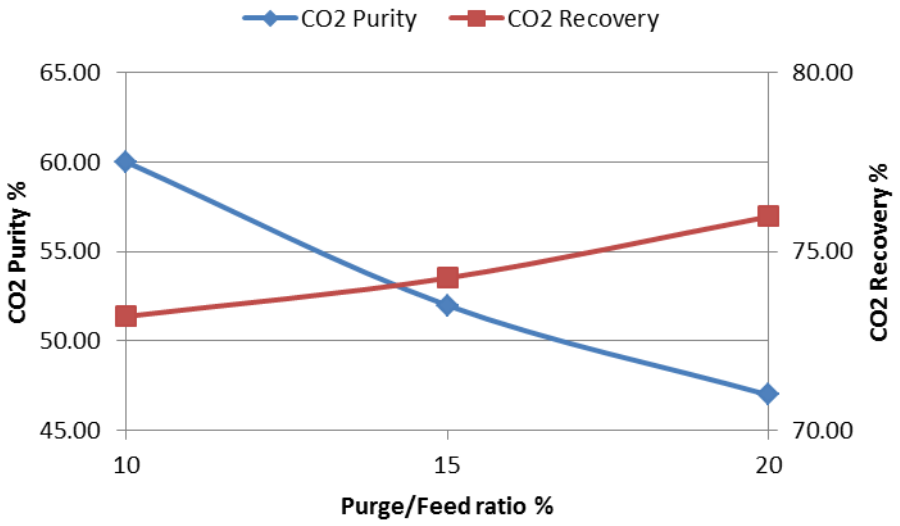

Figure 6-18: Variation of CO_2 purity and recovery for different purge to feed ratio in first stage of the capture unit (activated carbon – 5 KPa)

The model representing a 10% purge/feed ratio gives a concentrated CO_2 stream of purity 0.60 mole fraction. The other simulated models are less than 0.55 mole fraction CO_2. The product stream from the model representing the 10% purge/feed ratio was chosen as the inlet for stage 2 of the capturing unit. This meant stage 2 was receiving a concentrated CO_2 stream with purity of 60%. The recovery of carbon dioxide in the first stage was equal to 73.19%. In similarity to stage 1, the feed pressure was set to 110 kPa for stage 2. Stage 2 consists of a total of twenty three sections like the adsorption benchmark model. The total cycle time for stage 2 was set as 450s, in which adsorption and purge was twice the time of blowdown and pressurisation.

The second stage using AC was able to attain a purity of 95 mol% of CO_2 with a purge/feed ratio of 1%. The recovery of CO_2 in stage 2 is 91.02%. This meant the overall recovery of CO_2 for the capture unit using AC is equal to 66.62%. The captured CO_2 product stream from one section of stage 2 has a

flow rate of 158.55 kmol/h. With a total of twenty three sections in stage 2 the total flowrate of the captured carbon dioxide stream leaving the capture unit is equal to 3646.65 kmol/h (1.58 x 10^5 kg/h). This stream is then sent to the pre-transport compression unit to reach a final pressure of 11 MPa with a temperature of 30^{o}C and purity of 0.95 mole fraction CO_2. This fits the requirement for transport and storage.

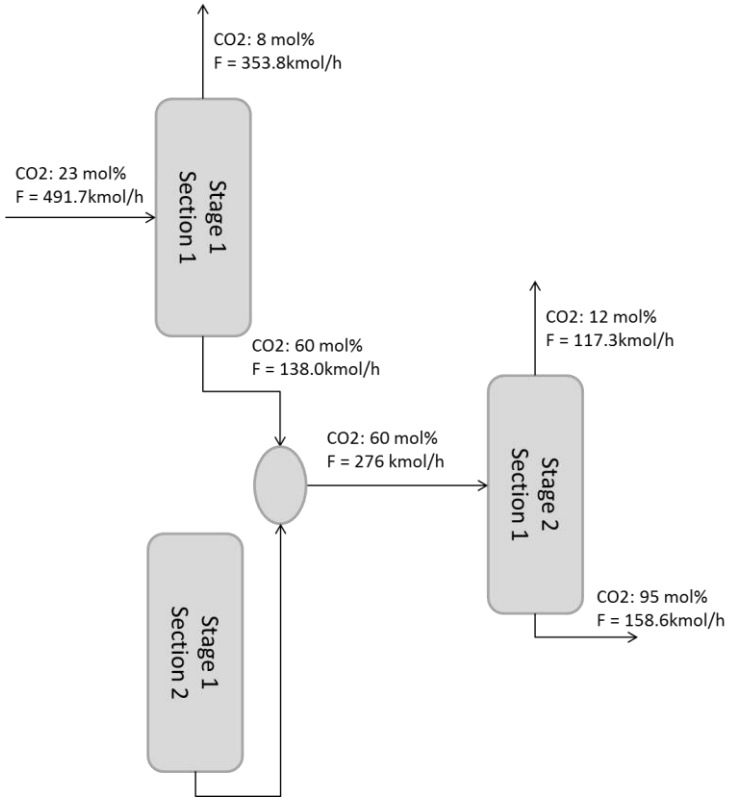

Figure 6-19: Mass balance of the two interacting stages of activated carbon capture (5kPa)

6.3.2 Economic evaluation of adsorption on ADSIM for CPS and TBH

The economy study was conducted for six different scenarios; costing with zeolite 13X at two different desorption pressures, costing using activated carbon, and all three above with complex controls with no intermediate tanks. The six different cases are summarised in Table 6-17. The ISBL boundary

starts after the desulphurisation of flue gas (Figure 6-11) and is assumed that the flue gas entering boundary is cleaned off particulates and oxides of sulphur. The pre-capture unit within the ISBL boundary varies in dependence of the sorbent used for capture. The stronger affinity of water molecules towards zeolite 13X requires a dehumidifier model with in pre-capture. Cases A-D will include the dehumidifier in economic analysis. This is not required for activated carbon so can be discarded for cases E and F. The rest of the units within the ISBL boundary are similar for all six cases.

Table 6-15: Summary of tables representing all six cases analysed for economic study

Cases		Sorbent	Controls complexity than MEA absorption	Desorption pressure (kPa)
A	with intermediate tanks	Zeolite 13X	66.7% more complex	5
B	no intermediate tanks	Zeolite 13X	166.7% more complex	5
C	with intermediate tanks	Zeolite 13X	66.7% more complex	10
D	no intermediate tanks	Zeolite 13X	166.7% more complex	10
E	with intermediate tanks	Activated carbon	66.7% more complex	5
F	no intermediate tanks	Activated carbon	166.7% more complex	5

6.3.2.1 CAPEX analysis

CAPEX analysis is calculated using the factorial method mentioned in Chapter 3. The factorial method represented by equation 3-3 was used to calculate the installed cost of all equipment in the ISBL boundary. The location factor and CEPCI index for 2013 are mentioned in Chapter 3 (Tables 3-1 and 3-2).

It was assumed that adsorption is more complex in controls and instrumentation, than the reference MEA capture model. This is due to the dynamic nature of adsorption. The adsorption models with intermediate tanks in between the capture stages (cases A, C and E) are assumed to be 66.7%

more complex than the MEA benchmark model. The elimination of intermediate tanks would increase controls and instrumentation complexity. This is due to interchanging compressors and vacuum pumps to operate with precision to time lag. Taking this into consideration it is assumed that the model without intermediate tanks (cases B, D, and F) will be 166.7% more complex than the MEA benchmark model. The complexity of controls and instrumentation will incur a high cost for capture. This is variation to the installed cost is included by changing the value f_i in equation 3-3.

6.3.2.1.1 Defining and sizing the dehumidifier unit

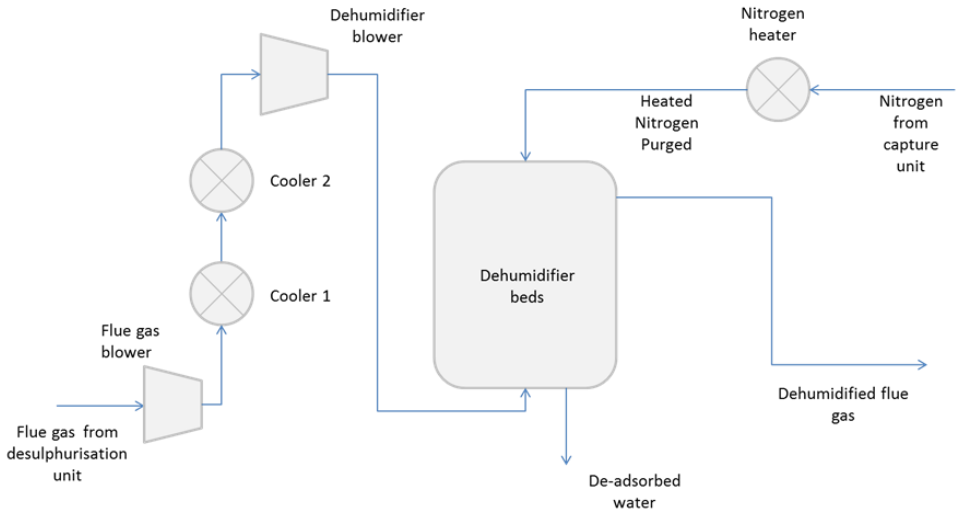

Figure 6-20: Pre-capture equipment for capturing using zeolite 13X

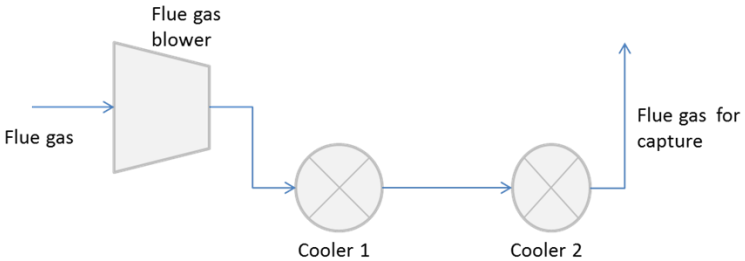

Figure 6-21: Pre-capture equipment for capturing using activated carbon

Figures 6-20 and 6-21 represents the pre-capture equipment for zeolite 13X and activated carbon respectively. Zeolite 13X needs to have a dehumidifier, to reduce moisture in flue gas to desired levels. There is less information in literature about desired flue gas humidity level that would have the least negative effects on carbon dioxide capture on zeolite 13X. Work done by Li et al. (2008) have looked into capturing carbon dioxide from 95% relative humid flue gas; the work concludes that high humidity has a detrimental effect on the capture level. It is mentioned by Li et al. (2008) that about 25% of the bed will be saturated by water molecules contributing to a lesser working capacity for carbon dioxide adsorption. In a pilot-scale experiment conducted by Wang et al. (2013) that the relative humidity of the flue gas entering the capture unit is set to less than or equal to 5%. There is no further mention if this level of humidity was sufficient to have the least detrimental consequence on capturing carbon dioxide.

The flue gas entering the ISBL boundary has a water content of approximately 50% relative humidity (Table 5-4 in Chapter 4). It is assumed in this study that the water content will be reduced to 5% or lower relative humidity to fall in line with the work conducted by Wang et al. (2013). A similar approach to Wang et al. (2013) using temperature swing adsorption with alumina as a sorbent has been considered as the dehumidifying model. The layout of the dehumidifying unit with pre-capture cooling is shown in Figure 6-20. Wang et al. (2013) have used a simple temperature swing desorption model, using the nitrogen separated in capture unit to regenerate the beds. In their work they have mentioned the nitrogen used to purge the dehumidifier beds needs to be heated to a temperature of 175^{o}C. Using the

isotherms presented by Serbezov (2003) on adsorption equilibria of water on activated alumina, the working capacity of the sorbent was estimated to be 0.04 kmol/kg. This working capacity is achievable with an adsorption temperature of 25^{o}C and a desorption temperature of 175^{o}C.

The flue gas from the desulphurisation unit enters the ISBL boundary at 50^{o}C and atmospheric pressure. It is blown through two heat exchangers to reduce the temperature to 25^{o}C, before it enters the dehumidifying blower. The dehumidifying blower blows the flue gas to elevate its pressure 110 kPa.

The flue gas entering the dehumidifying beds has a molar flow of 2.389x10^{4} kmol/h of which 5% is water. To achieve a relative humidity of 5% in the dehumidified flue gas, the dehumidifier should capture 1020.65 kmol of water per hour. The dehumidifier has got six beds undergoing two steps; adsorption and purge with heated nitrogen. Three beds are in adsorption phase for thirty minutes while the other three regenerate and cool down. It is also assumed that the adsorption of water on alumina is isothermal. Using these assumptions of how the beds are operating the working mass of alumina can be calculated for each bed to be 4252.71 kg. The size of the beds was calculated to accommodate the required mass of alumina. Similarly to the beds within the capture unit the beds within the dehumidification unit were set to have a height of 1m with a diameter to represent the required volume. The dehumidified flue gas from the alumina beds is then sent into the capture unit for adsorption of carbon dioxide. The nitrogen heater showed in Figure 5-19 heats a continuous flow of nitrogen stream from the capture unit. The flow rate of nitrogen used to purge the dehumidifying beds is assumed to be 10% of the flow rate of flue gas

entering the dehumidifying unit; therefore the nitrogen heater which is modelled as boiler uses steam to heat nitrogen, flowing at 2389kmol/h, from 25^{o}C to 175^{o}C.

6.3.2.1.2 CAPEX for all six cases

With the above definitions for the six different cases the installed CAPEX of all equipment within the ISBL boundary was calculated. The factorial method using equation 3-3 was used to calculate the individual unit cost and overall installed cost. The price of zeolite 13X is $5/kg of sorbent referenced from Ho et al. (2008b) and the price of alumina is assumed to be $20/kg. Activated carbon price is referenced from Xiao (2013) as $1.8/kg.

Table 6-16: Capital investment for all units within the IBSL for cases A-F

Equipment	Cost($M) case A	Cost($M) case B	Cost($M) case C	Cost($M) case D	Cost($M) case E	Cost($M) case F
Pre-capture						
Dehumidifier blower	2.92	2.92	2.92	2.92		
Dehumidifier beds	0.22	0.22	0.22	0.22		
Alumina	0.51	0.51	0.51	0.51		
Nitrogen heater	0.27	0.27	0.27	0.27		
Flue gas blower	2.97	2.97	2.97	2.97	2.97	2.97
Cooler 1	0.82	0.82	0.82	0.82	0.82	0.82
Cooler 2	1.23	1.23	1.23	1.23	1.23	1.23
Capture-Stage 1						
Adsorber beds	4.00	4.00	4.00	4.00	3.92	3.92
Sorbent	2.48	2.48	2.48	2.48	0.79	0.79
Compressors	10.98	11.95	10.98	11.95	10.98	11.95
Vacuum pumps	18.63	20.28	16.82	18.30	17.44	18.98
Capture-Stage 2						
Adsorber beds	2.06	2.06	2.06	2.06	2.06	2.06
Sorbent	1.48	1.48	1.48	1.48	0.53	0.53
Compressors	4.94	5.37	4.76	5.18	4.32	4.70
Vacuum pumps	11.32	12.32	9.76	10.62	9.90	10.77
Tanks						
Floating roof tanks	10.16		9.87		9.16	
Compression						
Compression unit	32.44	32.44	27.60	27.60	28.89	28.89
Total Installed ISBL CAPEX	107.36	101.32	98.73	92.60	93.00	87.60
OSBL + Contingency	1.60	1.60	1.60	1.60	1.60	1.60
Fixed Capital Investment (FCI)	171.77	162.11	157.97	148.16	148.80	140.16

In similarity to the MEA benchmark model the life span of all the units within the ISBL boundary is assumed to be 30 years. The FCI_{annual} mentioned in equation 3-4 was calculated for all six cases with an interest rate of 10%, and is summarised in Table 6-17.

Table 6-17: Annual fixed capital investment for all six cases

	Cost ($M/year)					
	Case A	Case B	Case C	Case D	Case E	Case F
Fixed Capital Investment (FCI)	18.22	17.20	16.76	15.72	15.78	14.87

6.3.2.2 OPEX analysis

In similarity to the MEA benchmark the operational hours per annum was set at 8000 to ensure more than 90% operation per year. The total operating cost (TOC) per annum is a summation of the fixed operational cost (FOC) and the variable operational cost (VOC) as mentioned in Chapter 3 (Sinnott and Towler, 2009, Karimi et al., 2011)

6.3.2.2.1 Fixed operating cost (FOC)

The breakdown of the factors contributing to FOC is detailed in Chapter 3 (Table 3-3). For capture using adsorption the overall FOC and its breakdown is summarised in Table 6-18 for cases A-F.

Table 6-18: Fixed operating costs for cases A-F

	Cost ($M/year)					
Costing Factor	**Case A**	**Case B**	**Case C**	**Case D**	**Case E**	**Case F**
Labour Cost	0.3	0.3	0.3	0.3	0.3	0.3
Supervision Cost	0.075	0.075	0.075	0.075	0.075	0.075
Direct Salary Overhead	0.153	0.153	0.153	0.153	0.153	0.153
Maintenance	3.22	3.04	2.96	2.78	2.79	2.63
Property Taxes and Insurance	1.07	1.01	0.10	0.93	0.93	0.88
Property Insurance	1.07	1.01	0.10	0.93	0.93	0.88
General Plant Overhead	1.50	1.43	1.40	1.32	1.33	1.26
Environmental Charges	1.72	1.62	1.58	1.48	1.49	1.40
Total (FOC)	9.11	8.64	8.44	7.96	7.99	7.57

6.3.2.2.2 Variable operating cost (VOC)

A total of five shift positions are assumed to be required to operate the plant, similarly to the benchmark model using MEA. A shift position costs

$60,000 per annum according to Sinnott and Towler (2009), therefore the total cost of labour is equal 0.3 million dollars per annum.

The VOC is made up of the following individual costs for the models representing adsorption using zeolite 13X and activated carbon

- Degradation of sorbent
- Electricity cost
- Cooling water cost
- Waste to landfill cost
- Alumina recycling cost (only for cases A-E)
- Steam for nitrogen heater (only for cases A-E)

The sorbent zeolite 13X used for capture has a life time of 5 years as mentioned by Xiao (2013) A thirty year lifetime capture unit would have six changes of sorbent in its lifetime. The lifetime of activated carbon is also five years as mentioned by Xiao (2013). Approximately 792.57 tonnes of zeolite 13X and 732.5 tonnes of activated carbon are used in the two stages of the capture unit. With the assumption of six changes for thirty years; cost of zeolite 13X per annum is $M 0.79 and cost of activated carbon per annum is $M 0.26. The price of zeolite 13X used is $5/kg and activated carbon is used as $1.8/kg (Ho et al., 2008b, Xiao, 2013).

The breakdown of electricity usage throughout the ISBL boundary for cases A-F is mentioned in Table 6-19. Equation 6-24 was used to calculate the electricity consumed by the blower and vacuum pump. With annual operational hours of 8000, the total kWh of electricity usage and its reference cost was

calculated for each case. Assuming that electricity is purchased from the wholesale market at a price of $0.07/kWh, the cost of electricity for all four cases were calculated (Sinnott and Towler, 2009). Cases A and B has a total electricity cost of $M 31.35 per annum. Cases C and D has total electricity cost of $M 25.97 per annum. Cases E and F has a total electricity cost $M 26.07 per annum.

Table 6-19: Electricity usage breakdown throughout the ISBL boundary for cases A-F

Unit	Electricity (MW) Case A & B	Electricity (MW) Case C & D	Electricity (MW) Case E & F
Pre-capture			
Blower	0.32	0.32	0.32
Dehumidifier blower	1.98	1.98	
Capture			
Compressors	1.90	1.86	1.77
Vacuum pumps	32.99	27.77	28.94
Compression			
Compression Unit	18.80	14.43	15.52
Total	55.99	46.37	46.56

The cost of cooling water treatment and makeup is assumed to be $0.0042 per tonne of water with reference to Sinnott and Towler (2009). The breakdown of water circulation within the units is mentioned in Table 6-20. The cost for cooling water for all cases A and B was calculated to be $M 0.11. The cost of cooling water for cases C-F was calculated to be $M 0.09.

Table 6-20: Cooling water circulation throughout the ISBL boundary for cases A-F

Unit	Cooling water circulation (kg/h)		
	Cases A & B	Cases C & D	Cases E & F
Pre-capture	3.59×10^5	3.59×10^5	3.59×10^5
Compression Unit	2.87×10^6	2.22×10^6	2.42×10^6
Total	3.23×10^6	2.58×10^6	2.78×10^6

As mentioned earlier about the life time of zeolite 13X and activated carbon to be 5 years. The end of life sorbent would be required to be sent to landfill once every five years. The total consumption of sorbent within the capture unit is 792.57 tonnes of zeolite 13X and 732.5 tonnes of activated carbon respectively. The cost to landfill mentioned by Sinnott and Towler (2009) is $50/tonne. The cost to landfill the end of life zeolite 13X is $7900 per annum (for cases A-D). Similarly the cost to landfill the expired activated carbon is $7300 per annum (for cases E-F).

The alumina used in the dehumidifier beds for zeolite 13X models is assumed to have a lifetime of 5 years. After five years the alumina is recycled at a cost of $10/kg. The total amount of alumina used in the dehumidifier beds is 25.51 tonnes. Therefore recycling alumina would cost $M 0.05 per annum (for cases A-D).

Steam at 180^{o}C and pressure of 1 MPa is used to heat the nitrogen that is used to purge the dehumidifier beds. 5083 kg/h of steam at the above conditions is required to heat the purging nitrogen stream from 25^{o}C to 175^{o}C. For a year the total steam used by the nitrogen heater is 40664 tonnes. The price of steam at the conditions required is assumed to be $13.5/tonne using the

information given by Sinnott and Towler (2009). The total cost of steam per annum is calculated to be $M 0.55 (for cases A-D).

The breakdown of all the individual operating cost contributing towards VOC is summarised in Table 6-21.

Table 6-21: Individual variable operating cost within ISBL cases A-F

	Cost ($M)/per year		
Variable Operating Cost	**Case A & B**	**Case C & D**	**Case E & F**
Electricity usage	31.35	25.97	26.07
Degrading of sorbent	0.79	0.79	0.26
Cooling water	0.11	0.09	0.09
Waste to landfill	0.008	0.008	0.007
Alumina recycling	0.05	0.05	
Steam generation	0.55	0.55	
Total VOC	32.86	27.45	26.44

The total operating cost (TOC) per annum for all six cases as a summation of FOC and VOC is summarised in Table 6-22.

Table 6-22: Total operating cost per annum for all cases A-F

	Cost ($M/year)					
	Case A	**Case B**	**Case C**	**Case D**	**Case E**	**Case F**
Fixed Operating Cost (FOC)	9.11	8.64	8.44	7.96	7.99	7.57
Variable Operating Cost (VOC)	32.86	32.86	27.45	27.45	26.44	26.44
Total Operating Cost (TOC)	41.97	41.50	35.89	35.42	34.43	34.01

6.3.2.3 Cost of capturing CO_2 – adsorption models

The total annual capture cost (TACC) is a summation of total operating cost (TOC) and annual fixed instalment cost (FIC_{annual}). For cases A-F the summary of TACC is highlighted in Table 6-23.

Table 6-23: Total annual capture cost for all cases A-F

	Cost ($M/year)					
	Case A	Case B	Case C	Case D	Case E	Case F
Fixed Investment Cost	18.22	17.20	16.76	15.72	15.78	14.87
Total Operating Cost	41.97	41.50	35.89	35.42	34.43	34.01
Total Annual Capture Cost	60.20	58.70	52.65	51.13	50.21	48.88

The amount of carbon dioxide captured for each case depends on the purity and flow rate of the captured stream leaving the compression unit. The results obtained from the technical analysis were used to obtain the amount of carbon dioxide captured for all six cases. It is summarised in Table 6-24.

Table 6-24: Amount of carbon dioxide capture for all cases (A-F)

Case	CO2 captured (Mtonnes/year)
A	1.50
B	1.50
C	1.14
D	1.14
E	1.22
F	1.22

Using equation 3-6 the cost of capturing carbon dioxide can be calculated. The cost of carbon dioxide captured for all six cases (A-F) is represented in Table 6-25.

Table 6-25: Cost of carbon dioxide captured for all cases (A-F)

	Case A	Case B	Case C	Case D	Case E	Case F
Cost of CO2 captured ($/tonne of CO2)	40.12	39.13	46.12	44.79	41.06	39.96

The cost of carbon dioxide avoided explained in Chapter 3, would be a better representation of the economic results to compare with published literature. Similarly to the MEA benchmark model indirect emissions from electricity and steam consumed will only be used. Other emissions from consumables such as cooling water and waste disposal are excluded. This assumption is based on the fact that steam and electricity are largest contributors for the variable costs.

The emissions for generating steam and electricity are 0.219kgCO_2/kWh_{th} and 0.491kgCO_2/kWh_e respectively as obtained from (DECC, 2011). Using these values the net carbon dioxide captured for each case was calculated. The results are shown in Table 6-26.

Table 6-26: Net CO_2 captured for all cases (A-F)

	CO_2 per annum (Mtonnes)		
	Case A & B	Case C & D	Case E & F
Total amount of CO_2 captured	1.50	1.14	1.22
CO_2 emitted form electricity usage	0.19	0.16	0.16
CO_2 emitted from steam usage	0.01	0.01	0.0
Net CO_2 captured	1.31	0.98	1.07

With the net carbon dioxide captured calculated. The cost of carbon dioxide avoidance can be calculated using equation 3-7. The results are shown below in Table 6-27.

Table 6-27: Cost of carbon dioxide avoided for all cases (A-F)

	Case A	Case B	Case C	Case D	Case E	Case F
Cost of CO2 avoided ($/tonne of CO2)	46.04	44.90	53.68	52.13	47.06	45.81

To compare the results obtained with published literature data, the cost needs to be amended to include the desulphurisation unit. In Chapter 5 the desulphurisation unit's installed ISBL CAPEX and OPEX were estimated using the work done by Singh et al. (2003). A similar approach was used for models using adsorption. The amended cost for including a desulphurisation unit is summarised in Table 6-28.

Table 6-28: Amended cost of carbon dioxide avoided for all cases with inclusion of the desulphurisation unit (A-F)

	Amended cost with desulphurisation unit included					
	Case A	*Case B*	*Case C*	*Case D*	*Case E*	*Case F*
Cost of CO2 avoided ($/tonne of CO2)	52.43	51.28	62.18	60.64	54.88	53.63

There are only few published works available that has analysed techno-economically the possibilities of applying large scale capture using adsorption. Most of the work is either lab-scale or pilot scale study, with no economic analysis. Ho et al. (2008b) have analysed capturing carbon dioxide using vacuum swing adsorption from flue gas of a coal fired power plant. The author concluded the cost of avoidance is \$56/tonne of CO_2 avoided. The author used zeolite 13X as the sorbent. The cost of capture is higher than case A and B in this study. It is mentioned by Ho et al. (2008b) that the high cost was contributed from the post-capture compression. The work done by Ho et al. (2008b) was only able to achieve a carbon dioxide purity of 48% mole. This increased the presence of other gaseous molecules in the final product stream. Therefore a large volume of gas needed to be compressed by the post-capture compressors leading to a higher cost. Kuramochi et al. (2012) have mentioned

in their work that capturing carbon dioxide using vacuum swing adsorption from the top gas recycling blast furnace costs approximately $53/tonne of CO_2 avoided. This is quoted from the work done by ULCOS. Top gas recycling blast furnace uses a complex process involving flue gas cooling before pre-capture and cryogenic separation in the final stage to reach required purity (Meijer et al., 2009). Therefore the process varies and is more complex than the one proposed in this study.

Overall it can be concluded that the results obtained in this study are similar to other published literate mentioned above. The cost of CO_2 capture using adsorption needs to be compared with the results obtained for amine scrubbing. The next chapter will consider this.

7 Discussion on Performance of Models

This chapter will look into the models created in HYSYS and ADSIM and comment on its performance in a discursive way.

7.1 Chemical Absorption Model on HYSYS

Chemical absorption is currently the most mature technology for carbon capture. As a benchmark study, capturing using MEA chemical absorption was modelled. The initial model created on Aspen HYSYS was compared with the work done by Tobiesen et al. (2007). The important design factors; CO_2 recovery, CO_2 production rate and steam consumption in the reboiler were compared. The model in HYSYS showed 0.13% and 0.02% less CO_2 recovery and production respectively. Steam consumption in the HYSYS model was showing an increase of 4.77%, when compared with the work of Tobiesen et al. (2007). Further investigation showed that the model in HYSYS had a comparatively lower temperature for the CO_2 rich solvent stream from the absorber column. This meant that the work by Tobiesen et al. (2007), had a comparatively higher temperature for the feed to regenerator column. Therefore reducing the duty of the reboiler, this showed 4.77% less steam consumption than that of the model created n HYSYS.

The heat of absorption in the absorber column was investigated by replicating a calorimeter experiment in HYSYS. The results were compared with the work of Kim and Svendsen (2007). The results showed that the equilibrium model in HYSYS was able to accurately display the heat of adsorption for solvent loadings below 0.5 mol CO_2/mol MEA. At solvent loadings higher to this value, the saturation point is reached and the heat of

absorption decreases quickly. This phenomenon was not displayed in HYSYS. Therefore it was concluded that the lean loading of the aqueous solvent fed to the absorber column should be below 0.5 mol CO_2/mol MEA.

7.1.1 Performance analysis of MEA scrubbing model for the steel mill

The model created in ASPEN HYSYS was modified to represent the studied steel mill. The percentage breakdown of the variable operational costs is shown in Figure 7-1. The largest variable operation cost is for the steam used in the reboiler to strip the MEA from the carbamate formed. This endothermic process involves high energy consumption and contributes to 61% of total variable operation cost. Electricity usage throughout the ISBL boundary contributes 27% of variable operation cost and is the second largest. The compression unit uses the most electricity when compared to two units (capture and pre-capture). A series of compressors followed by a pump is required to achieve the transport standard carbon dioxide product stream. The compressors and the pump in the compression unit use approximately 88% of the total electricity. A breakdown of the percentage electricity usage is shown in Figure 7-2.

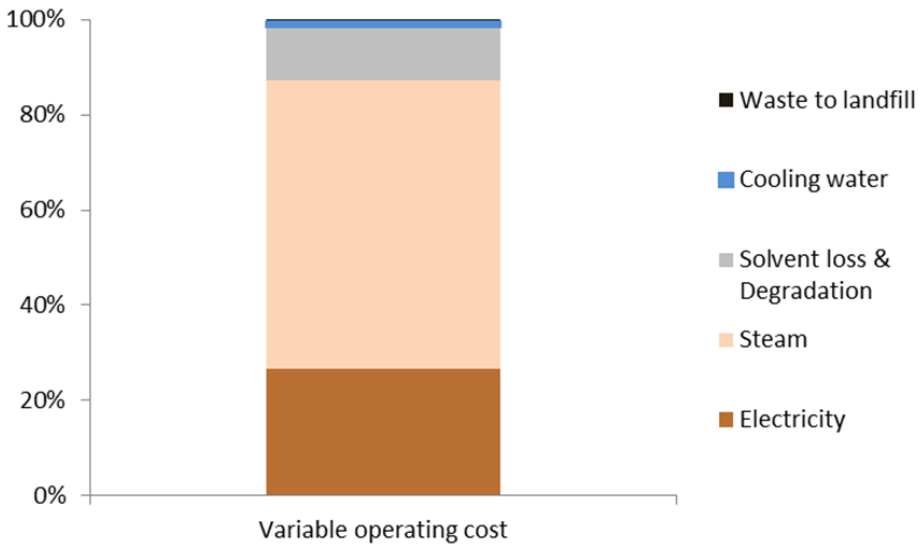

Figure 7-1: Breakdown of MEA benchmark model variable operation cost per annum (VOC total = $M 41.08)

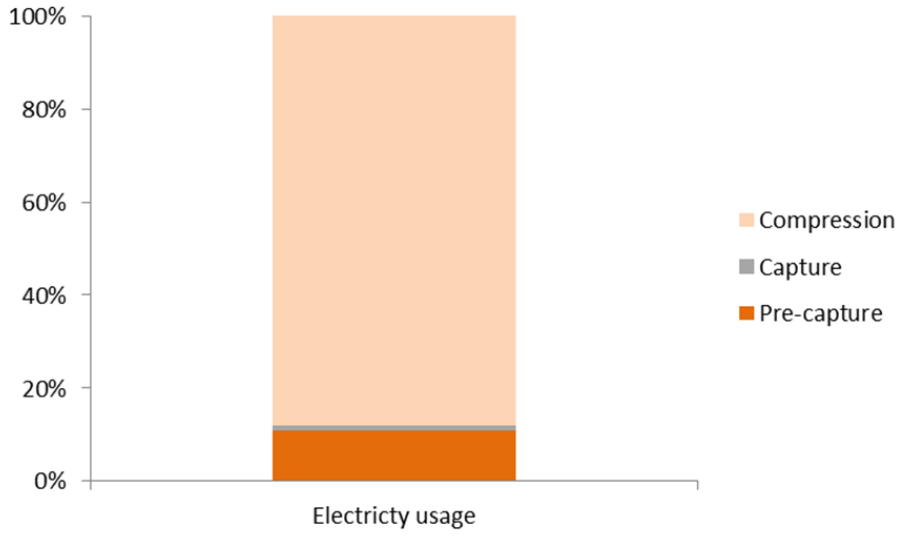

Figure 7-2: Breakdown of MEA benchmark electricity usage per annum (Total electricity usage = $M 10.9)

It is necessary for the model to represent accurately the steam consumption in the reboiler because this contributes the largest variable operational cost. There are few published studies available on capturing CO_2 from steel mill conditions using chemical absorption. Arasto et al. (2013) used rate based

chemical absorption in their study, and investigated capturing from an in-house power station in a steel mill. The MEA benchmark study in this research is similar to the work of Arasto et al. (2013), but has used equilibrium based separation and has considered a larger flow rate of flue gas. Other studies have investigated capturing from coal and natural gas fired power plants (Abu-Zahra et al., 2007b, Hamborg et al., 2014). The reboiler duty from this study was compared with published results and is illustrated in Table 7-1. The reboiler duty calculated by Aspen HYSYS as part of this study is within the range of published data, and therefore the operational cost can be considered accurate for conditions modelled.

Table 7-1: Comparison of reboiler duty of MEA benchmark model with other published work

	Reboiler duty ($MJ/kgCO_2$)	
This work	3.45	Flue gas from steel works
Aresto et al., 2013	3.40	Flue gas from steel works
Abu-Zahra et al., 2007a	3.9	Flue gas from coal fired burners
Hamborg et al., 2014	4.1	Flue gas from natural gas fired burners

The breakdown of capital instalment cost for MEA benchmark model is shown in Figure 7-3. It is clear that about 48% of the instalment cost is from the final phase of the process; the compression unit. The transport by pipeline standard requirement of carbon dioxide mentioned in literature is a liquefied phase of pressure 1.10×10^5 kPa (Baldwin, 2009, Karimi et al., 2011). The post-capture compressing unit consists an initial stage for compressing carbon dioxide to above its critical pressure and another stage for pumping the

liquefied carbon dioxide to 1.10 x 10^5 kPa. This is achieved by a series of compressors and pumps. It was seen earlier that the compression unit uses the largest percentage of the electricity consumed. It also has the largest percentage of installed cost due to it having many compressors, coolers and pumps to achieve the final standard of carbon dioxide for transport by pipeline.

The absorber and regenerator column contribute to about 26% of total installed cost; of which the absorber column is more expensive due to its larger size and more packing. This pattern has been observed by other studies on chemical absorption (Singh et al., 2003, Abu-Zahra et al., 2007a). Costing of the other equipment (heat exchangers, pumps and blowers), make up approximately 22% of the total installed cost. Make up tanks and raw materials required for start-up is approximately 4% of total installed cost.

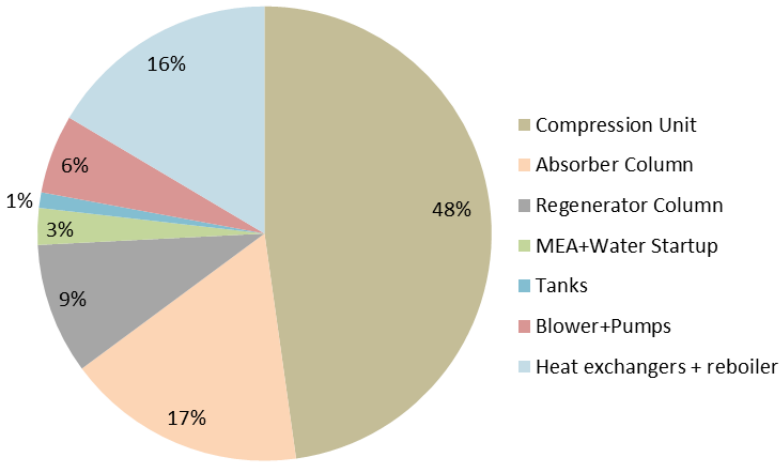

Figure 7-3: Breakdown of installed capital cost for MEA benchmark model (Total installed cost =$M 64.34)

Table 7-2 shows a comparison of installed cost for this study with the study done by Singh et al. (2003). Singh et al. (2003) have considered auxiliary units

and sulphur dioxide removal unit in their study. These have been excluded to match this study. The total carbon dioxide captured for the study done by Singh et al. (2003) is 2.41 Mtonnes/year, and is 40% more carbon dioxide captured than this research study. To normalise the scale of installed with the amount of CO_2 captured, installed cost per tonne of carbon dioxide captured per annum was calculated. This allows comparing of the installed cost of studies with different capacity. The results of installed cost for this study is less by approximately 3% when compared to the work of Singh et al. (2003).

Table 7-2: Comparison of ISBL installed cost of MEA benchmark model with published literature

	ISBL installed cost {$/[(tonne CO2 captured/year)]}
(Singh et al., 2003)	36.48
(This study)	37.63

In addition to installed ISBL (Inside Battery Limit) cost shown in Figure 7-3, the (OSBL) outside boundary limit and contingency charges needs to be included to calculate the fixed capital investment as explained in Chapter 3. There is a discrepancy of how the OSBL cost and contingency charge is calculated. Singh et al. (2003) have mentioned that the total OSBL and contingency charges are equal to approximately 45% of the installed ISBL cost. Sinnott and Towler (2009) have mentioned that OSBL and contingency is equal to 82% of total installed ISBL cost is the technology is uncertain. This research has assumed that the total OSBL and contingency charge is equal 60% of the ISBL installed cost. The normalised overall fixed capital investment in

terms of amount of carbon dioxide captured per annum compared with Singh et al. (2003) is shown in Table 7-3.

Table 7-3: Comparison of FCI cost of MEA benchmark model with published literature

	Fixed Capital Investment {$/[(tonne CO2 captured/year)]}
(Singh et al., 2003)	53.11
(This study)	58.32

The overall cost of carbon dioxide avoidance for this research was compared with other values in published literature and is within the range of captured cost as shown in Chapter 5. The overall cost of carbon dioxide avoidance for this study was calculated as \$44.92/tonne CO_2 without the desulphurisation unit. As seen earlier, a large percentage of this cost is from the installation and operation of the compression unit. If the captured carbon dioxide can be utilised on-site, the compression for transport/storage can be eliminated. There are different ways in which the captured carbon dioxide can be utilised on-site. Carbon dioxide mitigation by mineral carbonation and micro-algae farming have been mentioned as two promising methods for industries such as steel making (Metz et al., 2005). If the captured carbon dioxide can be utilised in these methods, the overall capture cost can be reduced.

Another large contribution for the overall cost is from the steam consumed in the reboiler of the regenerator. Using advanced solvent that has a lower regeneration energy requirement would enable reduction in steam usage. Arasto et al. (2013) have considered an advanced solvent, which requires steam

energy at 2.7 MJ/kg of CO_2 and noticed less steam usage for carbon dioxide recovery. A more advanced future model could use a solvent that uses a significantly lower temperature for regeneration than MEA. Arasto et al. (2013) have used a hypothetical solvent that regenerates at a temperature of 70^{o}C. This would be advantageous for the steel industry, because waste heat streams within steel making could be used for regeneration of the solvent.

Other possible measures to reduce cost of capture could be applied to the absorption and desorption columns. The columns are packed with stainless steel packing, because of the corrosive nature of the MEA solvent. Using less corrosive solvent would enable cheaper packing to be used and reduce overall cost. Abu-Zahra et al. (2007a) have identified this in their work

7.2 Adsorption Model on ADSIM

The models created in Aspen ADSIM (previously known as ASPEN Adsorption) to represent capture using vacuum swing adsorption (VSA) were assumed isothermal. Similar assumption have been made by Ho et al. (2008b), when modelling a techno-economic study for a large scale carbon dioxide capture study. The initial task in this study was to investigate equilibrium and kinetic parameters for adsorption for the two sorbents zeolite 13X and activated carbon. Breakthrough curves were modelled in Aspen ADSIM, for the two sorbents, to validate the parameters used. The results were compared with published literature of Shen et al. (2011) and Wang et al. (2012b). The results showed that the breakthrough curves from ADSIM agreed on the bed saturation point. The saturation point in the bed is when the breakthrough curve starts to show a variation to the CO_2 mole fraction in the decarbonised gas.

After the bed saturation point, the breakthrough curves differed in terms of steepness and the time elapsed for the full saturation of the bed. It was noted that the isothermal assumption, complex diffusivity and different forms of the equilibrium equation are the causes for the discrepancy in the breakthrough curves. It was also not that the nature of this study is investigating cyclic bulk CO_2 separation. For bulk cyclic separation the beds will get regenerated as soon as it reaches its saturation point, therefore the models in ADSIM are sufficient for this study.

The models created in Aspen ADSIM were then scaled up to investigate its performance in comparison with other lab scale cyclic process. Lab scale 4 step Skarstom cyclic process were mimicked in Aspen ADSIM with reference to the studies of Shen et al. (2012) and Wang et al. (2012a). ADSIM models showed an increase in purity and recovery of CO_2 when compared with the results of Shen et al. (2011) and Wang et al. (2012a). It was noted that isothermal assumption and not using pure N_2 to purge in ADSIM were the reason for the discrepancy.

The labs scale 4 step Skarstom cycle model was then scaled up to model CO_2 capture from the studied steel mill.

7.2.1 Performance analysis of adsorption for the steel mill

As part of this study, the two adsorbents zeolite 13X and activated carbon were modelled to capture the emission form the referenced steel mill. To achieve high purity in the final carbon dioxide product stream, there was a requirement to have more than one stage of separation. This required intermediate tanks

between the stages to control a steady a flow. As a further investigation, models were created excluding the intermediate tanks. These models were assumed to be 60% more complex in controls of the valves connected to the flue gas compressor and the vacuum pump, therefore having a higher installed capital expenditure. Overall six different cases were modelled and analysed techno-economically.

The overall percentage breakdown of the variable operating cost of the six cases is illustrated in Figure 7-4. It can be seen that in all six cases the largest contributor for the variable operating cost is electricity. Electricity contributes to more than 94% in all cases. Steam and alumina recycling cost are applicable for the cases using zeolite 13X only. They are used in the dehumidifier unit before capture for cases with zeolite 13X. Solvent loss and degradation is the second largest contributor for the overall variable operating cost. The price of zeolite 13X is more expensive than activated carbon; therefore sorbent replacement is more expensive. This variation in prices is showing that the models using zeolite 13X has a higher sorbent replacement cost than activated carbon. Other costs like waste to landfill and cooling water are small for both sorbents.

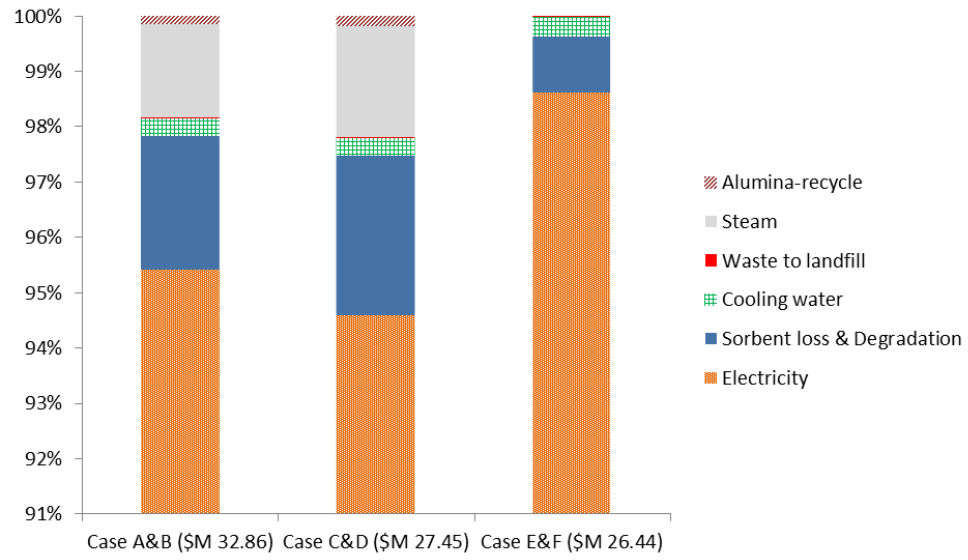

Figure 7-4: Percentage breakdown of variable operating cost per annum for all cases (A-F)

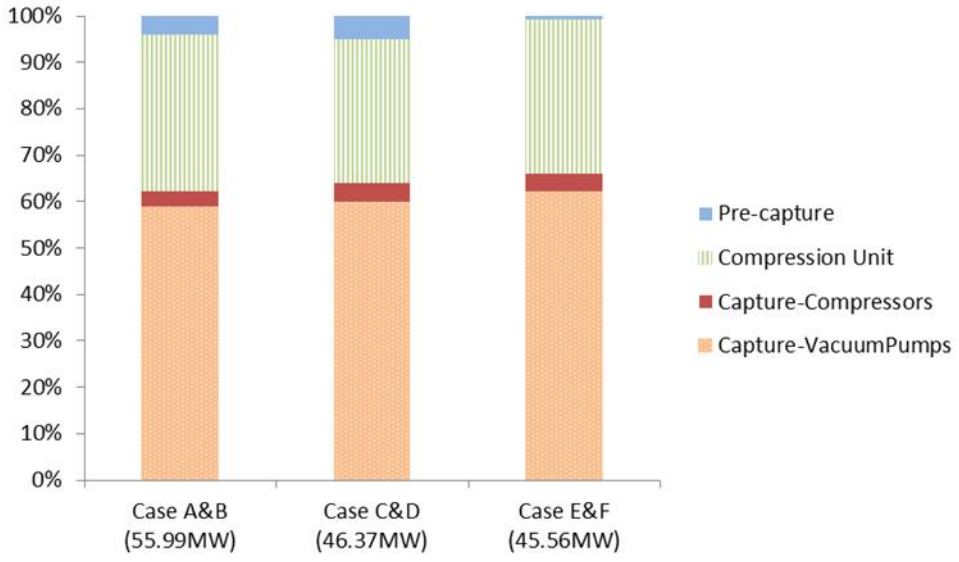

Figure 7-5: Percentage breakdown of electricity usage per annum within ISBL boundary for all cases (A-F)

To understand the breakdown of the electricity usage within the ISBL boundary a percentage breakdown of electricity usage was plotted for all cases. The results are illustrated in Figure 7-5. Vacuum pumps in the capture unit are the largest users of electricity; approximately 59-62% of electricity is consumed by the vacuum pumps in all six cases. This is the result of achieving

low vacuum pressures during regenerations of the beds. The feed gas compressors within the capture unit use comparatively less electricity than the vacuum pumps. The pressure ratios in which the feed gas compressors and the vacuum are operating defines the amount of electricity consumed. All cases have been modelled as vacuum swing adsorption; therefore the feed gas is compressed just above atmospheric pressure. In the models simulated the feed gas was compressed to a pressure of 110 kPa, therefore the pressure ratio is approximately 1.2: 1. The regeneration pressures varied for different cases; for cases A, B, E and F the pressure was set at 5 kPa and for the cases C and D the pressure was set at 10 kPa. The pressure ratios were approximately 20: 1 and 10: 1 for 5kPA and 10kPa respectively. To achieve these high pressure ratios a high amount of electricity is consumed in the vacuum pumps. Ho et al. (2008b) and Wang et al. (2013) have identified this in their studies. Working in low vacuum pressures to increase purity and recovery in the carbon dioxide product stream has a trade-off of a higher consumption of electricity.

To understand the power consumed by the feed gas compressors and vacuum pumps the specific power was calculated for capturing carbon dioxide. The specific power is given by the equation 7-1. The results are compared with other published literature (Shen et al., 2012, Wang et al., 2012a, Wang et al., 2013). The comparison is shown in Table 7-4. The specific power calculated in this study is within the range of 650-750 kJ/kgCO_2. This is similar to the other works compared in Table 7-4. It is to be noted that the other published works have considered different cyclic process, involving steps like pressure equalisation, and rinse. These steps are present to reduce energy usage in the

capture process. The models simulated in this study have not considered additional energy conserving steps.

Equation 7-1: Specific power consumption (feed gas compressors + vacuum pumps) for capturing carbon dioxide

$$Specific\ power\ = \frac{Electricty\ used\ per\ annum\ (Feed\ compressors + vacuum\ pumps)\ (kJ)}{CO_2\ captured\ per\ annum\ (kg)}$$

Table 7-4: Comparison of other published work on specific power for capturing carbon dioxide by adsorption (Z13: zeolite 13X and AC: activated carbon)

Process	*Adsorbent*	*Feed CO_2 mole %*	*Regeneration pressure*	*CO_2 purity %*	*CO_2 recovery %*	*Specific power (kJ/kgCO_2)*	*reference*
2 stage VPSA	AC	15	10 kPa	95.36	73.62	723.19	Shen et al., 2012
2 stage VPSA	AC	15	5 kPa	96.40	80.42	831.53	Shen et al., 2012
2 successive VPSA	Z13X	15	10 kPa	96.54	93.35	528.39	Wang et al., 2012a
2 successive VPSA	Z13X	15	6 kPa	96.61	97.88	594.01	Wang et al., 2012a
2 stage VPSA	Z13X first stage and AC second stage	16	First stage – 7-8 kPa Second stage – 20 kPa	95.6	90.2	756.0	Wang et al., 2013
2 stage VSA	Z13X	23	5 kPa	96	81.80	652.49	This study
2 stage VSA	Z13X	23	10 kPa	95	61.97	748.55	This study
2 stage VSA	AC	23	5 kPa	95	66.62	724.96	This study

The percentage breakdown of the ISBL installed cost for the six cases (A-F) is illustrated in Figure 7-6 and Figure 7-7. It is clear that the overall installed costs for cases without intermediate tanks are cheaper than their counterpart. The intermediate tanks were cost estimated as floating roof tanks, and was assumed that twelve tanks would be required in between the stages for the models. The tanks contribute to approximately 10% of the total installed cost, causing models having them to be more expensive than their counterparts even when they were modelled with high complexity in controls

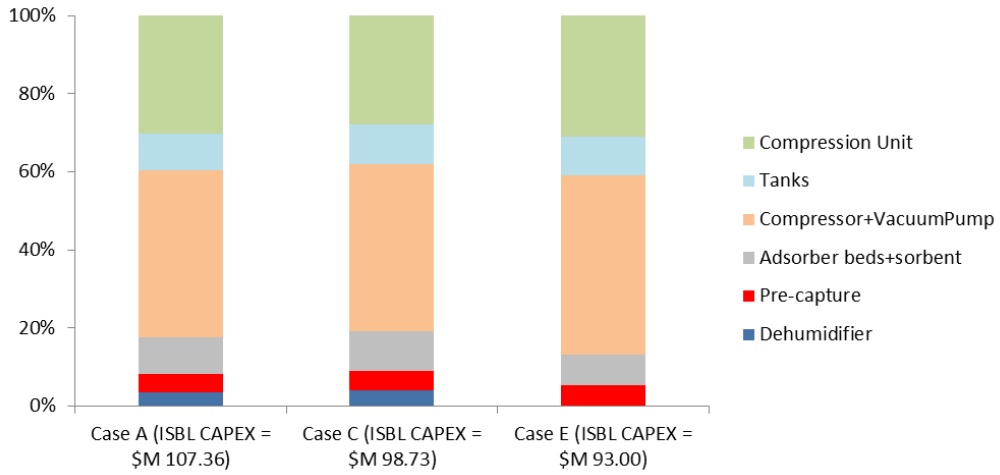

Figure 7-6: Percentage breakdown of ISBL installed cost for cases with intermediate tanks (A, C and E)

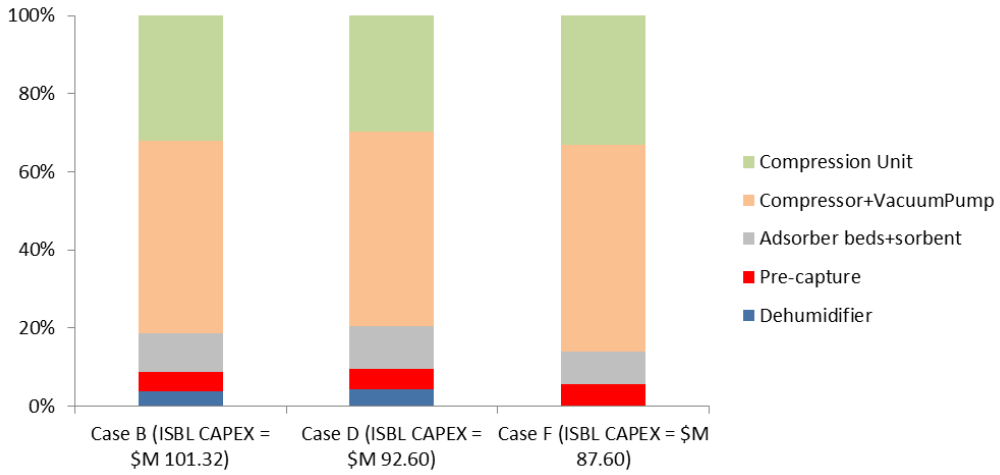

Figure 7-7: Percentage breakdown of ISBL installed cost of cases without intermediate tanks (B, D and F)

The largest contribution for the ISBL installed cost is from the compressors and vacuum pumps in the capture unit. The large flow rate of the flue gas required to be compressed by the compressors, and the high pressure ratio set to be achieved by vacuum pumps require an expensive installed cost. It contributes to approximately 43-53% of the total installed cost. In similar to the electricity usage, the total installed cost is largely contributed by vacuum

pumps. The post-capture compression unit is the second largest contributor to the total installed cost. It contributes approximately 29-32% of the total installed cost. The final carbon dioxide product is required to be compressed to 1.1 x 10^4 kPa for transport by pipelines and therefore requires a series of compressors and pumps to achieve this. The installed cost of vacuum pumps is more expensive than feed gas compressors, because of the high pressure ratio it works on. The cost of beds and sorbents in the capture unit are relatively less when compared to compressors and vacuum pumps. It contributes to approximately 8-11% of the total installed cost. Other costs from the dehumidifier and pre-capture unit contribute to approximately 5-10% of the total ISBL installed cost.

The need to work at very low vacuum to achieve desired purity and recovery of carbon dioxide is consuming a lot of electricity and requires a high capital investment. The equilibrium properties of the sorbent especially zeolite 13X requires regeneration at lower pressures. Working at higher vacuum reduces the overall recovery of carbon dioxide as seen from models using 10 kPa desorption pressure. With the decrease in overall recovery the specific power consumed by the compressors and vacuum pump increases, therefore increasing the cost of capture. This can be seen in Table 7-4.

7.3 Comparison of Chemical Absorption and Adsorption

The performance of capturing carbon dioxide by adsorption, for the six different cases, is compared with the benchmark model using MEA absorption. The results are summarised in Table 7-5.

Table 7-5: Technical and economic performance of capturing absorption using absorption and adsorption

	MEA reference case	Case A	Case B	Case C	Case D	Case E	Case F
CO_2 recovery rate (%)	85.71	81.8	81.8	61.97	61.97	66.62	66.62
CO_2 purity in captured steam (%)	>99	96	96	95	95	95	95
ISBL Cost of CO2 captured ($/tonne of CO2)	33.77	40.12	39.13	46.12	44.79	41.06	39.96

It is clear that all cases (A-F) are able to achieve the required purity for transport by pipelines which >95% (Karimi et al., 2011). The recovery of carbon dioxide differs for each case and it can be seen that cases A & B are the only models able to achieve a recovery of more than 80%. The models using activated carbon and a desorption pressure of 5 kPa (E and F) are only able to achieve an overall recovery of 67%. The models representing capture with a vacuum pressure of 10 kPa using sorbent zeolite 13X is the worst in recovery when compared with the other cases. It only recovers approximately 62% of carbon dioxide. The comparison of the overall recovery of carbon dioxide is illustrated in Figure 7-8. In a technical perspective the MEA benchmark model is the best performer, it achieves the highest purity with a recovery of approximately 86%.

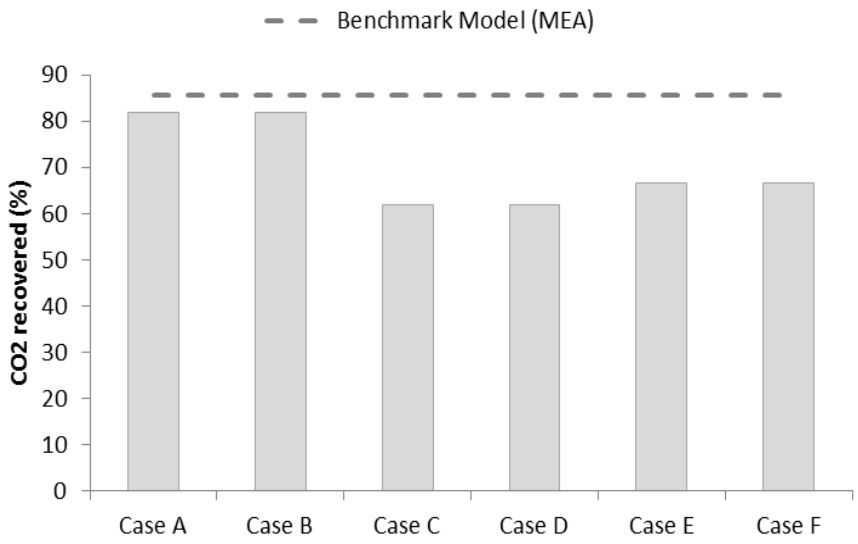

Figure 7-8: CO_2 recovery comparison of MEA model and adsorption models (A-F)

The cost of capturing carbon dioxide is the lowest for the MEA benchmark model. Capturing using 10 kPa regenerating pressure is the most expensive of all, because of the low CO_2 recovery. Capturing using zeolite 13X with a desorption pressure of 5 kPa is the least costly of the cases representing capture using adsorption. The higher recovery of carbon dioxide using zeolite 13X is reducing the overall capture cost when compared to activated carbon. Overall capturing using complex controls without intermediate tanks is cheaper than its counterpart.

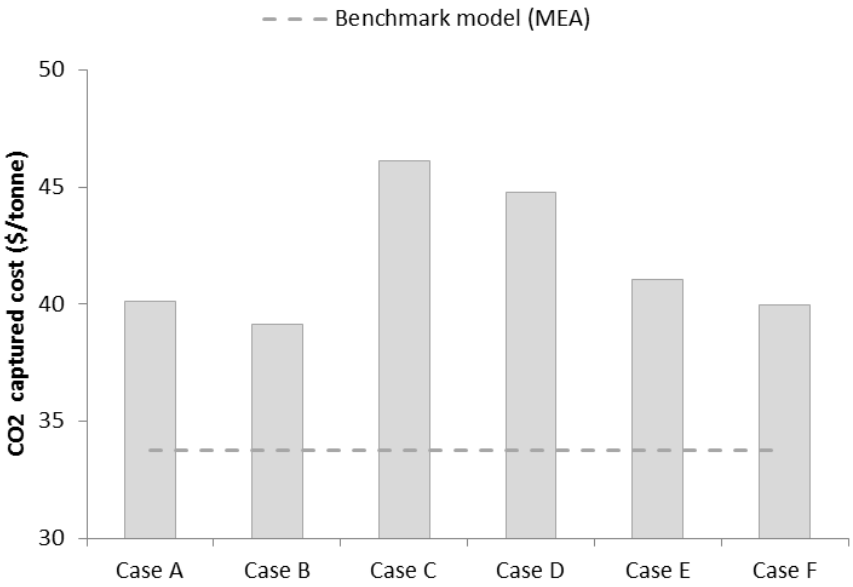

Figure 7-9: Comparison of carbon dioxide capture costs for all models

Even though the costs of carbon dioxide capture using adsorption is not economically favourable according to Figure 7-9. It is necessary to understand the cost of carbon dioxide avoidance to evaluate the overall economic performance. Consuming carbon emitting utilities and resources during capture process reduces the net carbon dioxide captured. This will have an overall increased cost for carbon dioxide reduction. The overall cost of carbon emission avoidance for all models is illustrated in Figure 7-10.

It is clear that the when considering the cost of carbon dioxide avoidance the benchmark model is comparably similar to cases A, B E and F. Assessing the cost of carbon dioxide avoidance shows that case B is approximately 0.04% cheaper that benchmark model. Cases A, E and F are approximately 2.0-4.8% more expensive than the benchmark case. The relative increase in cost of CO_2 avoidance for the benchmark model is due to its emissions from using utilities. The reboiler in the MEA benchmark model uses a large volume of steam,

therefore contributing a high indirect emission for capture. This reduces the net carbon dioxide captured and therefore increases the cost of avoidance. The overall net carbon dioxide captured with breakdown of indirect emissions is shown in Figure 7-11.

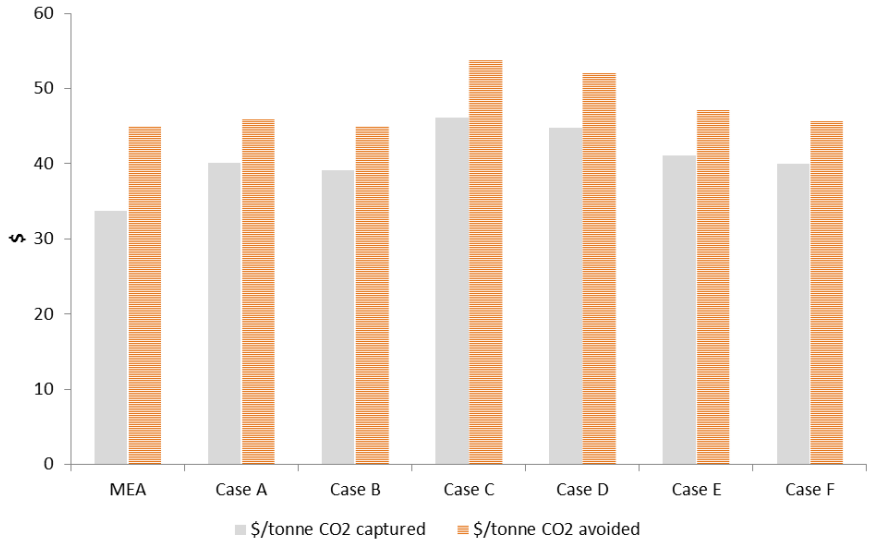

Figure 7-10: Comparison of cost of carbon capture vs. cost of carbon avoidance

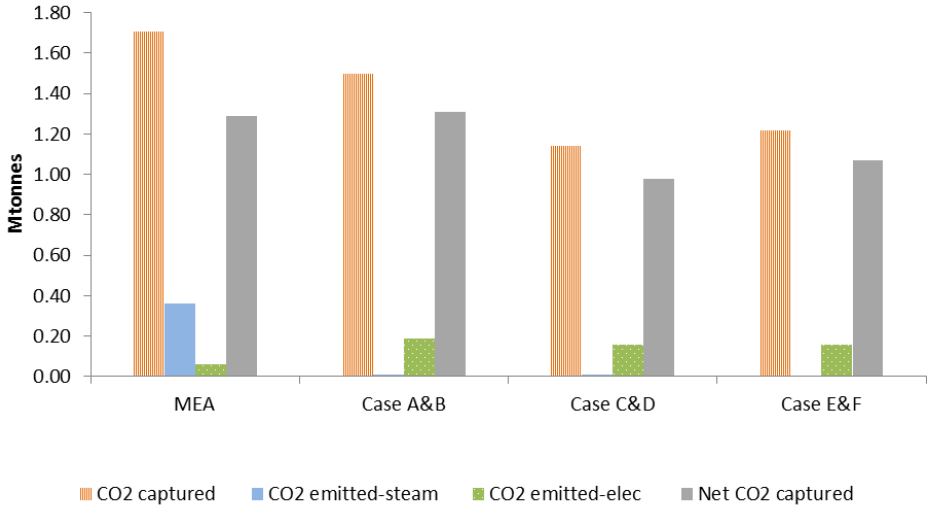

Figure 7-11: Net carbon dioxide emission for all models with breakdown of indirect emissions.

8 Conclusion and Recommendation of Future Work

8.1 Overview

The iron and steel industry contributes approximately 30% of CO_2 industrial direct emissions. It is approximated that a tonne of steel produce from raw materials emit 2.2 tonne of CO_2. Climate change due to the increase of CO_2 in the atmosphere has caused us to re-think and re-model the way we live in this world. Actions are needed and are being applied to tackle climate change. The steel industry is set achieve a decarbonised by 50% from today's emission levels by the year 2050.

TATA Steel collaborated with Nottingham University to research on applying CO_2 capture in parallel to steel making. CO_2 capture is considered as one of the important CO_2 mitigation technology that can be used to decarbonise not only the steel industry, but also to the power sector and other industries. This EngD degree was set to look at the technical perspective of applying CO_2 capture for an existing steel mill. An economic performance analysis was also required as part of this research to understand the techno-economic feasibly of the carbon capture for the steel mill.

8.1.1 The objectives set to achieve in this study

The ultimate outcome to be achieved through this research was an understanding the feasibility of CO_2 capture for an integrated steel mill. This required the following list of targets as part of this study:

- Understand steelmaking and its different point sources of CO_2 emissions
- Investigate CO_2 emissions from the steel mill, which will be used as part of this research
- Propose separation technologies that are suitable for the conditions of the steel mill
- Process model the CO_2 capture technology to understand its technical feasibility
- Apply an economic analysis to get the overall picture of the feasibility of CO_2 capture for the steel mill

8.2 Conclusions from CO_2 Mapping the Steel Mill

After examining the steel mill chosen for this research, it was clear that there were many point sources of CO_2 emissions within the mill. The CO_2 concentration and other conditions varied from one point to the other. The emissions were from different processes within the steel mill, which processed raw materials and produced steel.

It was understood that the work arising gases (WAGs) were used as a fuel at different units in the steel mill. WAGs are the process arising gases from different units, such as coke ovens and blast furnace. The steel mill studied had a power station and blower house, in close proximity that used the WAGs as fuel. A CO_2 mapping concluded that if post combustion capture can be applied

after the power station and the blower house, approximately 44% of CO_2 can be recovered. Therefore the conditions and compositions of the flue gas arising from these units in the steel mill were analysed. The CO_2 concentration in the flue gas from these units has a CO_2 concentration between 23-25 vol%. Using the CO_2 concentration information and a literature survey on different capture technologies, it was concluded that technologies such as adsorption and membrane would be suitable for these conditions. Given that the membrane technology is in very early stage of development, adsorption was chosen as a better choice for the conditions of the steel mill. In addition to adsorption, amine chemical absorption was also investigated as a benchmark study because of its maturity.

8.3 Conclusions from Process Modelling

The two technologies, chemical absorption and physical absorption were modelled in HYSYS and ADSIM respectively. The models were techno-economically assessed for conditions relating to the steel mill

8.3.1 Chemical absorption on HYSYS

The initial step taken towards modelling CO_2 capture using HYSYS was to create a model and validate it. A model representing work by SINTEF that looked at capturing CO_2 from the blast furnace top gas was recreated in HYSYS. The HYSYS model used Li-Mather thermodynamic model to represent vapour-liquid equilibrium for the amine systems. SINTEF used their own software that was proven with their pilot scale work; details of the vapour liquid equilibrium were not given.

It was concluded from the comparison study that HYSYS is able to represent CO_2 separation using MEA. There was a discrepancy in heat of absorption in the absorber column. After further investigating the heat of absorption discrepancy, it was concluded that the HYSYS model was representing heat of absorption for loading conditions of less than or equal to 0.5 mole CO_2/mole MEA. In the models created in HYSYS it was ensured that this was followed.

After completing the validation of the model in HYSYS, a scaled up model to study CO_2 absorption for the steel mill was created. The results obtained showed a capture of 85% or more CO_2 was achievable. In addition to this the final CO_2 product purity was above 99 mole%. This was promising because the final product was meeting the transport requirement. The reboiler duty was also agreeing with published literature.

8.3.2 Physical adsorption on ADSIM

Unlike to HYSYS, ADSIM is not fully developed. It has not got a library for sorbent and sorbate properties. This required investigating parameters and coefficients defining the adsorption process of CO_2 onto the sorbent. The isotherm parameters and mass transfer coefficient were obtained by using published literature.

After calculating the parameters required, a simple model in ADSIM was used to model a breakthrough study. This was to validate the accuracy of the parameters calculated. Breakthrough analysis was conducted for sorbents, zeolite 13X and activated carbon.

The models in ADSIM were further developed to investigate lab scale adsorption for both sorbents (activated carbon and zeolite 13X).

Finally it was concluded that the adsorption of CO_2 onto zeolite 13X and activated carbon can be represented by extended Langmuir equation and the linear driving force model can be used for mass transfer.

Full scale adsorption for the central power station and the turbo blower house was modelled in ADSIM for different conditions

- Adsorption onto zeolite 13X with a desorption pressure of 5 kPa
- Adsorption onto zeolite 13X with a desorption pressure of 10 kPa.
- Adsorption onto activated carbon with a desorption pressure of 5 kPa

All three models required two stages of separation, in which the first stage involved concentrating the product stream with CO_2. The second stage was required to achieve a purity of 95 mol% or more. The results showed that zeolite 13X was able to achieve 96 mol% purity and a recovery of more than 80%. The other models were able to achieve a purity of 95 mol%, but did not perform well with CO_2 recovery. They were only able to attain a CO_2 recovery within 60-70%.

8.4 Conclusions from Economic Analysis

The economic analysis was conducted for all models using the factorial method. The cost of CO_2 capture and the cost of CO_2 avoidance were calculated. For the models using adsorption, counterpart models without

intermediate tanks between the sections were analysed. It was assumed that the controls and instrumentations were more expensive for models that had no tanks in between stages. Overall the models without tanks were cheaper than their counter parts, because installing tanks were more expensive than to have a complex controls system.

MEA scrubbing and zeolite 13X with 5kPa desorption were concluded to be cheapest of all. It was calculated that the cost of CO_2 avoidance for the MEA scrubbing model was approximately \$44.92/tonne of CO_2. The cheapest adsorption model using zeolite 13X added up to \$44.90/tonne of CO_2. The price of CO_2 is high for the MEA model, because it contains large amount of indirect CO_2 emission from using a large volume of steam in the reboiler. It was concluded that CO_2 avoidance is a better costing parameter to investigate the real price of CO_2 mitigation.

It can be concluded that at these prices CO_2 capture for the steel mill does look attractive, because of the significantly low carbon price in the emission trading system (ETS). A detailed analysis of the ETS needs to be studied to understand, when a carbon capture unit with a cost of capture mentioned above will be economically beneficial to the company.

8.5 Recommendation for Future Work

Two stages were required for adsorption models because of the in-ability to reach purity of more than 95 mol% CO_2 in the first stage. Having two stages of separation is expensive in both CAPEX and OPEX. If we can limit the separation for one stage adsorption, the cost of CO_2 capture could be reduced. The following alterations might allow us to use one stage of separation

- Use oxy-combustion for the boilers in CPH and TBH, therefore increasing partial pressure of CO_2 in the flue so high purity of CO_2 can be achieved with one stage

- Use a hypothetical organic solvent as the purge gas, and condense the solvent after obtaining the CO_2 product stream from the bed. Purging with N_2 decreases purity in the CO_2 product stream.

- Using a hypothetical sorbent with a high working capacity and a high CO_2/N_2 selectivity would ensure a high recovery in each bed. Therefore a second stage would not be required.

Appendix A

Table A-1: Comparison of change in enthalpy during CO_2 absorption with published experimental results and Aspen HYSYS (in reference to Figure 5-6)

α – loading (mol CO_2 / mol MEA)	-H(abs) – Calorimeter experiment T=40°C & P=2MPa (kJ/mol of CO_2)	-H(abs) – HYSYS calculation (kJ/mol of CO_2)
0.041	83.575	89.472
0.084	82.801	88.152
0.124	83.694	88.064
0.167	84.065	87.844
0.211	84.322	87.624
0.256	84.359	87.272
0.31	84.362	86.744
0.352	84.325	86.348
0.397	84.344	85.864
0.451	84.333	85.423
0.494	84.311	85.115
0.535	84.529	84.851
0.576	82.283	84.587
0.608	80.373	84.411
0.64	78.418	84.323
0.662	77.063	84.191
0.684	75.714	84.059
0.704	74.537	83.927
0.715	73.931	83.883

Table A-2: Pre-capture units of MEA scrubbing costing parameters (in reference to Table 5-8)

Equipment	Size parameter, S	S (units)	Material	Cost (M$) -2007 US Gulf Coast
Flue gas blower	Volumetric flow	6.33×10^5 m^3/h	Carbon steel	2.83
Flue gas cooler	Area	416 m^2	Carbon steel	0.28

Table A-3: Capture unit of MEA scrubbing costing parameters (in reference to Table 5-8)

Equipment	Size parameter, S	S (units)	Material	Cost (M$) -2007 US Gulf Coast
Absorber column	Shell mass	2.23 x 10^4 kg	Stainless steel	1.32
Absorber packing	Column volume	1252 m^3	Stainless steel	8.64
Regenerator column	Shell mass	2.19 x 10^4 kg	Stainless steel	1.30
Regenerator packing	Column volume	600 m^3	Stainless steel	4.14
Rich Amine Pump (Centrifugal pump)	Flow rate	1038 L/s	Stainless steel	0.30
Rich Amine Pump (Driver motor)	Power	215 kW	Carbon steel	0.14
Rich/Lean Heat exchanger	Area	1.64 x 10^4 m^2	Stainless steel	4.15
Reboiler (regenerator)	Area	3915 m^2	Stainless steel	1.78
Condenser (regenerator)	Area	1233 m^2	Stainless steel	0.88
Lean amine cooler	Area	7247 m^2	Stainless steel	2.54
Amine tank (cone roof tank)	Volume	59.90 m^3	Stainless steel	0.11
Water tank (cone roof tank)	Volume	886 m^3	Carbon steel	0.53

Table A-4: Post capture compression unit for MEA scrubbing costing parameters (in reference to Table 5-8

Equipment	Size parameter, S	S (units)	Material	Cost (M$) -2007 US Gulf Coast
Compressor 1	Power	3.72 MW	Carbon steel	4.22
Compressor 2	Power	3.35 MW	Carbon steel	3.95
Compressor 3	Power	3.26 MW	Carbon steel	3.88
Compressor 4	Power	3.10 MW	Carbon steel	3.76
Compressor 5	Power	2.77 MW	Carbon steel	3.52
Compressor 6	Power	0.36 MW	Carbon steel	1.31
2 Phase separator 1	Shell mass	4525 kg	Carbon steel	0.15
2 Phase separator 1	Shell mass	5292 kg	Carbon steel	0.17
2 Phase separator 1	Shell mass	6150 kg	Carbon steel	0.18
2 Phase separator 1	Shell mass	6974 kg	Carbon steel	0.20
Cooler 1	Area	1575	Carbon steel	0.87
Cooler 2	Area	903	Carbon steel	0.60
Cooler 3	Area	869	Carbon steel	0.57
Cooler 4	Area	936	Carbon steel	0.62
Cooler 5	Area	1575	Carbon steel	0.87
Cooler 6	Area	5119	Carbon steel	1.77
Cooler 7	Area	1839	Carbon steel	0.96
Comp_pump (centrifugal pump)	Flow rate	99.5 L/s	Carbon steel	0.06
Comp_pump (driver motor)	Power	0.47MW	Carbon steel	0.22

Table A-5: CEPCI index used in estimating sizing of the desulphurisation unit (in reference to Table 5-13)

Chemical Engineering Cost Index (CEPCI)	
2003	402
2013	567.3

Table A-6: Location factor used for sizing of desulphurisation unit (in reference to Table 5-13)

Location factor	
Canada	1.0
UK	1.02

Table A-7: Variable operation cost calculation for the desulphurisation unit (in reference to Table 5-13)

	(Singh et al., 2003)	This study
Flue gas flow rate (kmol/h)	57338	23890
Operation & Maintenance (4% Installed cost) /(M$/year)	1.38	0.58
Raw materials (M$/year)	10.07	4.20
Total variable operational cost (M$/year)	11.45	4.78

Appendix B

Table B-1: Pre-capture unit costing for adsorption (cases A-F) (in reference to Table-6-16)

Equipment	Size parameter, S	S (units)	Material	Cost (M$) -2007 US Gulf Coast	Total equipment
		Cases A-F			
Flue gas blower	Volumetric flow	5.83×10^5 m^3/h	Carbon steel	2.69	1
Flue gas cooler 1	Area	1218 m^2	Carbon steel	0.75	1
Flue gas cooler 1	Area	2396 m^2	Carbon steel	1.12	1
		Cases A-D			
Dehumidifier blower	Volumetric flow	5.44×10^5 m^3/h	Carbon steel	2.58	1
Dehumidifier bed (1 bed)	Shell mass	24.3 kg	Carbon steel	0.03	6
Nitrogen heater	Area	345 m^2	Carbon steel	0.24	1

Table B-2: Capture unit of costing parameters for adsorption models A and B (in reference to Table 6-16)

Equipment	Size parameter, S	S (units)	Material	Cost (M$) -2007 US Gulf Coast		Total number of equipment
				Case A	Case B	
Stage 1						
Adsorber bed (1 bed)	Shell mass	173 kg	Carbon steel	0.04	0.04	92
Blower – pressurise	Volumetric flow	1.82 x 10^3 m^3	Carbon steel	0.10	0.11	23
Blower - feed	Volumetric flow	1.70 x 10^4 m^3	Carbon steel	0.38	0.41	23
Vacuum pump - blowdown	Volumetric flow	3.04 x 10^3 m^3	Carbon steel	0.14	0.15	23
Driver motor – blowdown	Power	317 kW	Carbon steel	0.21	0.23	23
Vacuum pump – purge	Volumetric flow	5.15 x 10^3 m^3	Carbon steel	0.18	0.20	23
Driver motor – purge	Power	537 kW	Carbon steel	0.29	0.31	23
Stage 2						
Adsorber bed (1 bed)	Shell mass	207 kg	Carbon steel	0.04	0.04	46
Blower – pressurise	Volumetric flow	1.82 x 10^3 m^3	Carbon steel	0.10	0.11	12
Blower – feed	Volumetric flow	1.24 x 10^4 m^3	Carbon steel	0.31	0.34	12
Vacuum pump – blowdown	Volumetric flow	7.30 x 10^3 m^3	Carbon steel	0.23	0.25	12
Driver motor – blowdown	Power	760 kW	Carbon steel	0.35	0.38	12
Vacuum pump – purge	Volumetric flow	3.39 x 10^3 m^3	Carbon steel	0.14	0.16	12
Driver motor – purge	Power	353 kW	Carbon steel	0.22	0.24	12
Floating roof tank (1 tank)	Volume	425 m^3	Carbon steel	0.77		12

Table B-3: Capture unit of costing parameters for adsorption models C and D (in reference to Table 6-16)

Equipment	Size parameter, S	S (units)	Material	Cost (M$) -2007 US Gulf Coast		Total number of equipment
				Case C	Case D	
Stage 1						
Adsorber bed (1 bed)	Shell mass	173 kg	Carbon steel	0.04	0.04	92
Blower – pressurise	Volumetric flow	1.82 x 10^3 m^3	Carbon steel	0.10	0.11	23
Blower - feed	Volumetric flow	1.70 x 10^4 m^3	Carbon steel	0.38	0.41	23
Vacuum pump - blowdown	Volumetric flow	1.95 x 10^3 m^3	Carbon steel	0.10	0.11	23
Driver motor – blowdown	Power	203 kW	Carbon steel	0.16	0.17	23
Vacuum pump - purge	Volumetric flow	5.18 x 10^3 m^3	Carbon steel	0.19	0.20	23
Driver motor – purge	Power	540 kW	Carbon steel	0.29	0.31	23
Stage 2						
Adsorber bed (1 bed)	Shell mass	207 kg	Carbon steel	0.04	0.04	46
Blower – pressurise	Volumetric flow	1.82 x 10^3 m^3	Carbon steel	0.10	0.11	12
Blower - feed	Volumetric flow	1.14 x 10^4 m^3	Carbon steel	0.30	0.32	12
Vacuum pump - blowdown	Volumetric flow	6.33 x 10^3 m^3	Carbon steel	0.21	0.23	12
Driver motor – blowdown	Power	659 kW	Carbon steel	0.32	0.35	12
Vacuum pump - purge	Volumetric flow	2.22 x 10^3 m^3	Carbon steel	0.11	0.12	12
Driver motor – purge	Power	231 kW	Carbon steel	0.17	0.19	12
Floating roof tank (1 tank)	Volume	394 m^3	Carbon steel	0.75		12

Table B-4: Capture unit of costing parameters for adsorption models E and F (in reference to Table 6-16)

Equipment	Size parameter, S	S (units)	Material	Cost (M$) -2007 US Gulf Coast		Total number of equipment
				Case E	Case F	
Stage 1						
Adsorber bed (1 bed)	Shell mass	152 kg	Carbon steel	0.04	0.04	92
Blower – pressurise	Volumetric flow	1.82×10^3 m³	Carbon steel	0.10	0.11	23
Blower - feed	Volumetric flow	1.70×10^4 m³	Carbon steel	0.38	0.41	23
Vacuum pump - blowdown	Volumetric flow	4.62×10^3 m³	Carbon steel	0.17	0.19	23
Driver motor – blowdown	Power	482 kW	Carbon steel	0.27	0.29	23
Vacuum pump - purge	Volumetric flow	2.72×10^3 m³	Carbon steel	0.13	0.14	23
Driver motor – purge	Power	284 kW	Carbon steel	0.19	0.21	23
Stage 2						
Adsorber bed (1 bed)	Shell mass	207 kg	Carbon steel	0.04	0.04	46
Blower – pressurise	Volumetric flow	1.82×10^3 m³	Carbon steel	0.10	0.11	12
Blower - feed	Volumetric flow	9.15×10^3 m³	Carbon steel	0.26	0.28	12
Vacuum pump - blowdown	Volumetric flow	7.30×10^3 m³	Carbon steel	0.23	0.25	12
Driver motor – blowdown	Power	760 kW	Carbon steel	0.35	0.38	12
Vacuum pump - purge	Volumetric flow	1.77×10^3 m³	Carbon steel	0.10	0.11	12
Driver motor – purge	Power	185 kW	Carbon steel	0.15	0.16	12
Floating roof tank (1 tank)	Volume	322 m³	Carbon steel	0.76		12

Table B-5: Costing parameters for compression unit used in adsorption (A and B) (in reference to Table 6-16)

Equipment	Size parameter, S	S (units)	Material	Cost (M$) -2007 US Gulf Coast
		Cases A & B		
Compressor 1	Power	3.03 MW	Carbon steel	3.71
Compressor 2	Power	3.06 MW	Carbon steel	3.73
Compressor 3	Power	3.04 MW	Carbon steel	3.72
Compressor 4	Power	2.98 MW	Carbon steel	3.67
Compressor 5	Power	2.86 MW	Carbon steel	3.58
Compressor 6	Power	2.62 MW	Carbon steel	3.40
Compressor 7	Power	0.86 MW	Carbon steel	1.87
Cooler 1	Area	1210	Carbon steel	0.74
Cooler 2	Area	675	Carbon steel	0.44
Cooler 3	Area	689	Carbon steel	0.45
Cooler 4	Area	720	Carbon steel	0.47
Cooler 5	Area	803	Carbon steel	0.53
Cooler 6	Area	1217	Carbon steel	0.75
Cooler 7	Area	5120	Carbon steel	1.77
Cooler 8	Area	909	Carbon steel	0.60
Comp_pump (centrifugal pump)	Flow rate	90.8 L/s	Carbon steel	0.06
Comp_pump (driver motor)	Power	0.37MW	Carbon steel	0.19

Table B-6: Costing parameters for compression unit used in adsorption (C and D) (in reference to Table 6-16)

Equipment	Size parameter, S	S (units)	Material	Cost (M$) -2007 US Gulf Coast
		Cases C & D		
Compressor 1	Power	2.32 MW	Carbon steel	3.16
Compressor 2	Power	2.35 MW	Carbon steel	3.18
Compressor 3	Power	2.32 MW	Carbon steel	3.17
Compressor 4	Power	2.28 MW	Carbon steel	3.13
Compressor 5	Power	2.19 MW	Carbon steel	3.06
Compressor 6	Power	2.01 MW	Carbon steel	2.91
Compressor 7	Power	0.67 MW	Carbon steel	1.67
Cooler 1	Area	926	Carbon steel	0.61
Cooler 2	Area	517	Carbon steel	0.34
Cooler 3	Area	528	Carbon steel	0.35
Cooler 4	Area	552	Carbon steel	0.36
Cooler 5	Area	615	Carbon steel	0.40
Cooler 6	Area	931	Carbon steel	0.62
Cooler 7	Area	3910	Carbon steel	1.50
Cooler 8	Area	858	Carbon steel	0.67
Comp_pump (centrifugal pump)	Flow rate	75.9 L/s	Carbon steel	0.05
Comp_pump (driver motor)	Power	0.31MW	Carbon steel	0.17

Table B-7: Costing parameters for compression unit used in adsorption (E and F) (in reference to Table 6-16)

Equipment	Size parameter, S	S (units)	Material	Cost (M$) -2007 US Gulf Coast
		Cases E & F		
Compressor 1	Power	2.49 MW	Carbon steel	3.30
Compressor 2	Power	2.52 MW	Carbon steel	3.32
Compressor 3	Power	2.50 MW	Carbon steel	3.30
Compressor 4	Power	2.45 MW	Carbon steel	3.27
Compressor 5	Power	2.35 MW	Carbon steel	3.19
Compressor 6	Power	2.16 MW	Carbon steel	3.03
Compressor 7	Power	0.72 MW	Carbon steel	1.73
Cooler 1	Area	995	Carbon steel	0.66
Cooler 2	Area	556	Carbon steel	0.37
Cooler 3	Area	567	Carbon steel	0.37
Cooler 4	Area	593	Carbon steel	0.39
Cooler 5	Area	661	Carbon steel	0.43
Cooler 6	Area	1001	Carbon steel	1.57
Cooler 7	Area	4203	Carbon steel	0.96
Cooler 8	Area	923	Carbon steel	0.61
Comp_pump (centrifugal pump)	Flow rate	81.6 L/s	Carbon steel	0.06
Comp_pump (driver motor)	Power	0.33 MW	Carbon steel	0.18

Bibliography

ABU-ZAHRA, M. R. M., NIEDERER, J. P. M., FERON, P. H. M. & VERSTEEG, G. F. 2007a. CO2 capture from power plants. Part II. A parametric study of the economical performance based on mono-ethanolamine. *International Journal of Greenhouse Gas Control,* 1**,** 135-142.

ABU-ZAHRA, M. R. M., SCHNEIDERS, L. H. J., NIEDERER, J. P. M., FERON, P. H. M. & VERSTEEG, G. F. 2007b. CO2 capture from power plants: Part I. A parametric study of the technical performance based on monoethanolamine. *International Journal of Greenhouse Gas Control,* 1**,** 37-46.

ALEXANDER, L., SIMON, A., BINDOFF, N., BRÉON, F., CHURCH, J. & CUBASCH, U. 2013. Working Group I Contribution to the IPCC Fifth Assessment Report, Climate Change 2013: The Physical Science Basis Summary for policymakers. *Intergovernmental Panel on Climate Change,* 5.

ALIE, C., BACKHAM, L., CROISET, E. & DOUGLAS, P. L. 2005. Simulation of CO2 capture using MEA scrubbing: a flowsheet decomposition method. *Energy Conversion and Management,* 46**,** 475-487.

ALLWOOD, J. M. & CULLEN, J. M. Steel, aluminium and carbon: alternative strategies for meeting the 2050 carbon emission targets. R'09 Conference, Davos, 2009.

ARASTO, A., TSUPARI, E., KÄRKI, J., PISILÄ, E. & SORSAMÄKI, L. 2013. Post-combustion capture of CO2 at an integrated steel mill – Part I: Technical concept analysis. *International Journal of Greenhouse Gas Control,* 16**,** 271-277.

ARESTA, M. 2003. Carbon dioxide recovery and utilization. Kluwer Academic Publishers.

ASPENTECH 2004. Adsorption Reference Guide. *ASPEN ADSIM*.

AUSTGEN, D. M., ROCHELLE, G. T., PENG, X. & CHEN, C. C. 1989. Model of vapor-liquid equilibria for aqueous acid gas-alkanolamine systems using the electrolyte-NRTL equation. *Industrial & Engineering Chemistry Research,* 28**,** 1060-1073.

BALDWIN, P. 2009. Low-cost, high-efficiency CO_2 compressors. *Carbon Capture J.,* 11**,** 19-21.

BERGER, A. H. & BHOWN, A. S. 2011. Comparing physisorption and chemisorption solid sorbents for use separating CO2 from flue gas using temperature swing adsorption. *Energy Procedia,* 4**,** 562-567.

BERNSTEIN, L., BOSCH, P., CANZIANI, O., CHEN, Z., CHRIST, R., DAVIDSON, O., HARE, W., HUQ, S., KAROLY, D. & KATTSOV, V. 2007. Climate change 2007: Synthesis report. Contribution of Working Groups I, II and III to the fourth assessment report of the Intergovernmental Panel on Climate Change. *IPCC: Geneva, Switzerland*.

BLOMEN, E., HENDRIKS, C. & NEELE, F. 2009. Capture technologies: Improvements and promising developments. *Energy Procedia,* 1**,** 1505-1512.

BROWN, T. A., GAMBHIR, A., FLORIN, N. & FENNELL, P. S. 2012. Reducing CO2 emissions from heavy industry: a review of technologies and considerations for policy makers.

BRUNETTI, A., SCURA, F., BARBIERI, G. & DRIOLI, E. 2010. Membrane technologies for CO2 separation. *Journal of Membrane Science,* 359**,** 115-125.

CAVENATI, S., GRANDE, C. A. & RODRIGUES, A. E. 2004. Adsorption Equilibrium of Methane, Carbon Dioxide, and Nitrogen on Zeolite 13X at High Pressures. *Journal of Chemical & Engineering Data,* 49**,** 1095-1101.

CEPCI. 2013. Chemical Engineering Plant Cost Index. *Chem. Eng.***,** 76.

CHAPEL, D. G., MARIZ, C. L. & ERNEST, J. Recovery of CO2 from flue gases: commercial trends. Canadian Society of Chemical Engineers Annual Meeting, 1999. 4-6.

CHOI, S., DRESE, J. H. & JONES, C. W. 2009. Adsorbent Materials for Carbon Dioxide Capture from Large Anthropogenic Point Sources. *ChemSusChem,* 2**,** 796-854.

CHOU, C.-T. & CHEN, C.-Y. 2004. Carbon dioxide recovery by vacuum swing adsorption. *Separation and Purification Technology,* 39**,** 51-65.

CHUE, K. T., KIM, J. N., YOO, Y. J., CHO, S. H. & YANG, R. T. 1995. Comparison of Activated Carbon and Zeolite 13X for CO2 Recovery from Flue Gas by Pressure Swing Adsorption. *Industrial & Engineering Chemistry Research,* 34**,** 591-598.

CUSSLER, E. L. 2009. *Diffusion: Mass Transfer in Fluid Systems*, Cambridge University Press.

DAVIS, J. & ROCHELLE, G. 2009. Thermal degradation of monoethanolamine at stripper conditions. *Energy Procedia,* 1**,** 327-333.

DECC, D. 2011. Guidelines to Defra/DECC's GHG Conversion Factors for Company Reporting. *London: Department for Environment, Food and Rural Affairs and Department for Energy and Climate Change*.

DREISBACH, F., STAUDT, R. & KELLER, J. U. 1999. High Pressure Adsorption Data of Methane, Nitrogen, Carbon Dioxide and their Binary and Ternary Mixtures on Activated Carbon. *Adsorption,* 5**,** 215-227.

FARLA, J. M., HENDRIKS, C. & BLOK, K. 1995. Carbon dioxide recovery from industrial processes. *Climatic Change,* 29**,** 439-461.

FIELD, C. B. & VAN AALST, M. 2014. *Climate change 2014: impacts, adaptation, and vulnerability*, IPCC.

FISHER, K. S., BEITLER, C., RUETER, C., SEARCY, K., ROCHELLE, G., JASSIM, M. & FIGUEROA, J. D. Integrating MEA regeneration with CO2 compression to reduce CO2 capture costs. Fourth Annual Conference on Carbon Capture and Sequestration DOE/NETL, 2005.

GLUECKAUF, E. 1955. Theory of chromatography. Part 10.-Formulae for diffusion into spheres and their application to chromatography. *Transactions of the Faraday Society,* 51**,** 1540-1551.

GOJIÆ, M. & KOÞUH, S. 2006. Development of direct reduction processes and smelting reduction processes for the steel production. *Kem. u Ind. ,* 55**,** 1-10.

GOMES, V. G. & YEE, K. W. K. 2002. Pressure swing adsorption for carbon dioxide sequestration from exhaust gases. *Separation and Purification Technology,* 28**,** 161-171.

HAMBORG, E. S., SMITH, V., CENTS, T., BRIGMAN, N., PEDERSEN, O. F., DE CAZENOVE, T., CHHAGANLAL, M., FESTE, J. K., ULLESTAD, Ø., ULVATN, H., GORSET, O., ASKESTAD, I., GRAM, L. K., FOSTÅS, B. F., SHAH, M. I., MAXSON, A. & THIMSEN, D. 2014. Results from MEA testing at the CO2 Technology Centre Mongstad. Part II: Verification of baseline results. *Energy Procedia,* 63**,** 5994-6011.

HO, M. T., ALLINSON, G. W. & WILEY, D. E. 2008a. Reducing the Cost of CO2 Capture from Flue Gases Using Membrane Technology. *Industrial & Engineering Chemistry Research,* 47**,** 1562-1568.

HO, M. T., ALLINSON, G. W. & WILEY, D. E. 2008b. Reducing the Cost of CO2 Capture from Flue Gases Using Pressure Swing Adsorption. *Industrial & Engineering Chemistry Research,* 47**,** 4883-4890.

HO, M. T., ALLINSON, G. W. & WILEY, D. E. 2011. Comparison of MEA capture cost for low CO2 emissions sources in Australia. *International Journal of Greenhouse Gas Control,* 5**,** 49-60.

HYSYS, A. 2007. User's Guide. Aspen Technology. *Inc., Burlington, Massachusetts*.

IEA. 2008. *CO2 Capture and Storage: A Key Carbon Abatement Option* [Online]. Paris: OECD Publishing. Available: http://dx.doi.org/10.1787/9789264041417-en.

IEA. 2010. *Key World Energy Statistics 2010* [Online]. Paris: OECD Publishing. Available: http://dx.doi.org/10.1787/9789264095243-en.

IEA. 2012a. *Energy Technology Perspectives 2012* [Online]. Paris: OECD Publishing. Available: http://dx.doi.org/10.1787/energy_tech-2012-en.

IEA. 2012b. *Key World Energy Statistics 2011* [Online]. OECD Publishing. Available: http://dx.doi.org/10.1787/key_energ_stat-2011-en.

IEA. 2014. *Key World Energy Statistics 2014* [Online]. Paris: OECD Publishing. Available: http://dx.doi.org/10.1787/key_energ_stat-2014-en.

ISHIBASHI, M., OTA, H., AKUTSU, N., UMEDA, S., TAJIKA, M., IZUMI, J., YASUTAKE, A., KABATA, T. & KAGEYAMA, Y. 1996. Technology for removing carbon dioxide from power plant flue gas by the physical adsorption method. *Energy Conversion and Management,* 37**,** 929-933.

JOHNSON, R. A. 2009. *Statistics: principles and methods,* John Wiley & Sons.

KANNICHE, M., GROS-BONNIVARD, R., JAUD, P., VALLE-MARCOS, J., AMANN, J.-M. & BOUALLOU, C. 2010. Pre-combustion, post-combustion and oxy-combustion in thermal power plant for CO2 capture. *Applied Thermal Engineering,* 30**,** 53-62.

KARIMI, M., HILLESTAD, M. & SVENDSEN, H. F. 2011. Capital costs and energy considerations of different alternative stripper configurations for post combustion CO2 capture. *Chemical Engineering Research and Design,* 89**,** 1229-1236.

KHAN, F. M., KRISHNAMOORTHI, V. & MAHMUD, T. 2011. Modelling reactive absorption of CO2 in packed columns for post-combustion carbon capture applications. *Chemical Engineering Research and Design,* 89**,** 1600-1608.

KIKKINIDES, E. S., YANG, R. T. & CHO, S. H. 1993. Concentration and recovery of carbon dioxide from flue gas by pressure swing adsorption. *Industrial & Engineering Chemistry Research,* 32**,** 2714-2720.

KIM, I. & SVENDSEN, H. F. 2007. Heat of Absorption of Carbon Dioxide (CO2) in Monoethanolamine (MEA) and 2-(Aminoethyl)ethanolamine (AEEA) Solutions. *Industrial & Engineering Chemistry Research,* 46**,** 5803-5809.

KIM, M.-B., RYU, Y.-K. & LEE, C.-H. 2005. Adsorption Equilibria of Water Vapor on Activated Carbon and DAY Zeolite. *Journal of Chemical & Engineering Data,* 50**,** 951-955.

KISTER, H. Z., SCHERFFIUS, J., AFSHAR, K. & ABKAR, E. 2007. Realistically predict capacity and pressure drop for packed columns. *AIChE meeting.* Houston, TX.

KO, D., SIRIWARDANE, R. & BIEGLER, L. T. 2002. Optimization of a Pressure-Swing Adsorption Process Using Zeolite 13X for CO2 Sequestration. *Industrial & Engineering Chemistry Research,* 42**,** 339-348.

KO, D., SIRIWARDANE, R. & BIEGLER, L. T. 2005. Optimization of Pressure Swing Adsorption and Fractionated Vacuum Pressure Swing Adsorption Processes for CO2 Capture. *Industrial & Engineering Chemistry Research,* 44**,** 8084-8094.

KOHL, A. L. & NIELSEN, R. B. 1997. Chapter 2 - Alkanolamines for Hydrogen Sulfide and Carbon Dioxide Removal. *Gas Purification (Fifth Edition).* Houston: Gulf Professional Publishing.

KURAMOCHI, T., RAMÍREZ, A., TURKENBURG, W. & FAAIJ, A. 2012. Comparative assessment of CO 2 capture technologies for carbon-intensive industrial processes. *Progress in energy and combustion science,* 38**,** 87-112.

KVAMSDAL, H. M., JAKOBSEN, J. P. & HOFF, K. A. 2009. Dynamic modeling and simulation of a CO2 absorber column for post-combustion CO2 capture. *Chemical Engineering and Processing: Process Intensification,* 48**,** 135-144.

KVAMSDAL, H. M. & ROCHELLE, G. T. 2008. Effects of the Temperature Bulge in CO2 Absorption from Flue Gas by Aqueous Monoethanolamine. *Industrial & Engineering Chemistry Research,* 47**,** 867-875.

LI, G., XIAO, P., WEBLEY, P., ZHANG, J., SINGH, R. & MARSHALL, M. 2008. Capture of CO2 from high humidity flue gas by vacuum swing adsorption with zeolite 13X. *Adsorption,* 14**,** 415-422.

LIE, J. A., VASSBOTN, T., HÄGG, M.-B., GRAINGER, D., KIM, T.-J. & MEJDELL, T. 2007. Optimization of a membrane process for CO2 capture in the steelmaking industry. *International Journal of Greenhouse Gas Control,* 1**,** 309-317.

LIU, X. 2014. *Rate based modelling of CO2 removal using alkanolamines.* Masters, Norwegian University of Science and Technology.

LIU, Y., ZHANG, L. & WATANASIRI, S. 1999a. Representing Vapor−Liquid Equilibrium for an Aqueous MEA−CO2 System Using the Electrolyte

Nonrandom-Two-Liquid Model. *Industrial & Engineering Chemistry Research,* 38**,** 2080-2090.

LIU, Z., LING, L., QIAO, W. & LIU, L. 1999b. Preparation of pitch-based spherical activated carbon with developed mesopore by the aid of ferrocene. *Carbon,* 37**,** 663-667.

MATHONAT, C., MAJER, V., MATHER, A. E. & GROLIER, J. P. E. 1997. Enthalpies of absorption and solubility of CO2 in aqueous solutions of methyldiethanolamine. *Fluid Phase Equilibria,* 140**,** 171-182.

MEIJER, K., DENYS, M., LASAR, J., BIRAT, J.-P., STILL, G. & OVERMAAT, B. 2009. ULCOS: ultra-low CO2 steelmaking. *Ironmaking & Steelmaking,* 36**,** 249-251.

METZ, B., DAVIDSON, O., DE CONINCK, H., LOOS, M. & MEYER, L. 2005. IPCC special report on carbon dioxide capture and storage. Prepared by Working Group III of the Intergovernmental Panel on Climate Change. *IPCC, Cambridge University Press: Cambridge, United Kingdom and New York, USA,* 4.

MIMURA, T., NOJO, T., ISHIDA, K., NAKASHOJI, H., TANAKA, H. & HIRATA, T. 2008. Amine recovery apparatus and decarbonation apparatus having same. Google Patents.

MUNASINGHE, A. S. K., ØI, L.E 2011. Process simulation of water wash in CO2 absorption using monoethanolamine. *3rd International Symposium on Environmental Management.* Zagreb, Croatia,.

ØI, L. E. 2007. Aspen HYSYS Simulation of CO2 Removal by Amine Absorption from a Gas Based Power Plant. *The 48th Scandinavian Conference on Simulation and Modeling (SIMS 2007), 30-31 October, 2007, Göteborg (Särö)***,** 73-81.

ØI, L. E. 2010. CO2 removal by absorption: challenges in modelling. *Mathematical and Computer Modelling of Dynamical Systems,* 16**,** 511-533.

OLAJIRE, A. A. 2010. CO2 capture and separation technologies for end-of-pipe applications - A review. *Energy,* 35**,** 2610-2628.

ORTH, A., ANASTASIJEVIC, N. & EICHBERGER, H. 2007. Low CO2 emission technologies for iron and steelmaking as well as titania slag production. *Minerals Engineering,* 20**,** 854-861.

RACKLEY, S. A. 2010. *Carbon capture and storage,* Burlington, MA, Butterworth-Heinemann/Elsevier.

RAO, A. B. & RUBIN, E. S. 2002. A Technical, Economic, and Environmental Assessment of Amine-Based CO2 Capture Technology for Power Plant Greenhouse Gas Control. *Environmental Science & Technology,* 36**,** 4467-4475.

REMUS, R., ROUDIER, S., AGUADO-MONSONET, M. A. & SANCHO, L. D. 2013. *Best Available Techniques (BAT) Reference Document for Iron and Steel Production: Industrial Emissions Directive 2010/75/EU: Integrated Pollution Prevention and Control*, Publications Office.

RICHARDSON, J. F., HARKER, J. H., BACKHURST, J. R. & COULSON, J. M. 2002. *Coulson and Richardson's chemical engineering: vol. 2 : particle technology and separation processes,* Oxford, Butterworth-Heinemann.

RUTHVEN, D. M. 1984. *Principles of Adsorption and Adsorption Processes*, Wiley.

SERBEZOV, A. 2003. Adsorption Equilibrium of Water Vapor on F-200 Activated Alumina. *Journal of Chemical & Engineering Data,* 48**,** 421-425.

SHEN, C., LIU, Z., LI, P. & YU, J. 2012. Two-stage VPSA process for CO2 capture from flue gas using activated carbon beads. *Industrial & Engineering Chemistry Research,* 51**,** 5011-5021.

SHEN, C., YU, J., LI, P., GRANDE, C. & RODRIGUES, A. 2011. Capture of CO2 from flue gas by vacuum pressure swing adsorption using activated carbon beads. *Adsorption,* 17**,** 179-188.

SINGH, D., CROISET, E., DOUGLAS, P. L. & DOUGLAS, M. A. 2003. Techno-economic study of CO2 capture from an existing coal-fired power plant: MEA scrubbing vs. O2/CO2 recycle combustion. *Energy Conversion and Management,* 44**,** 3073-3091.

SINNOTT, R. K. & TOWLER, G. 2009. *Chemical Engineering Design*, Butterworth-Heinemann.

SIRIWARDANE, R. V., SHEN, M.-S., FISHER, E. P. & POSTON, J. A. 2001. Adsorption of CO2 on Molecular Sieves and Activated Carbon. *Energy & Fuels,* 15**,** 279-284.

TAYLOR, R., KRISHNA, R. & KOOIJMAN, H. 2003. Real-world modeling of distillation. *transfer,* 1000**,** 1.

THOMAS, W. J. & CRITTENDEN, B. D. 1998. *Adsorption Technology and Design*, Butterworth-Heinemann.

TOBIESEN, F. A., SVENDSEN, H. F. & MEJDELL, T. 2007. Modeling of Blast Furnace CO2 Capture Using Amine Absorbents. *Industrial & Engineering Chemistry Research,* 46**,** 7811-7819.

TSUPARI, E., KÄRKI, J., ARASTO, A. & PISILÄ, E. 2013. Post-combustion capture of CO2 at an integrated steel mill – Part II: Economic feasibility. *International Journal of Greenhouse Gas Control,* 16**,** 278-286.

VALIA, H. S. 1994. *Coke production for blast furnace ironmaking* [Online]. Available: http://www.steel.org/making-steel/how-its-made/processes/processes-info/coke-production-for-blast-furnace-ironmaking.aspx [Accessed 12th Dec 2015].

WANG, L., LIU, Z., LI, P., WANG, J. & YU, J. 2012a. CO2 capture from flue gas by two successive VPSA units using 13XAPG. *Adsorption,* 18**,** 445-459.

WANG, L., LIU, Z., LI, P., YU, J. & RODRIGUES, A. E. 2012b. Experimental and modeling investigation on post-combustion carbon dioxide capture using zeolite 13X-APG by hybrid VTSA process. *Chemical Engineering Journal,* 197**,** 151-161.

WANG, L., YANG, Y., SHEN, W., KONG, X., LI, P., YU, J. & RODRIGUES, A. E. 2013. CO2 Capture from Flue Gas in an Existing Coal-Fired Power Plant by Two Successive Pilot-Scale VPSA Units. *Industrial & Engineering Chemistry Research,* 52**,** 7947-7955.

WANG, M., LAWAL, A., STEPHENSON, P., SIDDERS, J. & RAMSHAW, C. 2011. Post-combustion CO 2 capture with chemical absorption: a state-of-the-art review. *Chemical Engineering Research and Design,* 89**,** 1609-1624.

WHITMAN, W. 1923. The two-film theory of gas absorption. *Chem. metall. Engng.,* 29**,** 146-148.

WILCOX, J. 2012. *Carbon Capture,* Springer New York.

WILEY, D. E., HO, M. T. & BUSTAMANTE, A. 2011. Assessment of opportunities for CO2 capture at iron and steel mills: An Australian perspective. *Energy Procedia,* 4**,** 2654-2661.

WSA. 2008. *2008 Sustainability report of the world steel industry* [Online]. World Steel Association. Available: https://www.worldsteel.org/dms/internetDocumentList/bookshop/2008-Sustainability-Report/document/2008%20Sustainability%20Report.pdf [Accessed 30th Nov 2015].

WSA. 2014a. *Fact-sheet: Addressing climate change through technology transfer and research* [Online]. World Steel Association. Available: http://www.worldsteel.org/pictures/programfiles/Fact%20sheet_Breakthrough%20technologies.pdf [Accessed 30th Nov 2015].

WSA. 2014b. *Fact Sheet: Steel and Raw Materials* [Online]. World Steel Association. Available: https://www.worldsteel.org/publications/fact-sheets/content/00/text_files/file0/document/fact_raw%20materials_2014.pdf [Accessed 30th Nov 2015].

XIAO, G., WEBLEY, P, HOADLEY, A, HO, M, WILEY, D 2013. Low Cost Hybrid Capture Technology Development: Final Report. Canberra, Australia: CO2CRC.

YANG, H., XU, Z., FAN, M., GUPTA, R., SLIMANE, R. B., BLAND, A. E. & WRIGHT, I. 2008. Progress in carbon dioxide separation and capture: A review. *Journal of Environmental Sciences,* 20**,** 14-27.

YANG, R. T. 1997. *Gas Separation by Adsorption Processes*, Imperial College Press.

ZHANG, J., XIAO, P., LI, G. & WEBLEY, P. A. 2009a. Effect of flue gas impurities on CO2 capture performance from flue gas at coal-fired power stations by vacuum swing adsorption. *Energy Procedia,* 1**,** 1115-1122.

ZHANG, Y., CHEN, H., CHEN, C.-C., PLAZA, J. M., DUGAS, R. & ROCHELLE, G. T. 2009b. Rate-Based Process Modeling Study of CO2 Capture with Aqueous Monoethanolamine Solution. *Industrial & Engineering Chemistry Research,* 48**,** 9233-9246.

ZHANG, Z., ZHANG, W., CHEN, X., XIA, Q. & LI, Z. 2010. Adsorption of CO2 on Zeolite 13X and Activated Carbon with Higher Surface Area. *Separation Science and Technology,* 45**,** 710-719.